NUREG/IA-0003



# International Agreement Report

# Influence of the Wetting State of a Heated Surface on Heat Transfer and Pressure Loss in an Evaporator Tube

Prepared by
W. Köhler, D. Hein

Kraftmerk Union AG
Erlangen, Federal Republic of Germany



**Office of Nuclear Regulatory Research**
**U.S. Nuclear Regulatory Commission**
**Washington, DC 20555**

**September 1986**

Prepared as part of
The Agreement on Research Participation and Technical Exchange
under the International Thermal-Hydraulic Code Assessment
and Application Program (ICAP)

Published by
U.S. Nuclear Regulatory Commission

Available from

Superintendent of Documents
U.S. Government Printing Office
P.O. Box 37082
Washington, D.C. 20013-7082

and

National Technical Information Service
Springfield, VA 22161

---

NUREG/IA--0003

TI87 900030


**International Agreement Report**

# Influence of the Wetting State of a Heated Surface on Heat Transfer and Pressure Loss in an Evaporator Tube

Prepared by
W. Köhler, D. Hein

Kraftmerk Union AG
Erlangen, Federal Republic of Germany

**Office of Nuclear Regulatory Research**
**U.S. Nuclear Regulatory Commission**
**Washington, DC 20555**

**September 1986**



Prepared as part of
The Agreement on Research Participation and Technical Exchange
under the International Thermal-Hydraulic Code Assessment
and Application Program (ICAP)

Published by
U.S. Nuclear Regulatory Commission

NOTICE

This report documents work performed under the sponsorship of the Kraftwerk Union in the Federal Republic of Germany. The information in this report has been provided to the USNRC under the terms of an information exchange agreement between the United States and the Federal Republic of Germany (Technical Exchange and Cooperation Arrangement Between the United States Nuclear Regulatory Commission and the Bundesminister Fuer Forschung und Technologie of the Federal Republic of Germany in the field of reactor safety research and development, April 30, 1981). The Kraftwerk Union has consented to the publication of this report as a USNRC document in order that it may receive the widest possible circulation among the reactor safety community. Neither the United States Government nor the Kraftwerk Union or any agency thereof, or any of their employees, makes any warranty, expressed or implied, or assumes any legal liability of responsibility for any third party's use, or the results of such use, of any information, apparatus, product or process disclosed in this report, or represents that its use by such third party would not infringe privately owned rights.

## ABSTRACT

The influence of the wetting state of a heated surface on heat transfer and pressure loss in an evaporator tube was investigated for a parameter range occurring in fossil-fired steam generators. Included in the analysis are quantities which determine the wetting state in steady and transient flow.

The experimental work consists of the following:

- occurrence of critical heat flux (CHF) and post-CHF heat transfer in a vertical upflow evaporator tube
- influence of pressure and enthalpy transients on heat transfer in the unwetted region
- influence of pipe orientation on heat transfer
- two phase flow pressure loss in wetted and unwetted region.

Based on these experiments a method of predicting CHF for a vertical upflow evaporator tube was developed. The heat transfer in the unwetted region was newly formulated taking into account thermal nonequilibrium between the water and steam phases. Wall temperature excursions during pressure and enthalpy transients are interpreted with the help of the boiling curve and the Leidenfrost phenomenon. A method is developed by means of which it is possible to determine the influence of the pipe orientation on the location of the boiling crisis as well as on the heat transfer in the unwetted region. The influence of the wetting state of the heated surface on the two phase flow pressure loss is interpreted as "Wall effect" and is calculated using a simplified computer model.

TABLE OF CONTENTS


| | | Page |
|---|---|---|
| ABSTRACT | | iii |
| 1. | INTRODUCTION AND OBJECTIVE | 1 |
| 2. | TEST EQUIPMENT AND PROGRAM | 2 |
| 2.1 | Experimental Loop | 2 |
| 2.2 | Instrumentation of the Objects of Measurements | 2 |
| 2.3 | Processing of the Measured Data | 7 |
| 2.4 | Test Program | 7 |
| 3. | STEADY FLOW IN A VERTICAL UPFLOW TUBE | 8 |
| 3.1 | Flow Patterns and Heat Transfer Regions | 8 |
| 3.2 | Critical Boiling States | 10 |
| 3.2.1 | Forms of Boiling Crisis in an Evaporator Tube | 10 |
| 3.2.2 | Process for the Determination of Critical Boiling States in the Entire Steam Quality Range | 11 |
| 3.2.3 | Model Verification | 13 |
| 3.3 | Heat Transfer in the Post-Dryout Region | 18 |
| 3.3.1 | The Heat Transfer Mechanism | 18 |
| 3.3.2 | Method of Calculation from the Literature | 20 |
| 3.3.3 | Development of a Calculation Model for the Heat Transfer in the Post-Dryout Region | 23 |
| 3.3.3.1 | The Heat Transfer in a Developed Thermal Non-Equilibrium | 23 |
| 3.3.3.2 | The Heat Transfer at the Region Boundaries | 27 |
| 3.3.3.3 | Model Verification | 31 |
| 4. | PRESSURE AND ENTHALPY TRANSIENTS | 42 |
| 4.1 | Transient Behavior of an Evaporator Tube | 42 |
| 4.2 | Interpretation of the Transient Processes with Help of the Boiling Curve | 48 |
| 4.3 | Influence of the Leidenfrost Temperature | 53 |
| 4.4 | Mathematical Model for the Determination of the Influence of Pressure and Enthalpy Transients on the Heat Transfer | 57 |
| 5. | INFLUENCE OF THE TUBE ORIENTATION ON THE HEAT TRANSFER | 63 |
| 5.1 | Flow Patterns and Heat Transfer Regions | 63 |
| 5.2 | Heat Transfer in the Wetted Region | 65 |
| 5.3 | Critical Boiling States | 67 |
| 5.4 | Heat Transfer in the Post-Dryout Region | 78 |

TABLE OF CONTENTS (Continued)


| | Page |
|---|---|
| 6. PRESSURE DROP | 88 |
| 6.1 Pressure Drop Components in an Evaporator Tube | 88 |
| 6.2 Friction Pressure Loss in the Wetted and Unwetted Regions | 89 |
| 6.2.1 Experimental Observations and Their Interpretation | 89 |
| 6.2.2 Comparison of Various Pressure Loss Correlations | 91 |
| 6.2.3 Influence of the Heating and Entrance Effects | 98 |
| 6.3 Recommendations for the Determination of the Friction Pressure Loss of a Two-Phase Flow | 106 |
| 7. SUMMARY | 114 |
| NOMENCLATURE | 116 |
| BIBLIOGRAPHY | 119 |

# 1 INTRODUCTION AND OBJECTIVE

In many technical apparatuses a fluid evaporates through the supply of heat. If the evaporation takes place in a fluid carrying pipe and if the fluid is completely converted into steam, the heated surface lies partially in the wetted and partially in the unwetted regions. A typical example of this are the evaporator tubes of a fossil-fired steam generator. The wetted region is characterized by high heat transfer coefficients while in the unwetted region (post-dryout region) the heat transfer is usually greatly reduced. The boiling crisis constitutes the boundary between both regions.

In view of the design of the evaporator heating surfaces of fossil-fired steam generators the heat transfer in the unwetted region is of prime interest, since the herein occurring material temperatures influence the service life of the evaporator tubes. The heat transfer in the unwetted region depends greatly on the thermal non-equilibrium between the steam flow and the water droplets. Therefore, this effect has to be included in these studies.

Also the location of the boiling crisis influences the maximum heating surface temperatures in the unwetted region. Should the boiling crisis occur already at low steam qualities, the steam velocity and, thus, the cooling through steam convection is still low and as a result the heating surface temperatures are higher than those that occur at high steam qualities. The pressure and enthalpy transients that occur near the critical pressure can displace the location of the boiling crisis to lower steam qualities, thus leading to a considerable increase of the heating surface temperatures in the unwetted region.

The orientation of the tube influences the distribution of the phases over the flow cross-section and thus also the occurrence of critical boiling states as well as the heat transfer in the unwetted region. Since the influence of the orientation of the tube on the heat transfer depends on many parameters (e.g., pressure, mass flow density, tube diameter) extensive investigations have to be conducted in this respect.

For the flow-related design of evaporator tubes it is of interest to which extent the pressure loss of the two-phase flow is influenced by the occurrence of the boiling crisis. Since heat transfer calculations are frequently based on the pressure loss, by comparison between calculation and measurement it can be determined if heat transfer models are based on the actually occurring pressure losses. The formulation of the heat transfer in the unwetted region can be verified in this manner.

It is the aim of this study to investigate the influence of the wetting state of a heated surface on the heat transfer and the pressure loss in an evaporator tube. An essential part of this task is the determination and analysis of the relevant quantities which determine the wetting state of a heated surface.

## 2 TEST EQUIPMENT AND PROGRAM

### 2.1 Experimental Loop

A high-pressure loop (Figures 2-1 and 2-2) was available for the tests. Due to the wide operating range of the test rig it was possible to simulate the conditions existing in fossil-fired evaporators under full and partial load.

| | |
|---|---|
| Pressure | up to 330 bar |
| Flow rate | up to 15 $m^3/h$ |
| Heating capacity | up to 1000 kW |
| Tube Length | up to 6.1 m |

The installation was operated in once-through mode with low flow rates (up to 2 $m^3/h$. The demineralized and degassed water was therein carried with a piston pump through the preheater and the test tube, and wholly or partially evaporated in the process. It was condensed and subcooled in the spray condenser and finally carried to the drain via a pressure-reducing valve. The piston pump was equipped with six pistons and a surge tank on the outlet side. Thus, it was possible to limit the flow rate oscillations to a value of less than 0.5%.

In the case of high flow rates, the tests were conducted in recirculation operation by means of a centrifugal pump.

The test tubes were horizontally and vertically installed. The heating was by direct current, both axially and circumferentially uniform, whereby the tube wall served as dissipative resistance.

A detailed description of the experimental installation is contained in /1/.*

### 2.2 Instrumentation of the Objects of Measurements

The measurements of heat transfer and pressure loss were conducted on three measuring sections with tube dimensions of 17.15 x 2.31 mm, 18 x 2 mm and 33.4 x 4.55 mm. The instrumentation of the measuring sections are shown in Figures 2-3 and 2-4. The temperature measuring points were installed along an upper, a lateral and a lower surface line on the outside of the tubes. Only thermocouples of one surface line were connected to the data logger in the case of experiments with a vertical measuring section. Thermocouples with insulated measuring points had to be used because of the direct heating of the tubes. For the analysis, the measured outside-wall temperatures were converted to the tube inside-wall values.

A mixing chamber was installed at the outlet of the test section. It had the task to evaporate water droplets which could still exist in the superheated fluid. Thus, energy balances can be performed, containing the preheater and test section. Fluid thermocouples were installed at the inlet, and outlet, of the test section as well as downstream of the mixing chamber. The determination of the static pressure was made after a steadying stage at the pipe inlet and downstream of the mixing chamber.

---

*Editor's note: Reference citations in this report are designated by slashes bounding the number listed in the Bibliography.

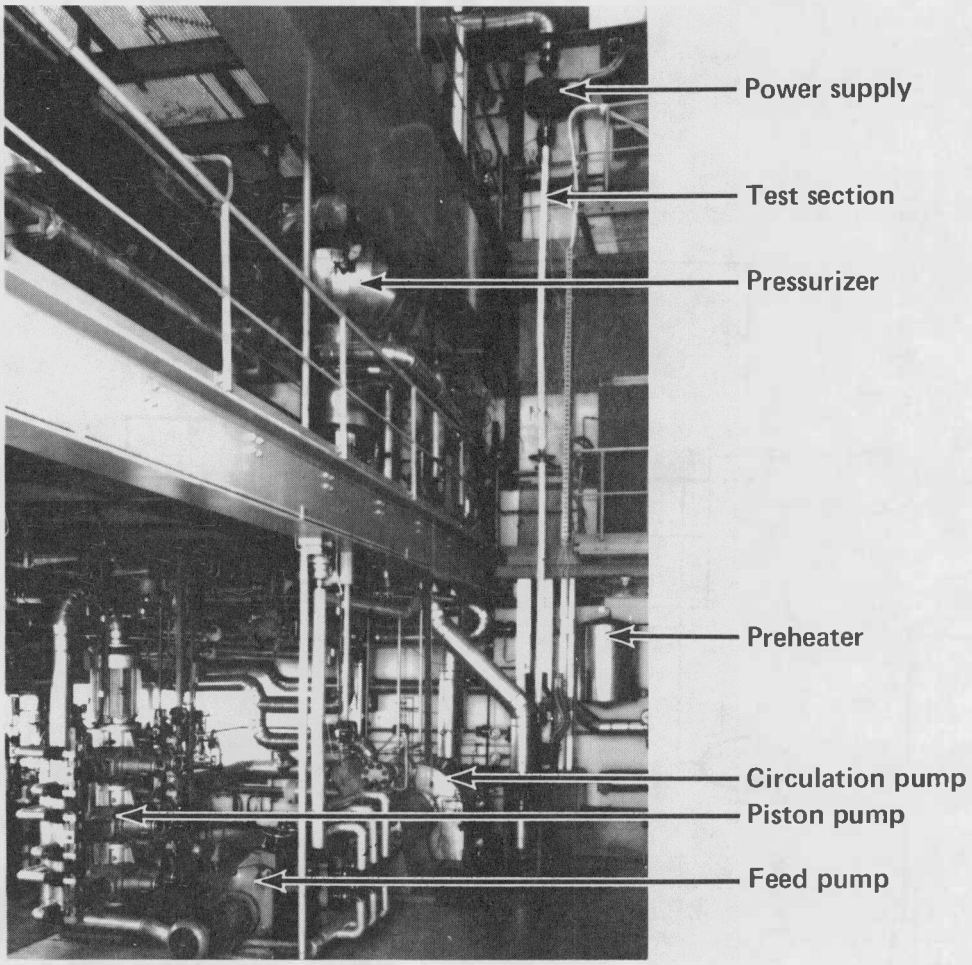


Figure 2-1 The BENSON test rig

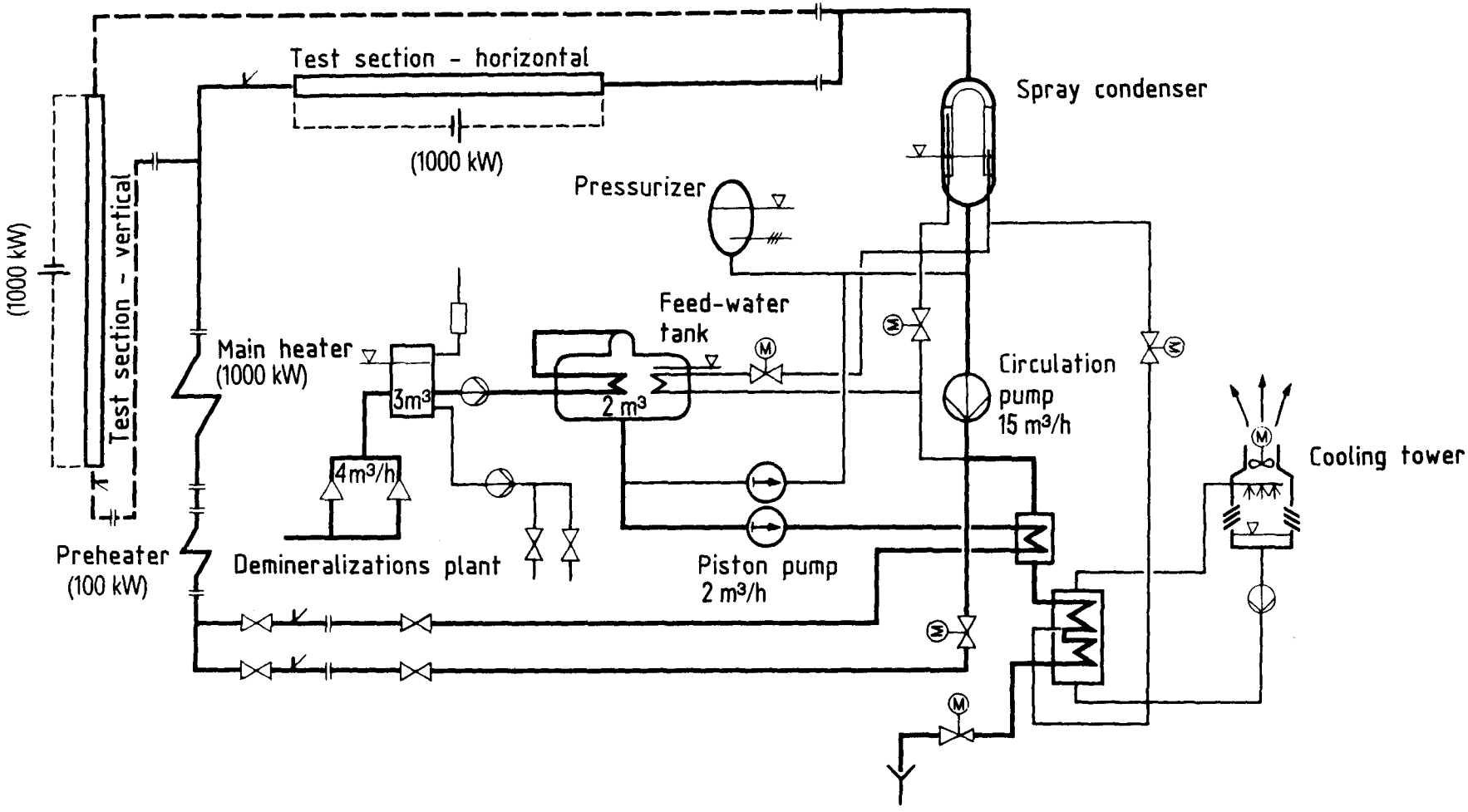


Figure 2-2 The BENSON test rig (circuit diagram)

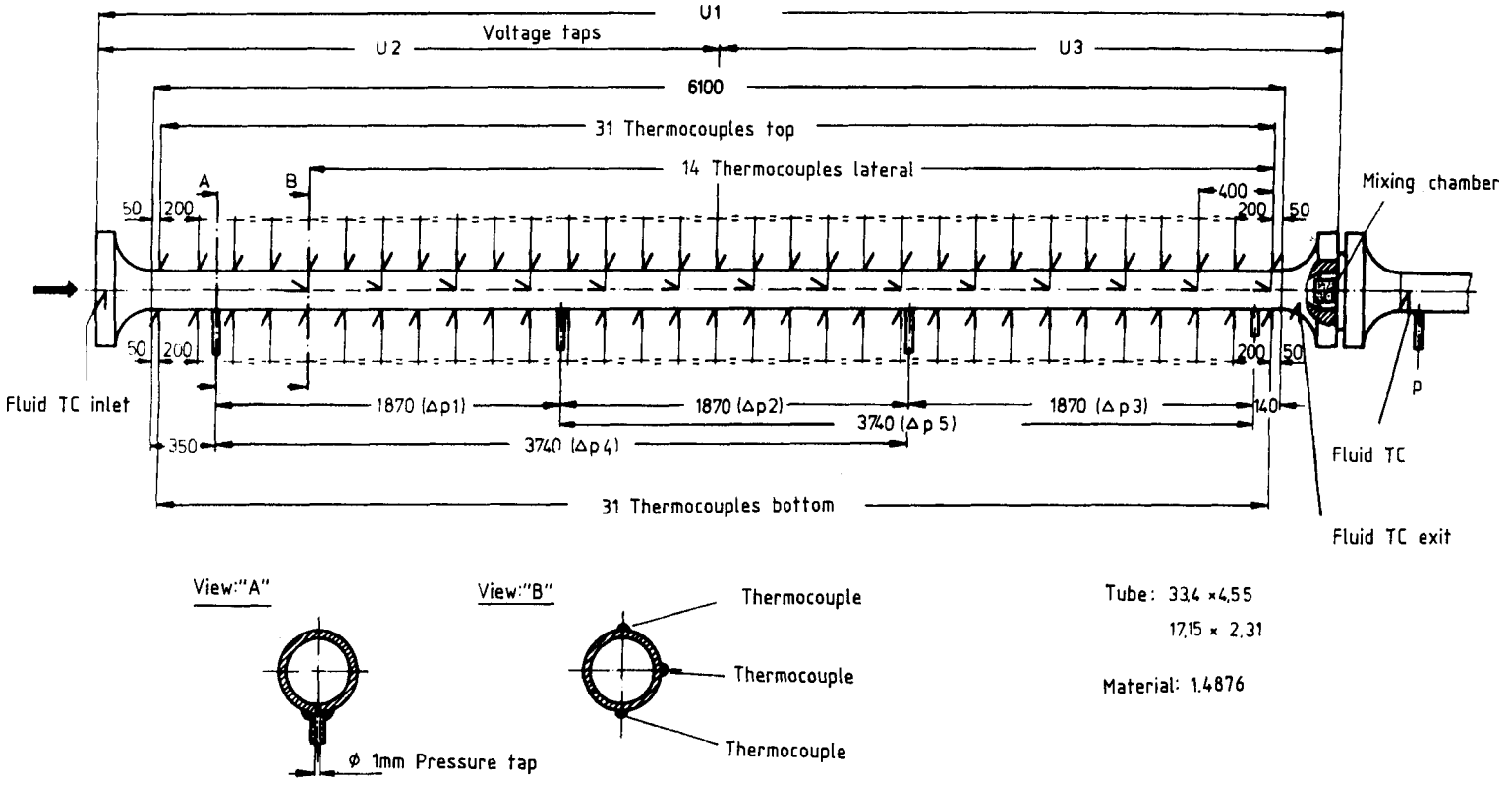


Figure 2-3 Instrumentation of the test tubes with inside diameters of 12.5 and 24.3 mm

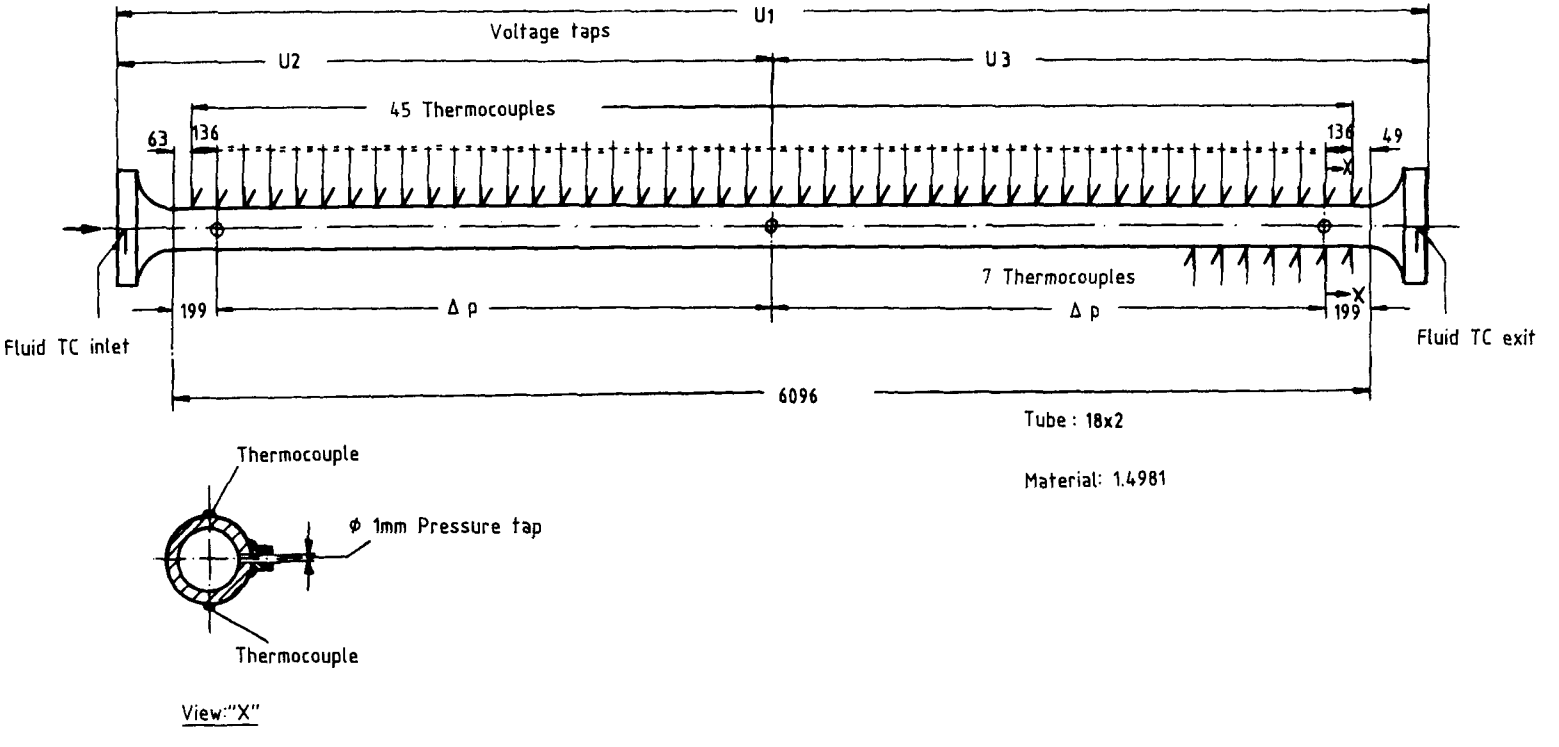


Figure 2-4 Instrumentation of the test tube with an inside diameter of 14 mm

Furthermore, the pressure loss was measured over 3 tube sections.

The supplied power - and therefrom the heat flux - was determined by a voltage and current measurement. For this purpose, total voltage and partial voltage taps were installed within the test tube.

## 2.3 Processing of the Measured Data

A digital data logger with 64, and 96, channels was used for the recording of the measured data. Software was available which scanned all measuring stations once a second and recorded them on a magnetic tape. In order to eliminate temporary oscillations, the measured valued of one test point were recorded for approximately 150 seconds.

The stored data were further processed using both the data logger as well as the KWU main frame computer.

## 2.4 Test Program

The test program comprises the determination of the critical boiling conditions, of the heat transfer in the post-dryout region and of the pressure loss in the two-phase region. Furthermore, the influence of the pipe orientation on heat transfer and pressure loss was also studies. Finally, the influence of pressure- and enthalpy drops on the heat transfer in the post-dryout region was determined.

The parameter range of the experimental investigations overlaps the operating range of fossil-fired steam generators under partial- and full load operations. The main influence parameters were varied as follows:

| | | | |
|---|---|---|---|
| System pressure | 50 | to 250 | bar |
| Mass velocity | 300 | to 2500 | $kg/m^2s$ |
| Heat flux | up | to 600 | $kW/m^2$ |

Mass velocities of 1000 and 2000 $kg/m^2s$ were used for the investigations on the influence of pressure- and enthalpy drops on the heat transfer in the post-dryout region.

# 3 STEADY FLOW IN A VERTICAL UPFLOW TUBE

## 3.1 Flow Patterns and Heat Transfer Regions

The distribution of the steam and water phase over the flow cross-section is symmetrical in a vertical upflow evaporator tube. Figure 3-1 shows the possible flow patterns in a vertical evaporator tube, whereby with increasing steam quality all shown flow configurations are not always transversed. With the help of flow pattern charts /2,3,4/ it is possible to determine the flow pattern which occurs at a given parameter combination. However, not too high expectations should be placed in the accuracy of these charts.

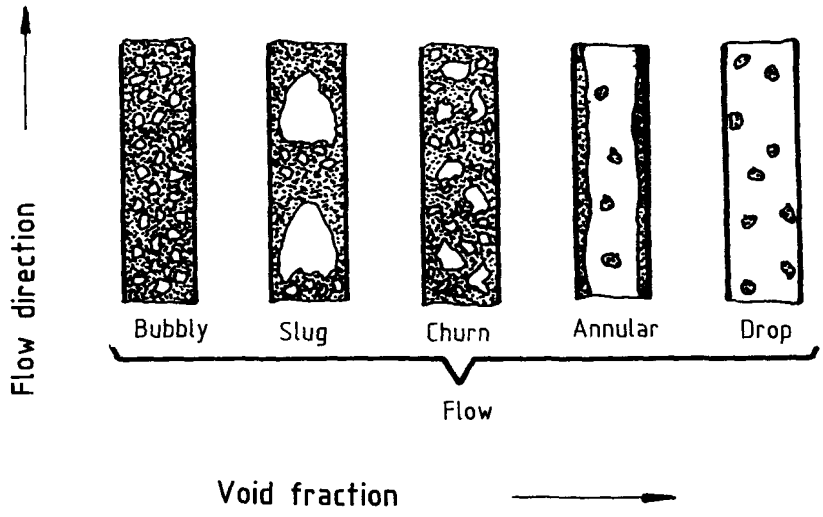


Figure 3-1 Flow patterns in a vertical upflow tube

Figure 3-2 shows the typical flow patterns and heat transfer regions in a vertical upflow evaporator tube:

The fluid is subcooled at the tube inlet. Single-phase flow with convective heat transfer takes place. If the wall temperature slightly exceeds the saturation temperature of the fluid subcooled boiling sets in at the wall. Most of the steam bubbles condense within the fluid. The wall temperature remains almost constant with increasing enthalpy.

Once the mean fluid temperature reaches the saturation temperature, the steam quality increases corresponding to the further enthalpy increase. The very good heat transfer remains almost constant.

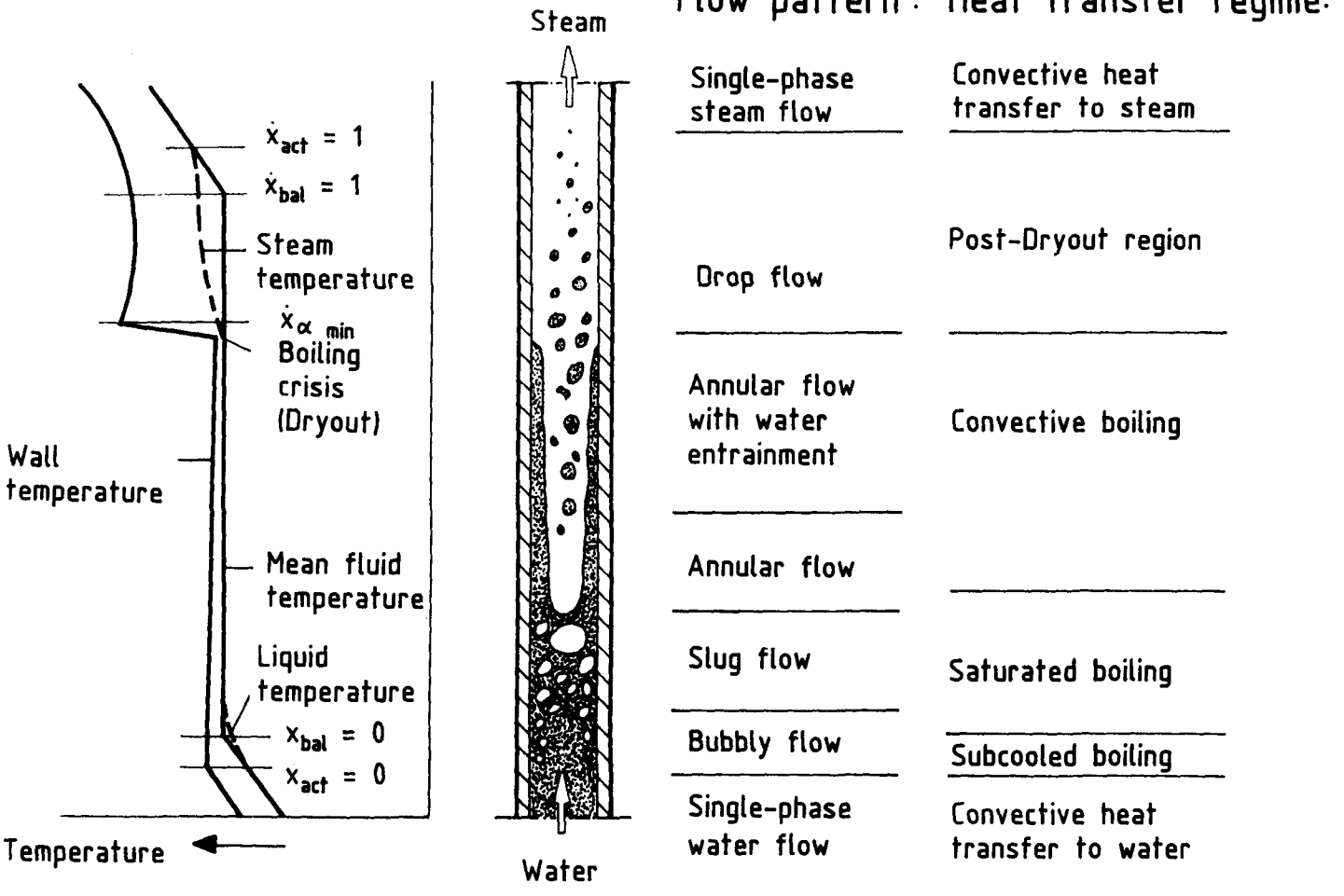


Figure 3-2 Flow patterns and heat transfer regions in a vertical evaporator tube

Annular flow sets in once a certain steam quality, which depends on the chosen parameters, is reached. Therein, the fluid flows partially as film along the wall and partially in the form of droplets in the flow core.

With high flow velocities the heat transfer improves somewhat compared with the conditions under nucleate boiling.

With a further enthalpy increase a state is reached (critical boiling state) at which the wetting of the heating surface can no longer be maintained. A boiling crisis sets in because the fluid loses its contact with the wall. The boiling crisis in a steam generator is usually caused by dryout of the heating surface. Therein, the heat transfer is reduced most of the times and the wall temperature increases correspondingly in the next region (post-dryout region). If all fluid droplets are evaporated, the region with a single-phase convective steam flow follows.

From Figure 3-2 it can be gathered that, at the beginning and at the end of the evaporation zone, the water and steam phases are not in thermal equilibrium. While voids at saturation temperature exist in subcooled fluid during subcooled boiling, in the post-dryout region there are water droplets at saturation temperature present in a superheated steam flow.

## 3.2 Critical Boiling States

### 3.2.1 Forms of Boiling Crisis in an Evaporator Tube

The location at which the boiling crisis occurs separates the wetted and the unwetted regions in an evaporator tube.

The occurrence of the boiling crisis is essentially determined by the parameters for heat flux density, mass flow density, steam mass quality, pressure, and hydraulic diameter. In connection with the occurrence of the boiling crisis there is of interest either the steam quality (critical steam quality) or the heat flux (critical heat flux), at which critical boiling states occur. IN the case of upward flow in vertical tubes, according to /5/, the critical heat flux can be represented as function of the critical steam quality by three characteristic curve segments (Figure 3-3):

Zone 1:

The void fraction in the flow is low, i.e., water is the continuous phase. At the location of the boiling crisis is formed a steam film on the tube wall, which separates the water from the heating surface (film boiling). In the literature this process is also called boiling crisis of the first kind, respectively "Departure from Nucleate Boiling (DNB)." The extent of the critical heat flux depends on the steam quality of the flow. An increase of the heat flux of the flow displaces the onset of the film boiling to lower steam qualities.

Zone 2:

Steam becomes the continuous phase with increasing steam quality in the flow. At the location of the boiling crisis the still existing water film breaks off from the tube wall, or it dries out. In the literature this process is also called boiling crisis of the second kind, or "dryout." Here the critical heat flux decreases considerably with increasing steam quality.

Zone 3:

With a further decrease of the heat flux a movement of the location of the boiling crisis moves towards higher steam qualities is observed. Obviously, water droplets can thereby increasingly deposit on the tube wall, a reason why this process is called "Deposition Controlled Burnout." As well as in Zone 2, the occurrence of the boiling crisis is herein connected with a dryout of the heating surface.

The processes which lead to critical boiling states in the individual steam quality zones are, to a great extent, still beyond the possibility of an analytical calculation, so that practical equations for a rather extensive range of parameters are of empirical nature.

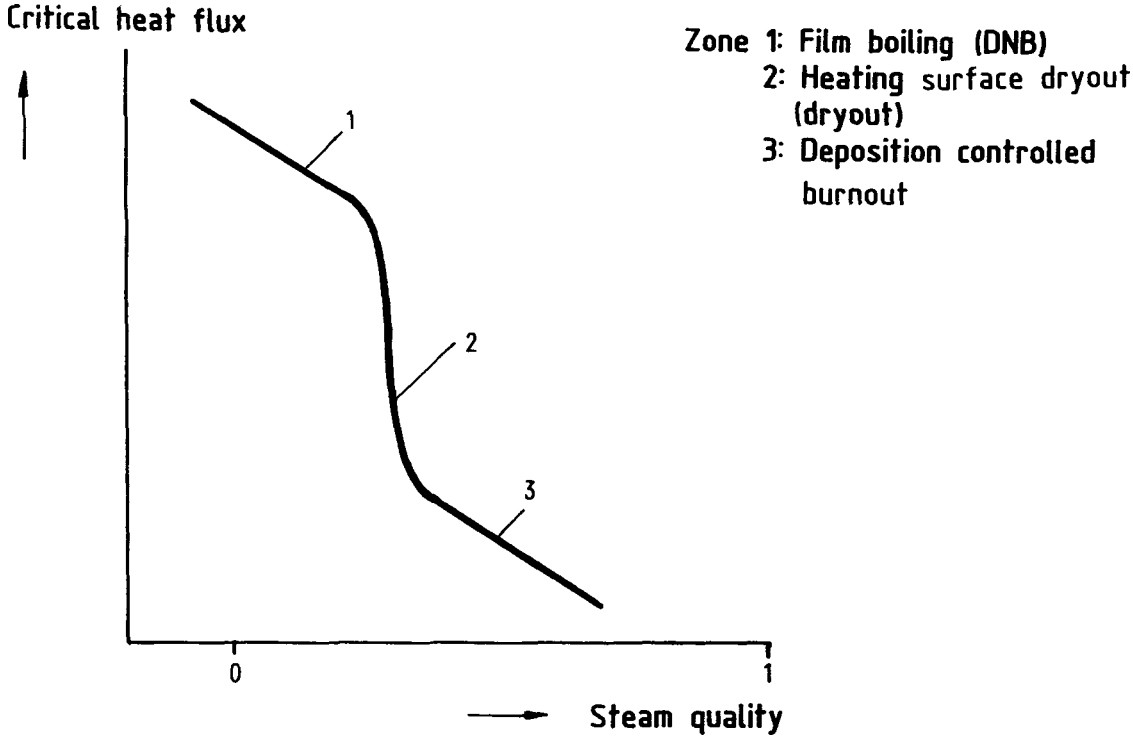


Figure 3-3 Typical path of the critical heat flux

3.2.2 Process for the Determination of Critical Boiling States in the Entire Steam Quality Range

The hitherto existing equations for the determination of the critical heat flux always determine only portions of the critical boiling states. Of a process for the determination of the critical heat flux in the entire steam quality range it is required however, that the equations chosen for all allowable parameter combinations lead to a constant path along the limits of validity. This aim was attained with the following method:

If one starts from Figure 3-3, which shows the critical heat flux as a function of the local steam quality, one can see that with increasing steam quality the

critical heat flux in the film boiling region decreases less than in the dryout region. If for each region there is chosen a suitable equation, the intersection of the two curves, determined with the two equations, represents the limit between the two mechanisms of the boiling crisis. Mathematically, the choice of region can be made by a comparison of the critical heat fluxes calculated according to the two equations for a determined steam quality, in considering as valid the lower value.

For the film boiling region (Zone 1 in Figure 3-3) there were chosen the tabular values of V.E. DOROSHCHUK /6,7/. According to KEMNER /8/, these values proved to be superior to other correlations in the case of high heat fluxes, as they occur in nuclear fuel assembles. However, due to the easier use - even with a slight loss of accuracy - there was used the empirical equation developed by DOROSHCHUK from the tables:

$$\dot{q}_{Kr} = 10^3 \cdot [10.3 - 17.5(p/p_c) + 8(p/p_c)^2] \cdot (8 \cdot 10^{-3}/d)^{0.5} \cdot e^{-1.5 \cdot \dot{x}} \cdot \quad (3\text{-}1)$$

$$(\dot{m}/1000)^{(0.68(p/p_c)-1.2\,\dot{x}\,-0.3)}$$

It has the following region of validity:

$$29 \leqq p \leqq 196 \text{ bar}$$

$$500 \leqq \dot{m} \leqq 5000 \text{ kg/m}^2\text{s}$$

$$0 \leqq \Delta\vartheta_{\mu} \leqq 75 \text{ K}$$

$$4 \cdot 10^{-3} \leqq d \leqq 16 \cdot 10^{-3} \text{ m}$$

In equation (3-1) $\dot{x}$ is the steam quality. It is defined as the proportion of steam mass flow in the total mass flow.

Based on a study by FECHNER /9/ which covers the parameters of the fossil-fired steam generators, the KON'KOV /10/ equation was used for the region of the dryout of the heating surfaces (Zones 2 and 3 in Figure 3-3):

| | Pressure region p(bars) |
|---|---|
| $\dot{q}_{Kr} = 1.8447 \cdot 10^8 \dot{x}^{-8} \dot{m}^{-2.664} (d \cdot 1000)^{-0.56} e^{0.1372} \cdot p$ | 4.9 - 29.4 |
| $\dot{q}_{Kr} = 2.0048 \cdot 10^{10} \dot{x}^{-8} \dot{m}^{-2.664} (d \cdot 1000)^{-0.56} e^{-0.0204} \cdot p$ | 29.4 - 98 (3-2) |
| $\dot{q}_{Kr} = 1.1853 \cdot 10^{12} \dot{x}^{-8} \dot{m}^{-2.664} (d \cdot 1000)^{-0.56} e^{-0.00636} \cdot p$ | 98 - 196 |

It has the following region of validity:

$$\dot{q} < 1200 \text{ kW/m}^2$$

$$200 \leqq \dot{m} \leqq 5000 \text{ kg/m}^2\text{s}$$

$$4 \cdot 10^{-3} \leqq d \leqq 32 \cdot 10^{-3} \text{ m}$$

The Figures 3-4 to 3-6 show typical courses of the critical heat flux as function of the steam quality, arrived at a combining of equations (3-1) and (3-2). From these figures it can be gathered that the KON'KOV equation also covers the "Deposition Controlled Burnout" region due to its form of construction.

Since the KON'KOV equation is used with the DOROSHCHUK equation up to the intersection, in respect to the heat flux there occurs in part an exceeding of the validity region given by KON'KOV. This procedure is necessary, however, in order to prevent "gaps" in the desired parameter region.

3.2.3 Model Verification

The determination of the critical heat flux according to the chosen procedure was checked by means of 3044 test points (/5/ and /11 to 22/). Of these, 1663 test points were assigned to the film boiling, which was calculated by equation (3-1) with a mean value of 0.99 and a standard deviation of 0.16. The mean value was formed therein by the quotient of calculated and measured critical heat flux:

$$M = \frac{1}{n} \Sigma \frac{\dot{q}_{Kr_R}}{\dot{q}_{Kr_M}} \tag{3-3}$$

The standard deviation refers also to the quotient of calculated and measured critical heat flux.

For the remaining 1381 test points, in view of the choice of region described in chapter 3.2.2, dryout of the heating surface was assumed, which was calculated by equation (3-2) with a mean deviation of -0.04 and a standard deviation of 0.10. Due to the considerable decrease of the critical heat flux in this region, the comparison was made by means of the measured and calculated critical steam quality, whereby the mean deviation was defined as follows:

$$\overline{\Delta \dot{x}} = \frac{1}{n} \Sigma (\dot{x}_{Kr_R} - \dot{x}_{Kr_M}) \tag{3-4}$$

This error criterion ensures a constant weighted deviation in the entire steam quality region. Herein, the standard deviation refers to the difference of calculated and measured critical steam quality. Table 3.1 shows a list of the test parameters of the various authors as well as of the accuracy of equations (3-1) and (3-2). From the test calculation it can also be gathered that equation (3-1) can be applied beyond the given region of validity for the tube bore of 16 mm. Up to a tube bore of 24 mm there was not observed a vitiated result accuracy. The equation (3-2) can also be used beyond the given region of validity for the heat flux.

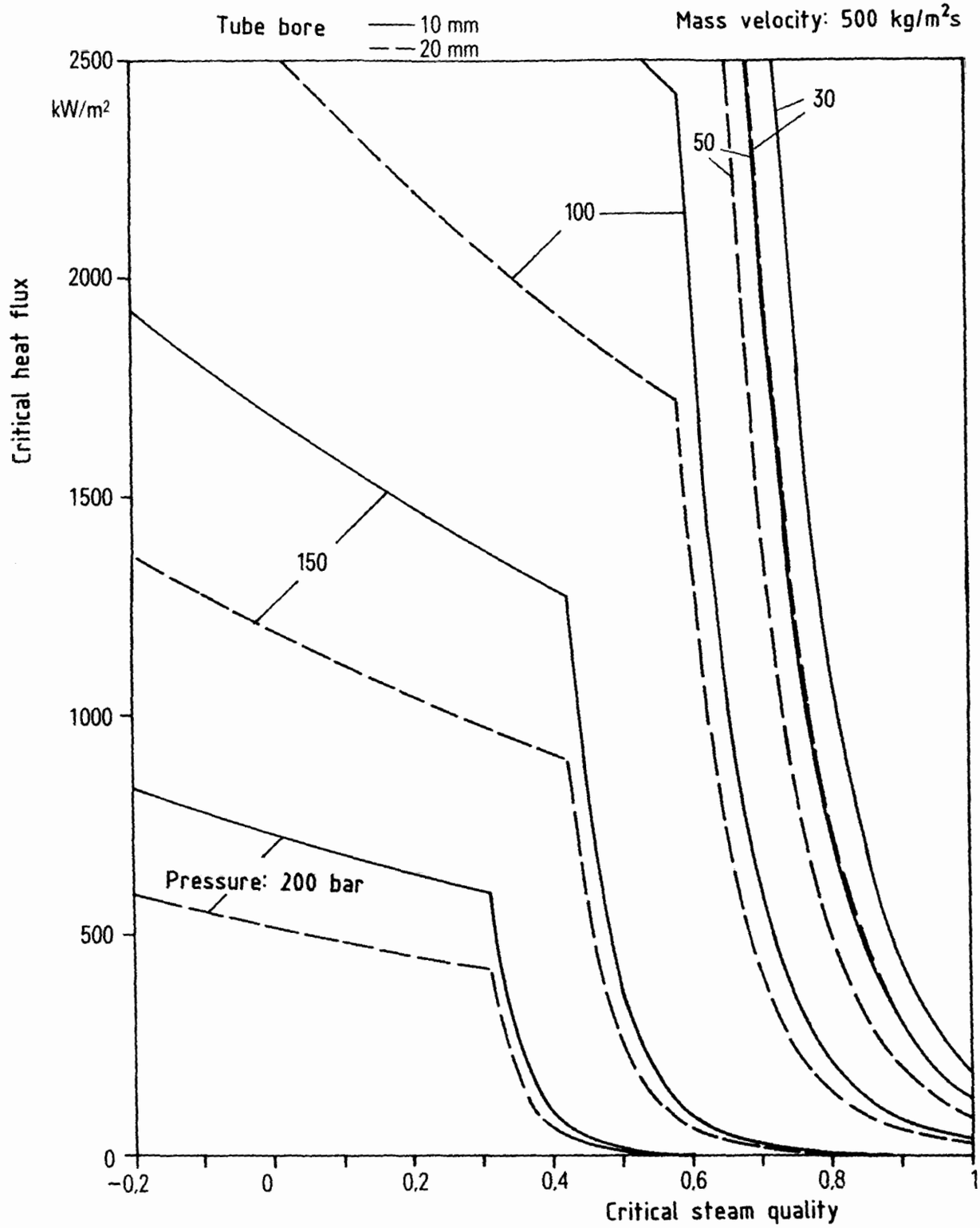


Figure 3-4 Critical heat flux as a function of the critical steam quality

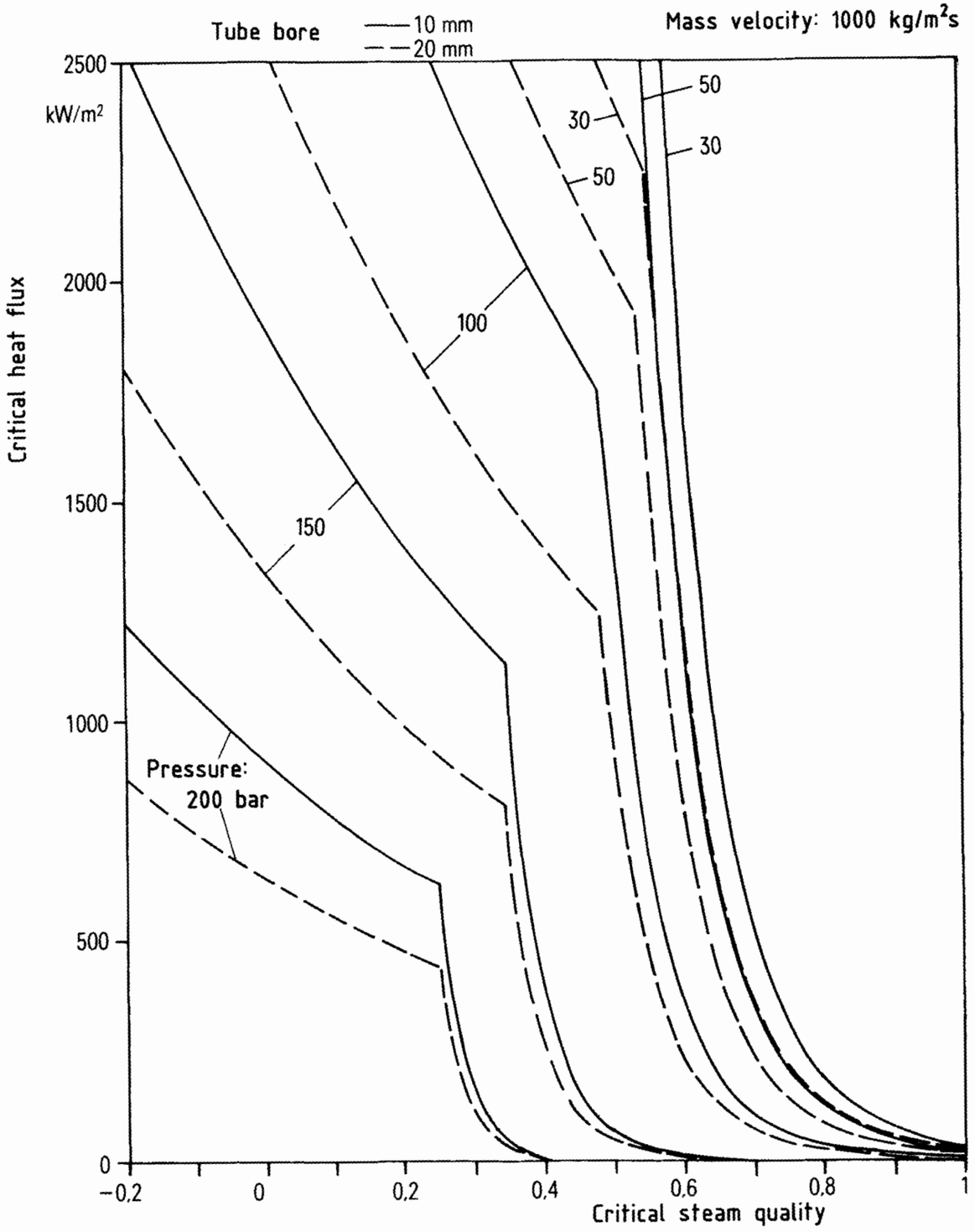


Figure 3-5 Critical heat flux as function of the critical steam quality

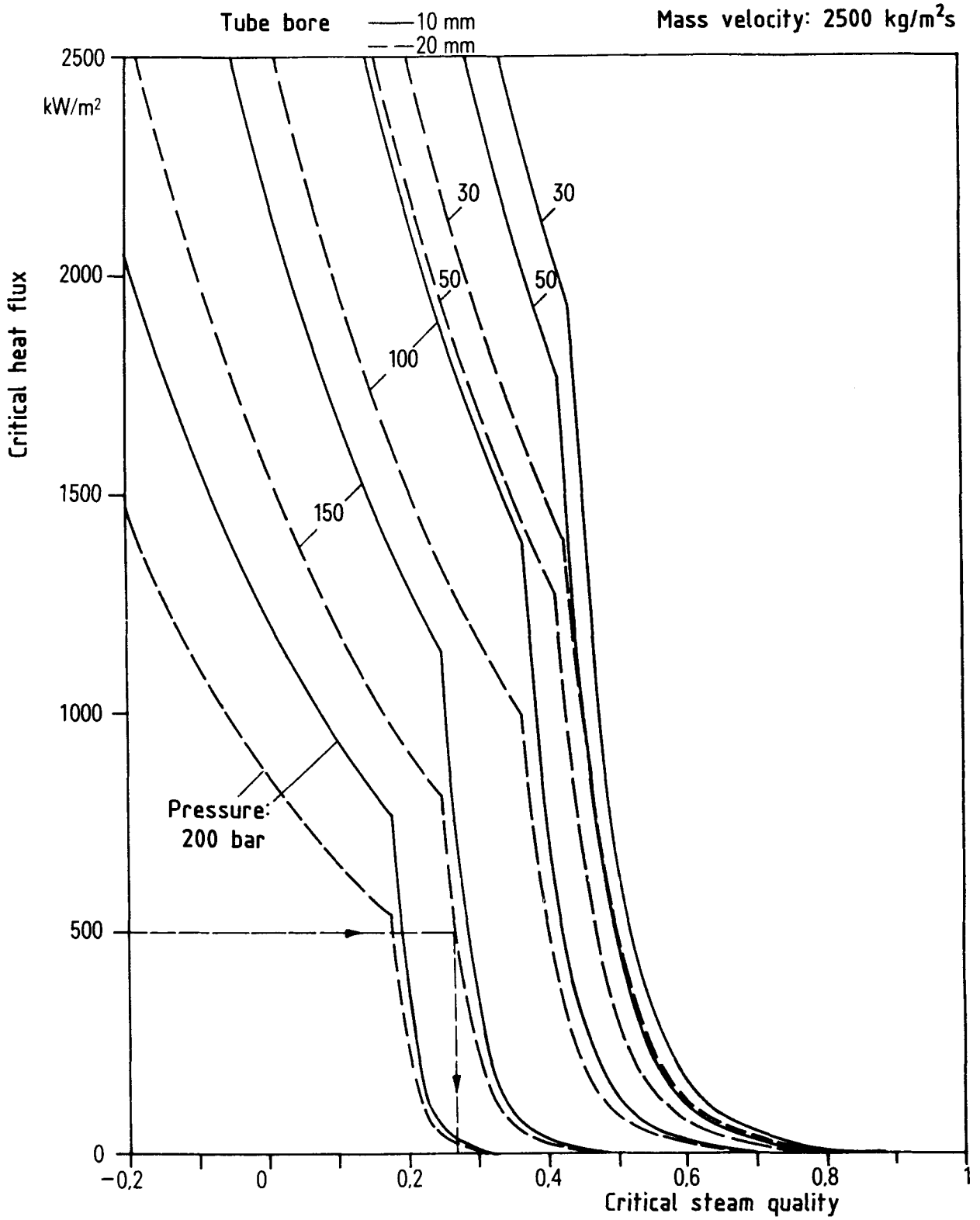


Figure 3-6 Critical heat flux as function of the critical steam quality

Table 3.1 Result accuracies of equations (3-1) and (3-2)

| Author | Calc. acc. to eq. (3-1) | | | Calc. acc. to eq. (3-2) | | | Test parameter | | | |
|---|---|---|---|---|---|---|---|---|---|---|
| | Number | Mean Value | Standard deviation | Number | Mean deviation | Standard deviation | Pressure (bar) | Mass velocity ($kg/m^2s$) | Tube bore (mm) | Heat flux ($W/m^2 10^{-4}$) |
| 11 | 263 | 1.03 | 0.14 | 27 | 0.07 | 0.08 | 38 - 138 | 528 - 4855 | 4.6 - 23.6 | 59 - 621 |
| 12 | 75 | 1.03 | 0.11 | 13 | 0.01 | 0.07 | 30 - 90 | 501 - 4410 | 5.6 - 25.0 | 150 - 545 |
| 13 | 89 | 0.93 | 0.08 | 4 | 0.02 | 0.13 | 77 - 137 | 552 - 2805 | 10.0 | 30 - 548 |
| 14 | 965 | 0.99 | 0.16 | 354 | 0.05 | 0.14 | 29 - 138 | 500 - 4977 | 4.6 - 23.6 | 59 - 997 |
| 15 | 136 | 1.05 | 0.13 | 195 | 0.05 | 0.07 | 29 - 92 | 517 - 4795 | 10.0 | 93 - 344 |
| 5 | - | - | - | 162 | 0.07 | 0.05 | 67 - 73 | 506 - 2036 | 13.0 | 28 - 87 |
| 16 | - | - | - | 21 | 0.08 | 0.06 | 40 - 71 | 664 - 1383 | 15.0 | 71 - 113 |
| 17 | - | - | - | 83 | 0.09 | 0.07 | 160 - 180 | 650 - 2700 | 12.8 | 15 - 80 |
| 18 | 42 | 0.99 | 0.24 | 61 | 0.05 | 0.08 | 49 - 176 | 600 - 4800 | 10.4 | 70 - 186 |
| 19 | 4 | 1.11 | 0.14 | 55 | 0.03 | 0.05 | 50 - 150 | 501 - 2293 | 24.7 | 30 - 126 |
| 20 | - | - | - | 43 | 0.02 | 0.13 | 49 - 174 | 510 - 2539 | 14.0 | 9 - 61 |
| 21 | - | - | - | 61 | 0.06 | 0.05 | 68 - 70 | 994 - 2013 | 10.0 | 20 - 81 |
| 22 | 90 | 0.91 | 0.21 | 302 | 0.02 | 0.07 | 39 - 195 | 501 - 4828 | 5.1 - 24.7 | 23 - 250 |

By way of example, in Figure 3-7 there are compared for each of the authors the measured critical heat flux and the one calculated with the aid of equation (3-1) as well as the measured critical steam quality and the one calculated with the aid of equation (3-2).

Due to the high result accuracy it is possible to apply the chosen procedure for the determination of the critical boiling states in a large pressure-, mass velocity and diameter range. In the evaluation of the occurring errors it has to be considered that even reproducibility tests /21/ may have an average deviation of approximately 6%.

## 3.3 Heat Transfer in the Post-Dryout Region

### 3.3.1 The Heat Transfer Mechanism

According to ILOEJE /23/, the following mechanisms are possible after reaching the boiling crisis:

1. Convective heat transfer from the heating surface to the steam, which thus becomes superheated.

2. Heat transfer from the heating surface to the water droplets, whereby a difference is made between the direct form of heat transfer, by wetting of the droplets on the wall, and the indirect form, by heat absorption in the superheated boundary layer.

3. Heat transfer by radiation from the heating surface to steam and droplets.

It is only in the case of very high wall temperatures that the radiation contributes considerably to the heat transfer. According to ILOEJE /23/, also the heat transfer between heating surface and fluid decreases very much with an increasing difference between heat surface and saturation temperatures, so that, according to MAYINGER /24/, this fraction has to be considered only during transient boiling.

Thus, points 2 and 3 can be neglected for the parameter range of the fossil-fired steam generators compared with point 1. Essentially, heat transfer takes place in two stages:

First, the heat from the heating surface is transferred to the steam by convective heat transfer. Thereby, the steam is superheated and is no longer in thermal equilibrium with the entrained water droplets. In a second phase, the heat is transported by the superheated steam to the water droplets. The higher the temperature difference between steam and water droplets, the more heat is transferred from the steam to the droplets, which evaporate thereby.

This two-stages model, developed by BENNET and HEWITT /25/ in 1967, is the basis of many heat transfer models in the post-dryout region.

For the heat transfer between steam and droplets there are two extreme cases:

1. No heat transfer between steam and water droplets, i.e., the water fraction in the flow remains constant starting from the location of the boiling crisis. The supplied heat is exclusively used for the superheating of the

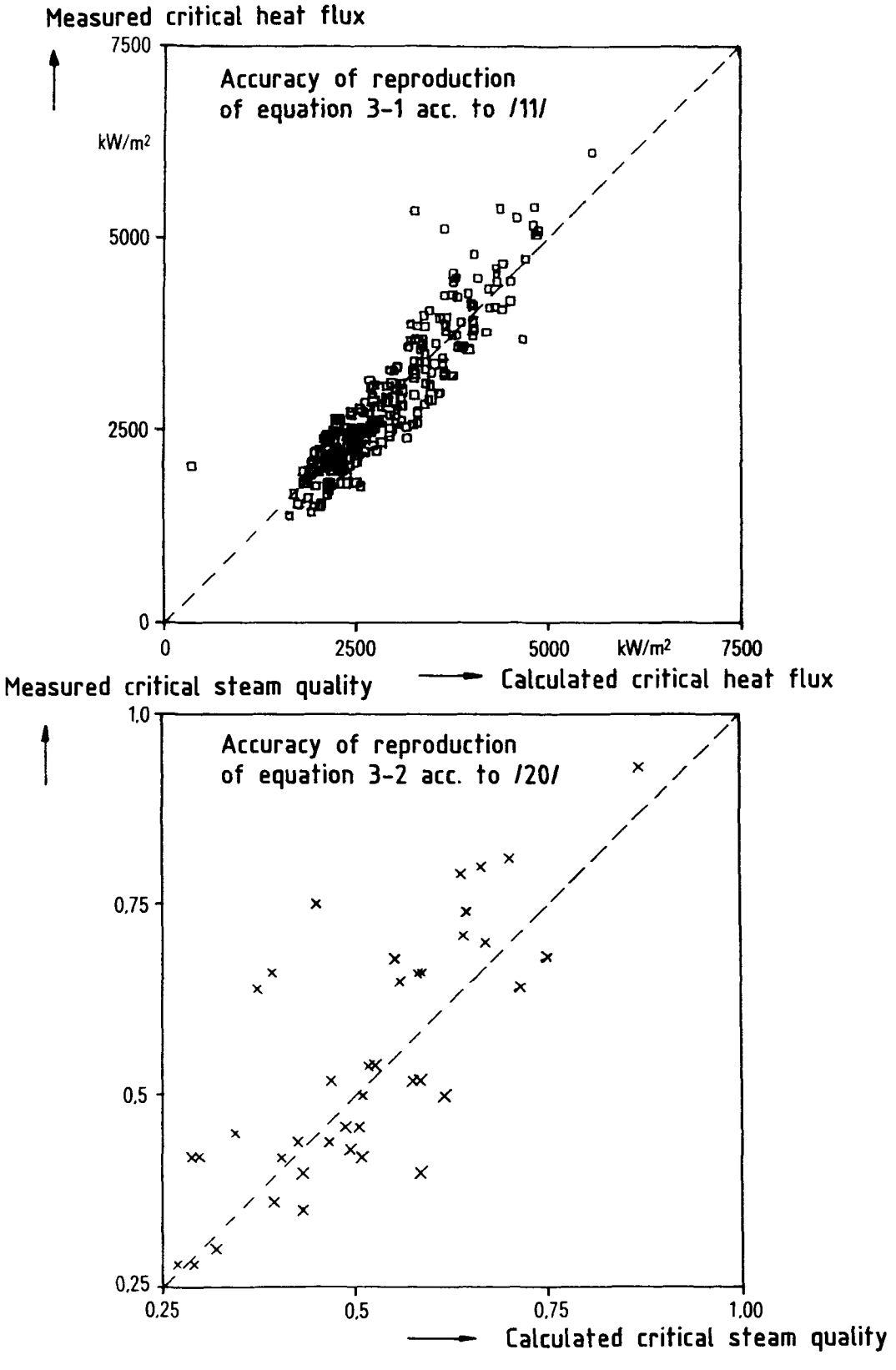


Figure 3-7 Comparison between calculated and measured critical boiling states

steam, whereby the steam temperature and the temperature of the heating surfaces increase continually (cf. Figure 3-8a).

2. An ideal heat transfer takes place between steam and water droplets, i.e., a superheating of the steam does not occur. The supplied heat is exclusively used for the evaporation of the water droplets. The steam quality increases also after the location of the boiling crisis same as before whereby, because of increasing steam velocity, the cooling increases and the temperature of the heating surface drops again (cf. Figure 3-8b).

While case 1 occurs with low pressure and low mass velocity, case 2 is present with high pressure and high mass velocity. From Figure 3-9 the manner can be gathered in which the heat transfer mechanism changes with increasing pressure from case 1 to case 2.

### 3.3.2 Method of Calculation from the Literature

The methods of calculation for the determination of the heat transfer after the dryout of the heating surface, gathered from the literature, can be grouped into two categories:

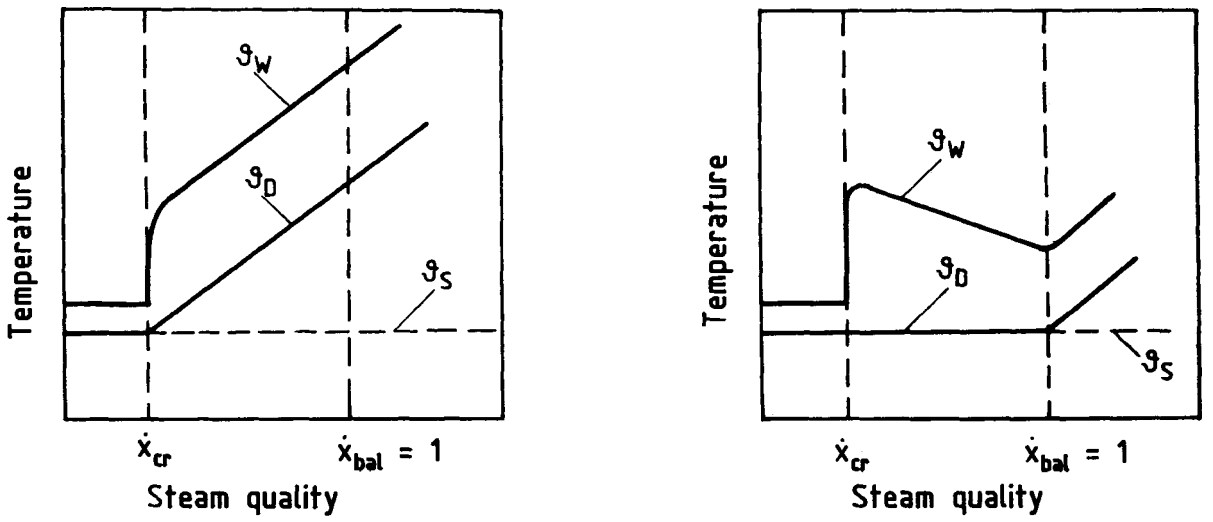


a) Maximum degree of non-equilibrium

b) Complete thermal equilibrium

Figure 3-8 Influence of the thermal non-equilibrium on the course of the steam and heating surface temperatures

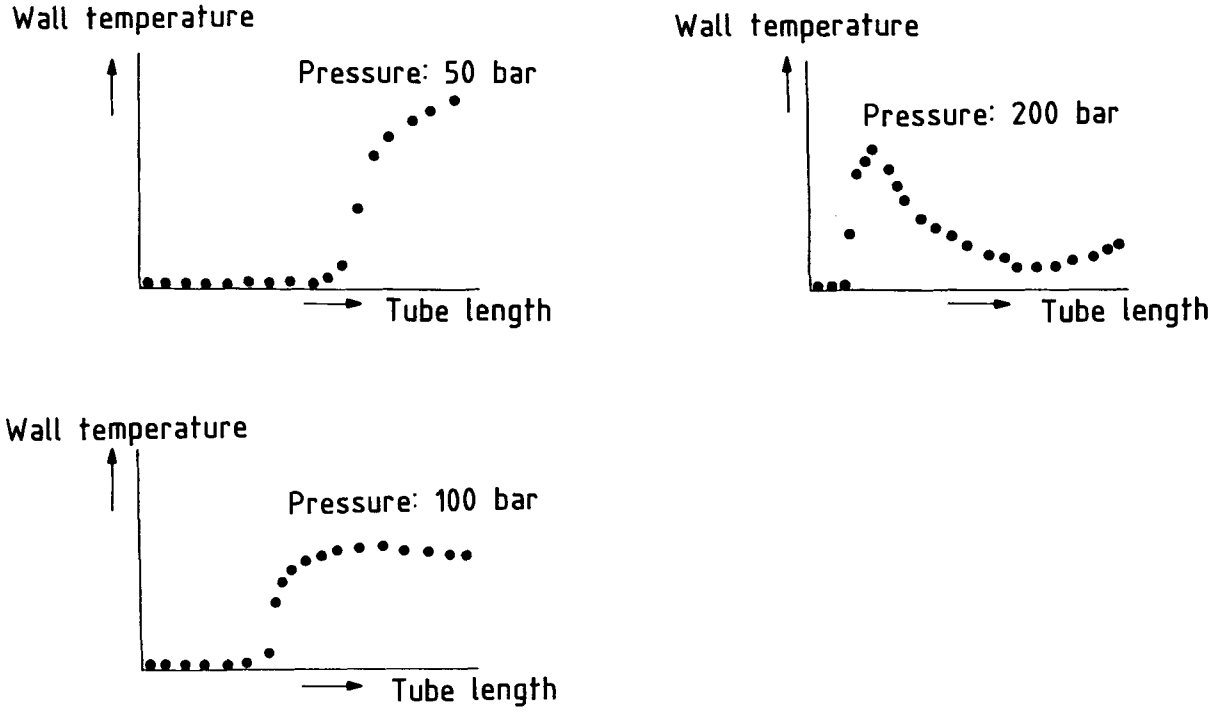


Figure 3-9 Typical wall temperature courses in dependence of pressure

1. Empirical equations

   These are modifications of single-phase heat transfer equations, which take into account the two-phase flow through special definitions of a "two-phase" Reynolds number and steam-quality dependent factors.

2. Models, which consider the thermal non-equilibrium between steam and water droplets.

Although empirical equations are easy to use, they have only a limited accuracy. Figure 3-10 shows a typical comparison between measured values and known empirical equations from the literature. From the figure it can also be gathered that the connection with the single-phase steam flow region ($\dot{x}_{Bil} \rightarrow 1$) is not uniform, since with neglect of the thermal non-equilibrium one would have to reckon with wall temperatures that correspond approximately to the values of the DOUGALL/ROHSENOW equation /26/.

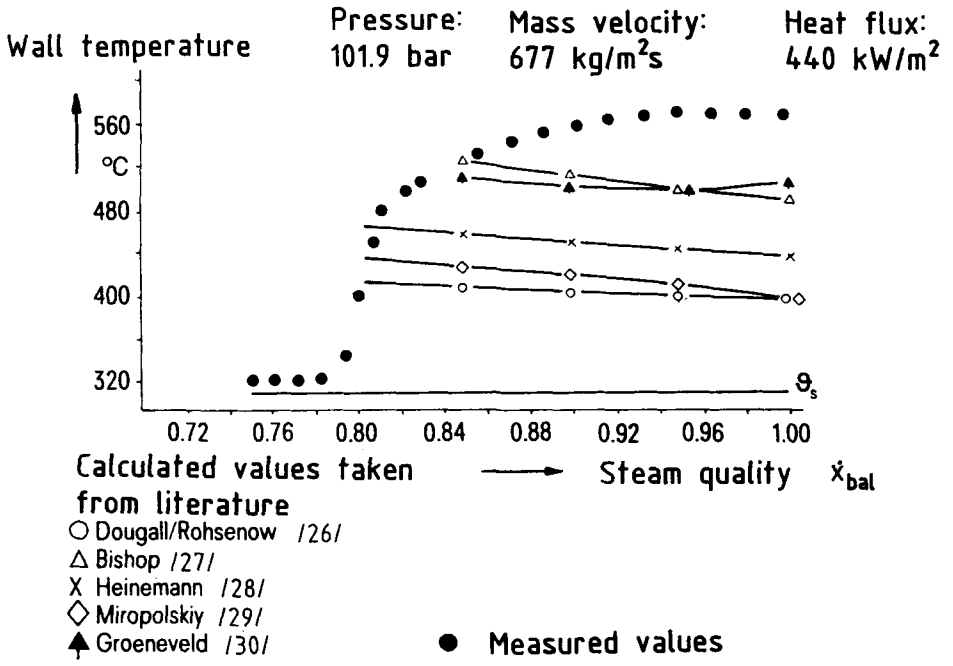


Figure 3-10 Comparison between calculated and measured wall temperatures

Models which take into account the thermal non-equilibrium between the phases allow a greater accuracy in the calculation of the heating surface temperatures. They can also be divided into two main groups:

1. Models which have an empirical statement for the actual steam quality in the flow. The actual steam quality is therein expressed as function of the balance-determined steam quality and some other parameters. Hereto belong the PLUMMER /31/ and GROENEVELD and DELORME /32/ models.

2. Models which determine the thermal non-equilibrium and therefrom the actual steam quality, based on relationships between heating surface and steam flow for the heat transfer as well as for the heat transfer between phases. The empiricism shifts herein to the determination of the heat transfer between steam and water droplets and of the representative droplet diameter. The models SAHA /33/ and KOIZUMI /34/ belong to this category.

Due to their higher modelling degree, the models of the second category can determine better than those of the first one the heat transfer in the post-dryout region. However, the determination of the representative droplet diameter presents some difficulties, since this value does not only depend on the system parameters but also that it changes, e.g., due to droplet disintegration along the evaporation path. SCHNITTGER /35/ developed a model for this.

### 3.3.3 Development of a Calculation Model for the Heat Transfer in the Post-Dryout Region

#### 3.3.3.1 The Heat Transfer in a Developed Thermal Non-Equilibrium

The water and steam fractions of the two-phase flow have still the same temperature at the location of the boiling crisis. Downstream, the steam can become superheated while the water droplets remain at saturation temperature. A thermal non-equilibrium develops between the phases. The development of the thermal non-equilibrium will be terminated after a certain tube length; i.e., there a developed thermal non-equilibrium is present. Due to the higher velocity of the two-phase flow and thus of the increased turbulence, with increasing steam quality there can occur a reduction of the thermal non-equilibrium caused, e.g., by the droplet disintegration. At that time, the heat transfer increases to a greater extent than corresponding to the increase of convection by the increasing mixture velocity. However, the highest heating surface temperatures occur when the thermal non-equilibrium has just developed. If it is possible to calculate them with sufficient accuracy, the deviations before and after this zone are of secondary importance for the design of the evaporator heating surfaces. This type of consideration leads to a considerable simplification of the calculation of the heat transfer in an evaporator tube. Therein one starts from the premise, that for each parameter combination there exists a value for the developed thermal non-equilibrium, through which the course of the heating surface temperature is determined.

The extent of the developed thermal non-equilibrium can be determined from a heat balance (Figure 3-11). The steam enthalpy would not change along the flow path, so that it is possible to enter $h_{D1} = h_{D2}$. The supplied heat is exclusively used for the evaporation and superheating of the newly originating steam.

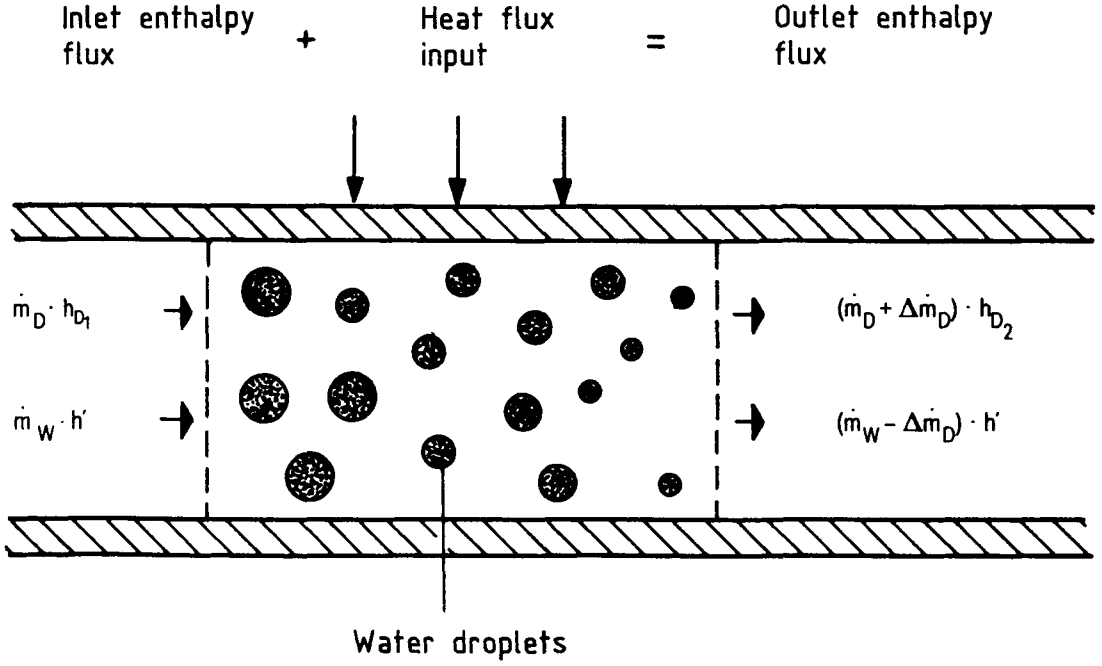


Figure 3-11 Determination of the thermal non-equilibrium with help of a energy balance

Under this premise, the superheating of the steam is:

$$\Delta\vartheta_u = \vartheta_D - \vartheta_S = \frac{\Delta h_v}{2 \cdot c_D}\left[\sqrt{1 + \frac{4 \cdot c_D \cdot \dot{q}}{\Delta h_v (\alpha \cdot F)_{Tr}}} - 1\right] \tag{3-5}$$

Herein, only the product $(\alpha \cdot F)_{Tr}$ from the heat transfer coefficient between water droplets and steam and the surface of the evaporating water droplets is unknown. Therein, the water droplets surface is in respect to a surface unit of the heated tube wall.

In the literature there are frequently used the heat transfer equations for spheres in flows for the heat transfer between droplets and steam for the determination of the value of $(\alpha \cdot F)_{Tr}$ (SAHA /33/ and KOIZUMI /34/). The Nusselt number relative to the droplet diameter is therein calculated by

$$Nu_{Tr} = 2 + a \cdot Re_{Tr}^{b} \cdot Pr_D^{c} \tag{3-6}$$

wherein different values are entered for the constants a, b and c.

This procedure requires knowledge about the representative droplet diameter and the relative velocity between droplets and steam along the evaporation path of the droplets. If, as already mentioned, one starts from the premise that for each combination of system parameters there exists a value for the developed thermal non-equilibrium, through which the course of the heating surface temperature along the flow path can be approximately determined, there can be omitted a detailed modelling of the heat transfer between droplets and steam. For each parameter combination a value for $(\alpha \cdot F)_{Tr}$, can then be assigned which is assumed independently of the local steam quality and thus constant along the flow path.

From the test values, whose parameter range was given in Chapter 2, an empirical equation for the heat transfer coefficient and the heat-exchanging surface between steam and water phase could be determined:

$$(\alpha \cdot F)_{Tr} = \begin{cases} 1.473 \cdot 10^{-7} \cdot (\dot{m}/A)^{1.33} & \text{for } \dot{m}/A \leq 1767 \cdot 10^3 \\ 3.078 \cdot 10^{-24} \cdot (\dot{m}/A)^{4} & \text{for } \dot{m}/A > 1767 \cdot 10^3 \end{cases} \tag{3-7}$$

Herein, $\dot{m}$ is the mass velocity and A the Laplace constant.

From a heat balance the actual steam quality can be determined:

$$\dot{x}_{Real} = \frac{h - h'}{\Delta h_v + c_D \cdot \Delta\vartheta_u} \tag{3-8}$$

Here, h is the enthalpy of the flow, which depends on heating and mass flow and is determined with the aid of a heat balance.

In case that no superheating of the steam exists, i.e., the water droplets and the steam are in thermal equilibrium, equation (3-8) becomes the definition equation for the steam quality according to the balance:

$$\dot{x}_{Bil} = \frac{h - h'}{\Delta h_v} \tag{3-9}$$

For the definition of the thermal non-equilibrium there is frequently used the non-equilibrium factor $\dot{\omega}$ which represents the ratio of the actual steam quality to that of the balance:

$$\dot{\omega} = \frac{\dot{x}_{Real}}{\dot{x}_{Bil}} \tag{3-10}$$

With equations (3-5), (3-8), (3-9), and (3-10) one obtains:

$$\dot{\omega} = 2/\left(\sqrt{1 + (4 \cdot c_D \dot{q})/[\Delta h_v (\alpha \cdot F)_{Tr}]} + 1\right) \tag{3-11}$$

In Figures 3-12 to 3-13 there are entered the thermal non-equilibrium factors, calculated according to equation (3-11), for pressures between 50 and 210 bars, mass velocities between 500 and 3500 kg/m$^2$s and heat fluxes up to 1000 kW/m$^2$.

The connection between the thermal non-equilibrium factor and steam superheating can be gathered from Figure 3-14.

Figures 3-12 to 3-14 can serve for the rough determination of the steam superheating with developed thermal non-equilibrium.

For the determination of the wall temperature there is still need for the heat transfer coefficient between the steam flow and the tube wall. For this the GNIELINSKI /36/ equation proven for simple-phase flow is used:

$$NU = \frac{(\xi/8) \cdot (Re - 1000) \cdot Pr}{1 + 12.7\sqrt{\xi/8} \cdot (Pr^{2/3} - 1)} \tag{3-12}$$

where

$$\xi = (1.82 \cdot \log_{10} Re - 1.64)^{-2} \tag{3-13}$$

The Reynolds number is formed herein with the mean velocity of the two-phase flow. If one postulates that in the post-dryout region the phase slip can be neglected, one obtains as Reynolds number of the two-phase flow:

$$Re = \frac{\dot{m} \cdot d}{\eta_D} \left[ \dot{x}_{Real} + (1 - \dot{x}_{Real}) \cdot (\rho_D / \rho_W) \right] \tag{3-14}$$

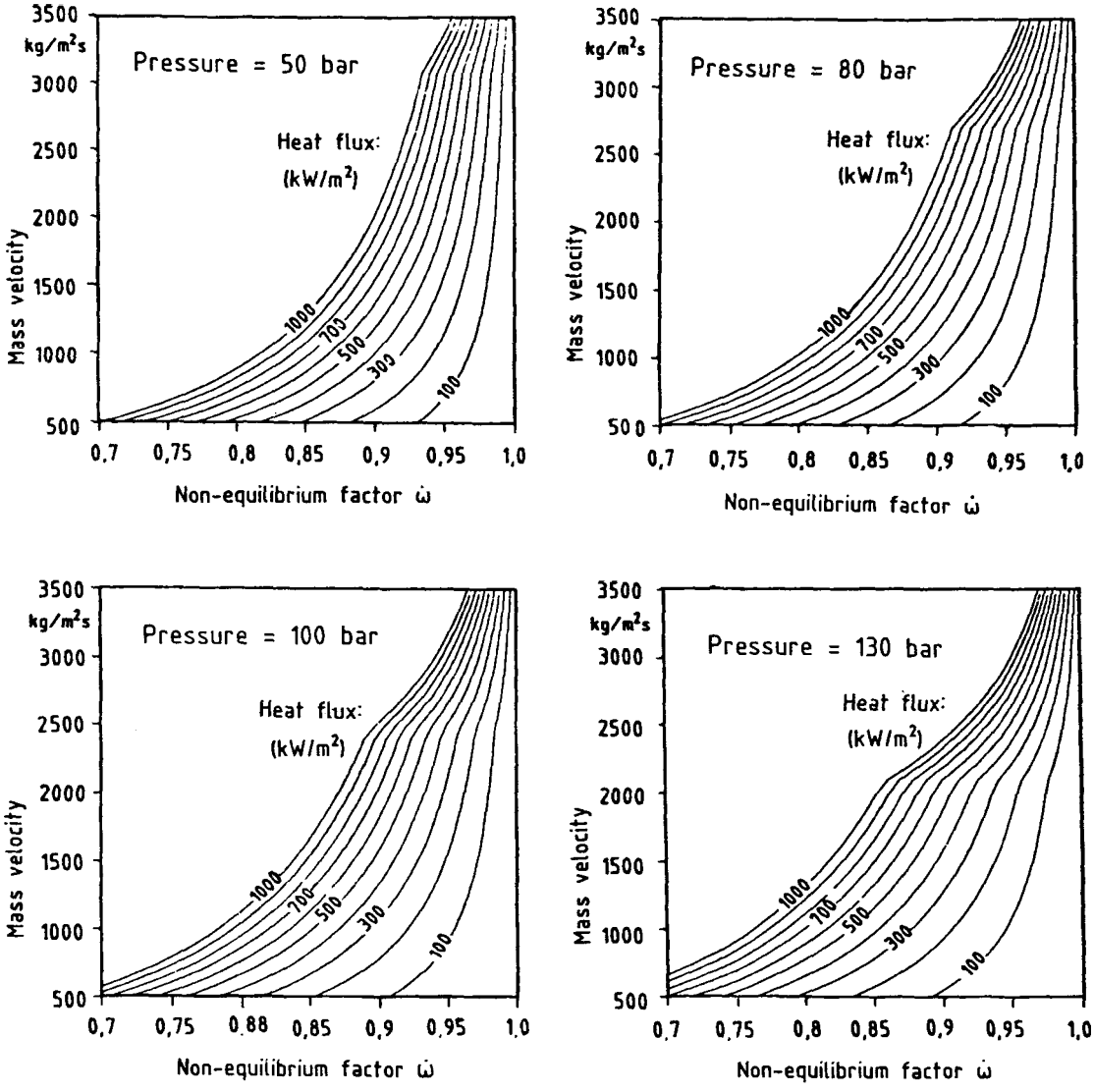


Figure 3-12 Determination of the thermal non-equilibrium factor

The Reynolds number determined with equation (3-14) is identical with the Reynolds number given in Chapter 6, equation (3-18), for the determination of the pressure loss with unwetted wall. For the determination of the pressure loss and also for the determination of the heat transfer in the post-dryout region it is assumed, that the properties of the steam determine the momentum and heat exchange with the heating surface.

As reference temperature for the characteristic values in equation (3-12) there has to be used the mean boundary layer temperature, which is obtained from the arithmetical mean of the steam and wall temperatures.

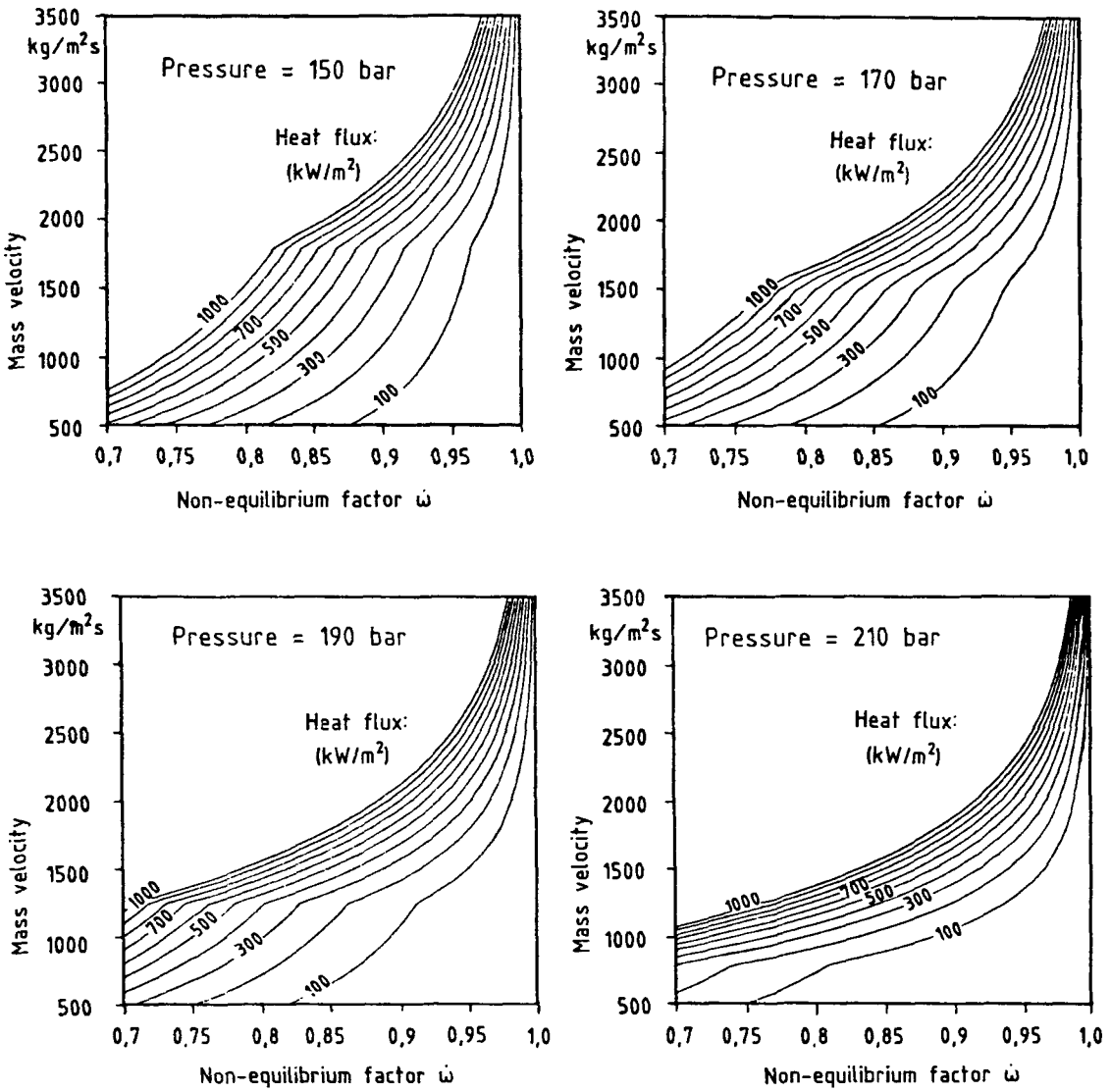


Figure 3-13 Determination of the thermal non-equilibrium factor

Finally, one obtains the wall temperature from the sum of the saturation temperature $\vartheta_s$, the superheating temperature of the steam $\Delta\vartheta_u$ and the wall excess temperature $\dot{q}/\alpha_D$ of the steam flow:

$$\vartheta_W = \vartheta_S + \Delta\vartheta_u + \dot{q}/\alpha_D \qquad (3\text{-}15)$$

3.3.3.2 The Heat Transfer at the Region Boundaries

The post-dryout region in an evaporator tube is bounded on the side with low enthalpy by the wetted part of the evaporator with nucleate boiling or

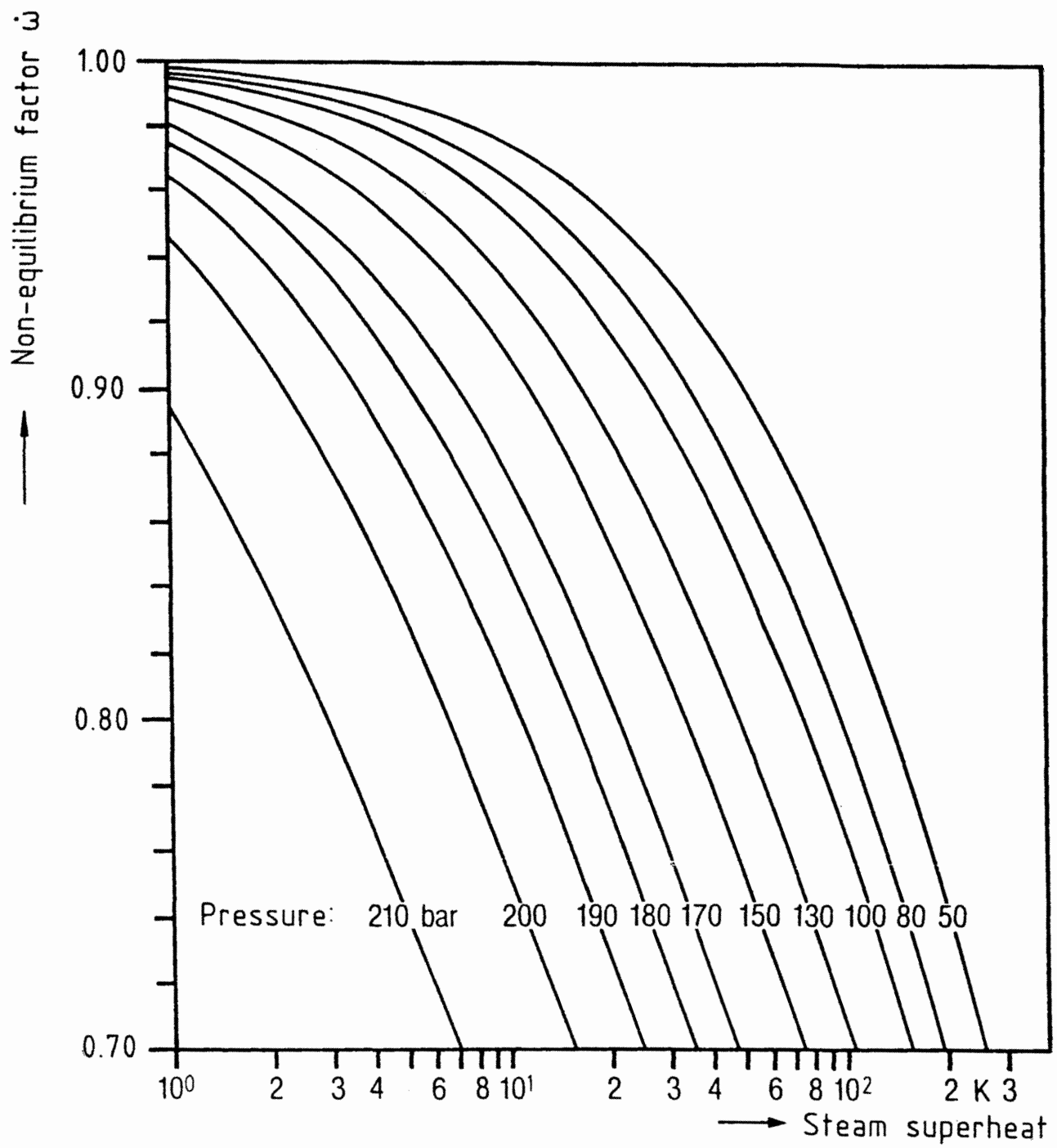


Figure 3-14 Determination of the steam superheating

convective boiling and on the side with higher enthalpy by the region of the one-phase steam flow.

Up to the location of the boiling crisis ($\dot{x}_{Kr}$), the flow is practically in thermal equilibrium, i.e., water and steam have the same temperature. After the location of the boiling crisis, the tube wall is unwetted and is essentially cooled by the steam which thereby heats up. Since the entrained water droplets remain at saturation temperature, the temperature difference between the water and steam phase increases until at the location of the minimum heat transfer ($\dot{x}_{\alpha_{min}}$) the thermal non-equilibrium is fully developed (Figure 3-15). With a further enthalpy increase the wall temperature decreases again because of the better steam cooling due to an increasing steam velocity.

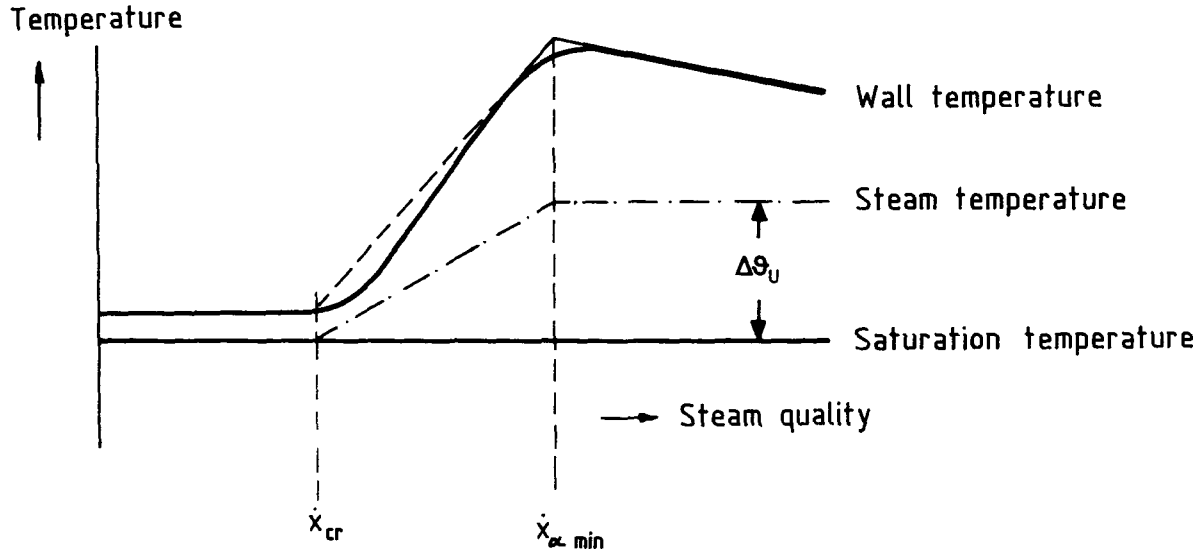


Figure 3-15 Development of the thermal non-equilibrium

The following method is suggested for the calculation of the location of the minimum heat transfer:

From the location of the boiling crisis to the location of the minimum heat transfer it is assumed, that the entire supplied heat is used for the heating-up of the steam originated until then.

Thus, from the energy balance the value ($\dot{x}_{\alpha_{min}}$), can be determined at which the steam attains the superheating temperature which corresponds to the developed thermal non-equilibrium:

$$\dot{x}_{\alpha_{min}} = \dot{x}_{Kr} + \frac{\dot{x}_{Kr} \cdot c_D \cdot \Delta\vartheta_u}{\Delta h_v} \qquad (3\text{-}16)$$

In Figure 3-16 the thus calculated difference of the steam mass quality between the location of the minimum heat transfer and that of the boiling crisis was compared. Calculation and measurement show, that with increasing mass velocity this value decreases, while it is the opposite with the influence of the heat flux.

By way of comparison, in Fig. 3-16 there was plotted a curve from HEIN et al. /22/, which is based on a statistical evaluation of the measurement results.

The described calculation model for the determination of the wall temperatures has to be modified at the transition to the simple-phase steam flow. From the tests it can be gathered, that starting from a determined, pressure-dependent steam quality the wall temperatures do not continue to decrease with increasing steam quality. This is caused by the decreasing surface of the entrained water droplets, since the two-phase flow becomes increasingly "drier." This has the result, that the steam temperature increases and thus compensates the effect of the better heat transfer, which is brought about by the higher steam velocity.

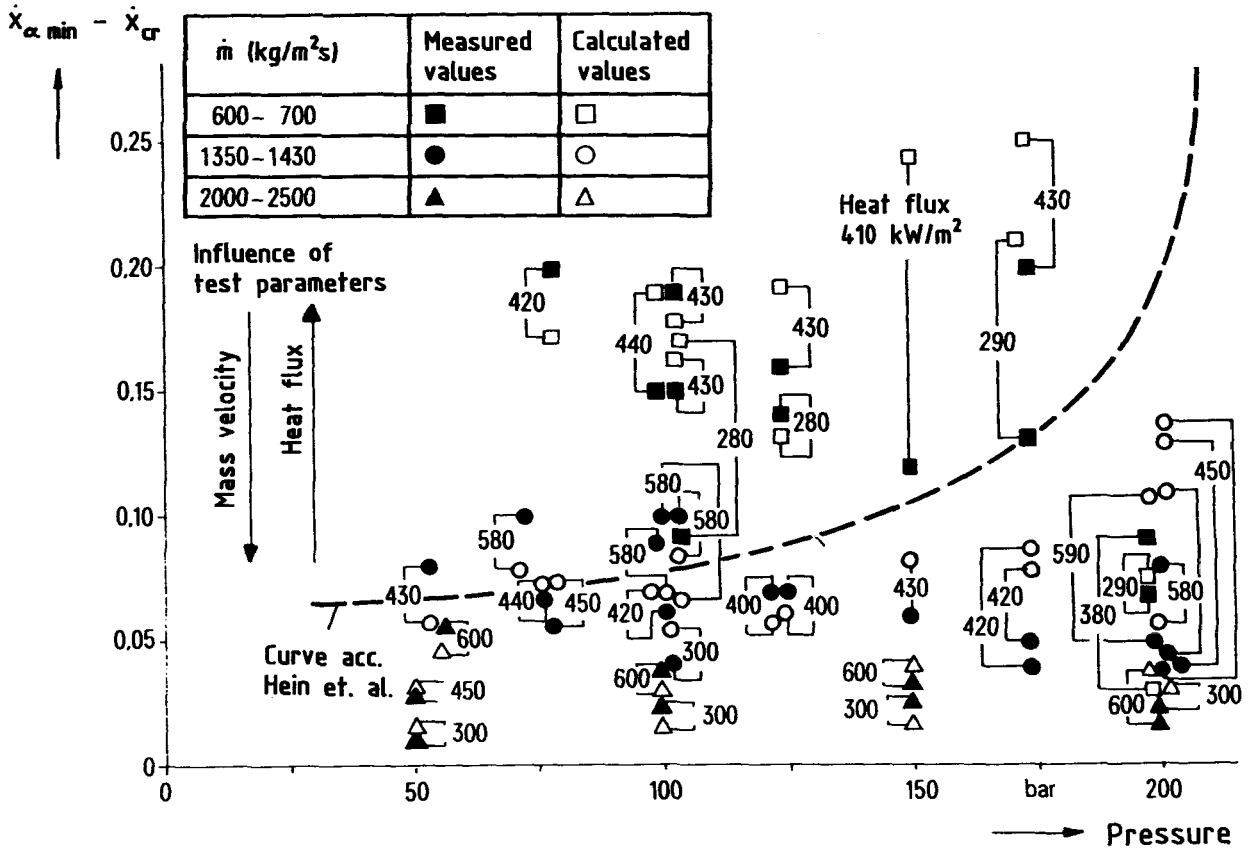


Figure 3-16 Difference of the steam quality between the location of the minimum heat transfer and that of the boiling crisis

This effect is simulated in the calculation model in such a manner, that starting from a determined steam quality ($\dot{x}_{Lim}$), the wall temperatures are maintained constant until all water droplets have evaporated, i.e., until the single phase steam flow state is attained. The boundary steam quality is a function of the pressure:

$$\dot{x}_{Lim} = 0.7 + 0.002 \cdot p \qquad (3\text{-}17)$$

If one assumes that steam and water droplets in the post-dryout region flow approximately with the same velocity, the steam quality $\dot{x}_{Lim}$ corresponds to a void fraction which lies always above 0.99.

The mathematical simulation of the transition to steam flow can be gathered from the figures in Chapter 3.3.3.3.

3.3.3.3 Model Verification

The model was verified with the aid of 368 comparison calculations with heat transfer tests of HERKENRATH /37/ and tests on the BENSON test rig. Figures 3-17 to 3-20 show typical comparisons between calculation and measurement with vertical flow. In the upper halves of the figures are represented wall temperatures with low mass velocities in the bottom part of the wall temperature with high mass velocities.

With horizontal flow, the heat transfer in the post-dryout region can be well simulated if there is no influence of the tube orientation on the heat transfer (e.g.; in Fig. 3-21). The conditions which lead to an influence by the tube orientation on the heat transfer can be determined according to Chapter 5. The location of the boiling crisis was determined with the procedure given in Chapter 3.2.

Figures 3-17 and 3-21 show that also the development of the thermal non-equilibrium from the location of the boiling crisis to the location with the lowest heat transfer coefficient is simulated with sufficient accuracy by the model. The greatest deviations between calculation and measurement are caused by the errors in the determination of the location of the boiling crisis and are therefore independent of the used calculation model for the heat transfer in the post-dryout region. This type of comparison was chosen since it illustrates that a calculation model for the heat transfer in the post-dryout region can be only as good as the model with which the critical boiling state is determined.

In order to have an overview of the accuracy to be obtained with the calculation mode, Figure 3-22 shows the differences between the measured and calculated maximum wall temperatures in the post-dryout region. As abscissa the quotient from mass velocity and the Laplace constant was chosen since this magnitude is characteristic for the heat transfer between water and steam phase in the used calculation model (cf. equation 3-7). With this it is possible to verify the empirical relationship for the heat transfer between steam and water phase in a large pressure and mass velocity region.

From Figure 3-22 it can be gathered that the studied diameter range from 70 to 24 mm was well simulated by the model. Greater deviations between calculation and measurement have to be almost exclusively attributed to tests which film

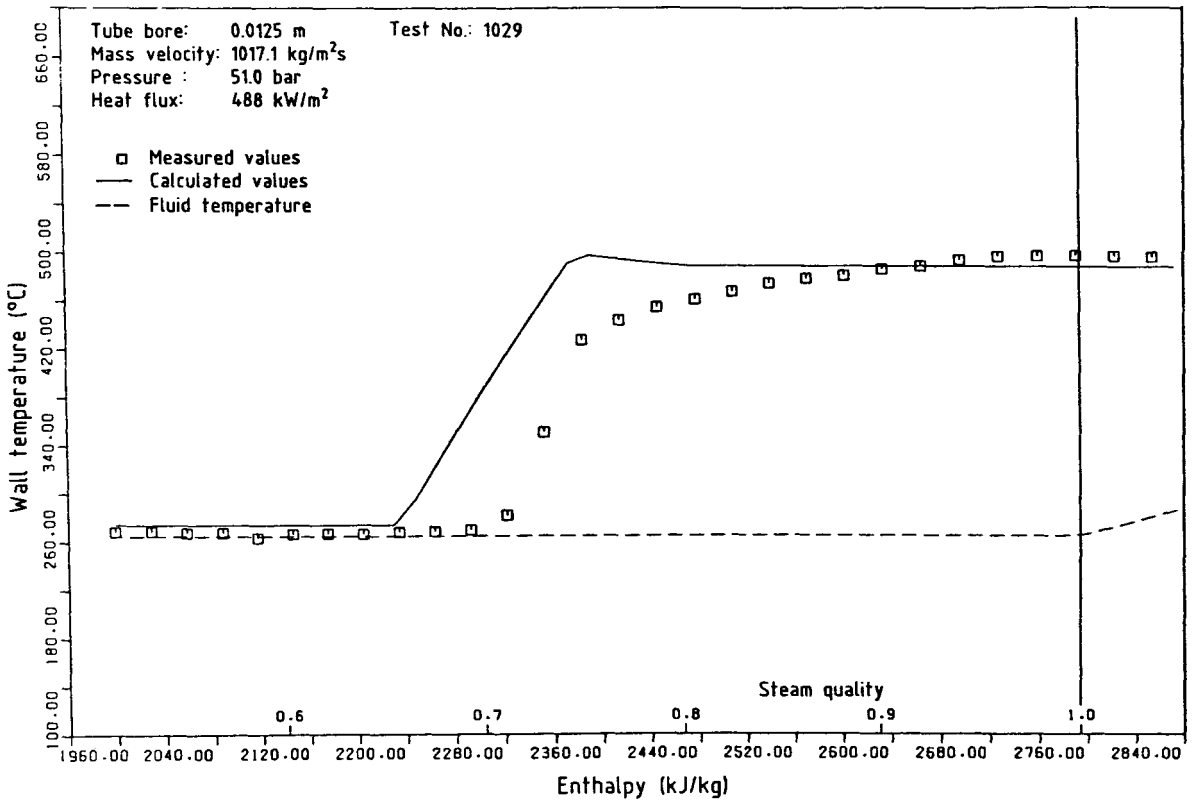


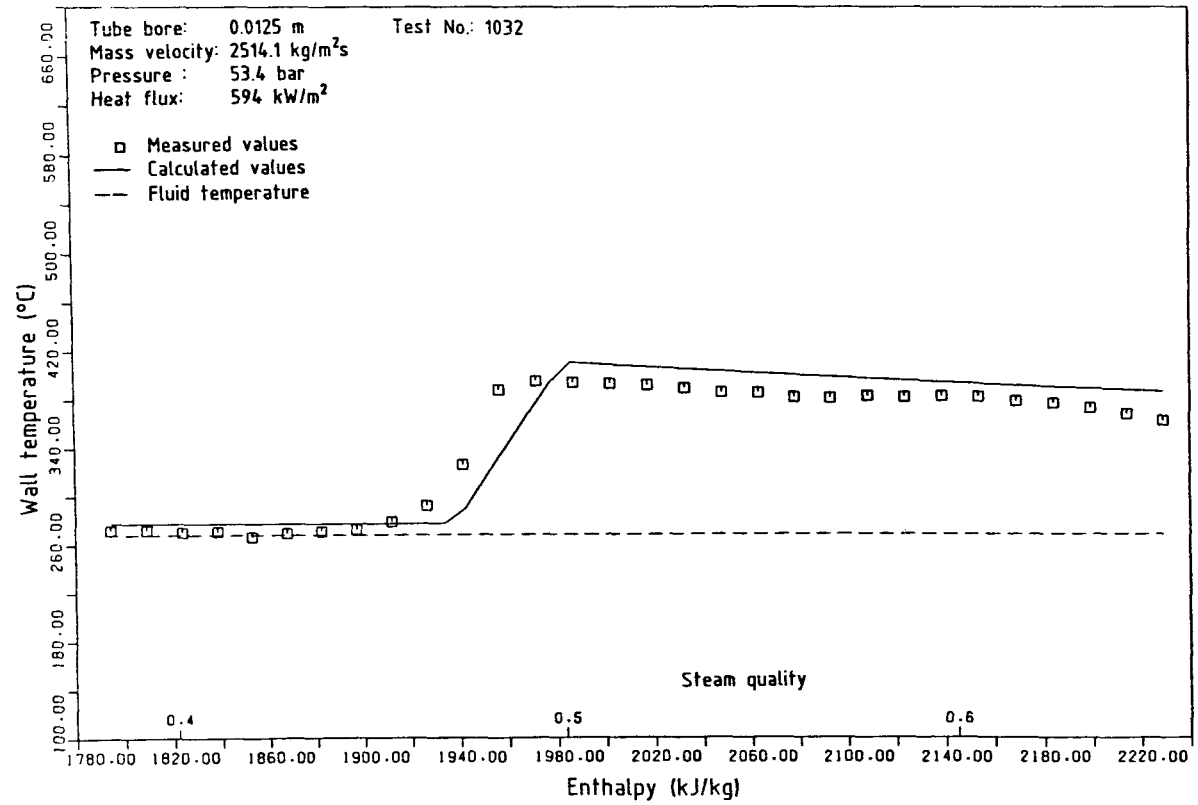


Figure 3-17 Calculated and measured wall temperature course with vertical flow

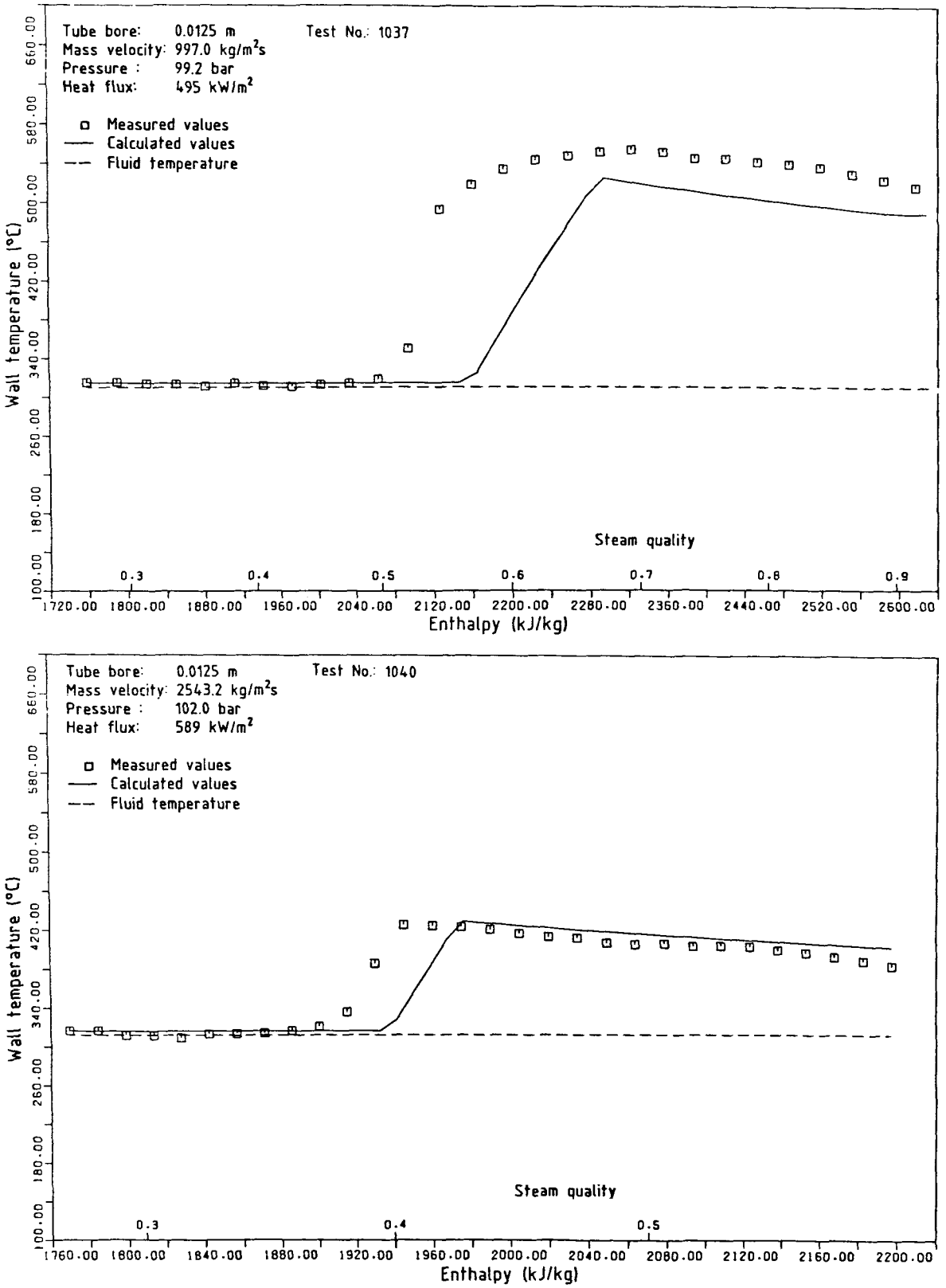


Figure 3-18 Calculated and measured wall temperature course with vertical flow

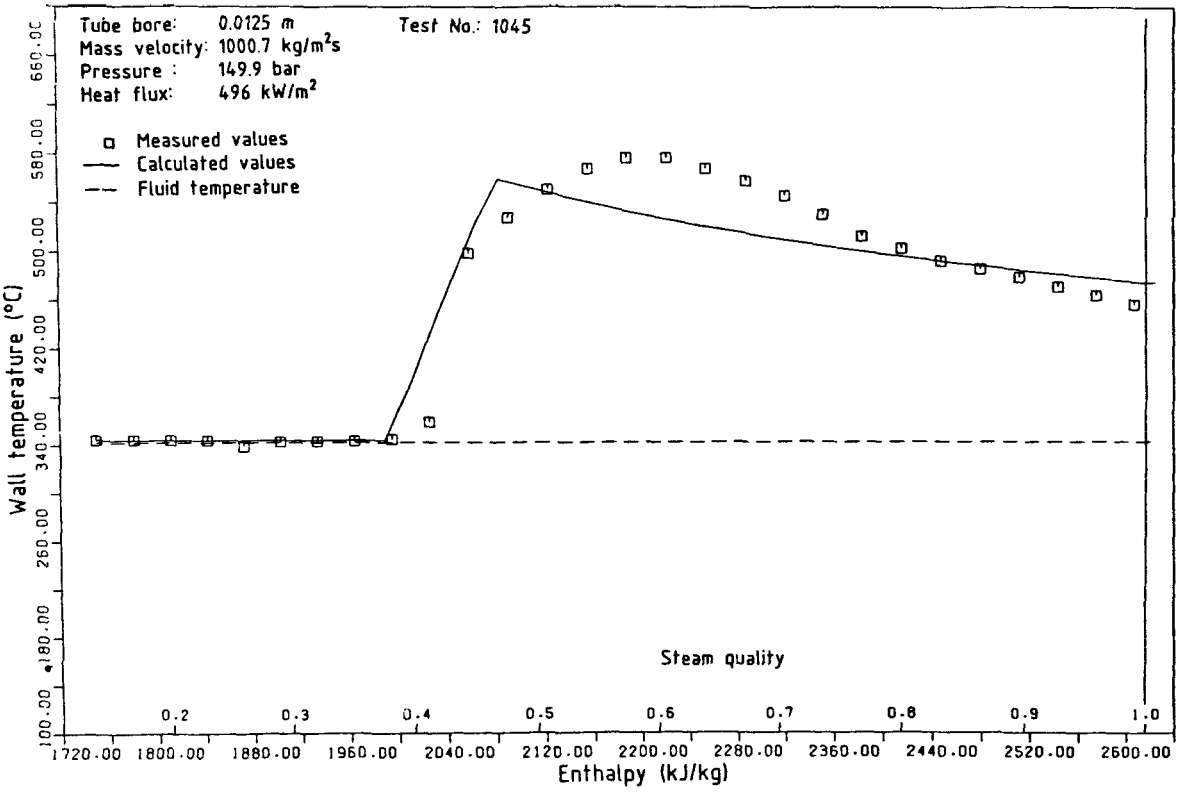


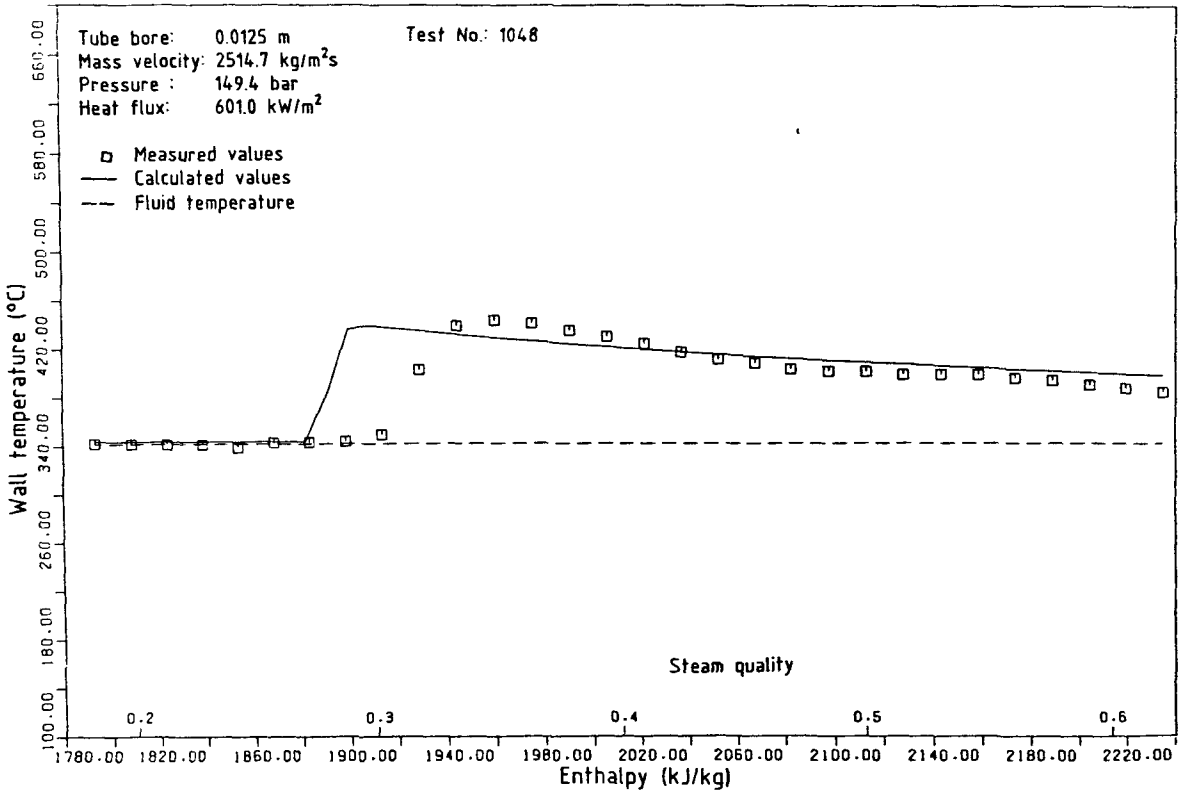


Figure 3-19 Calculated and measured wall temperature course with vertical flow

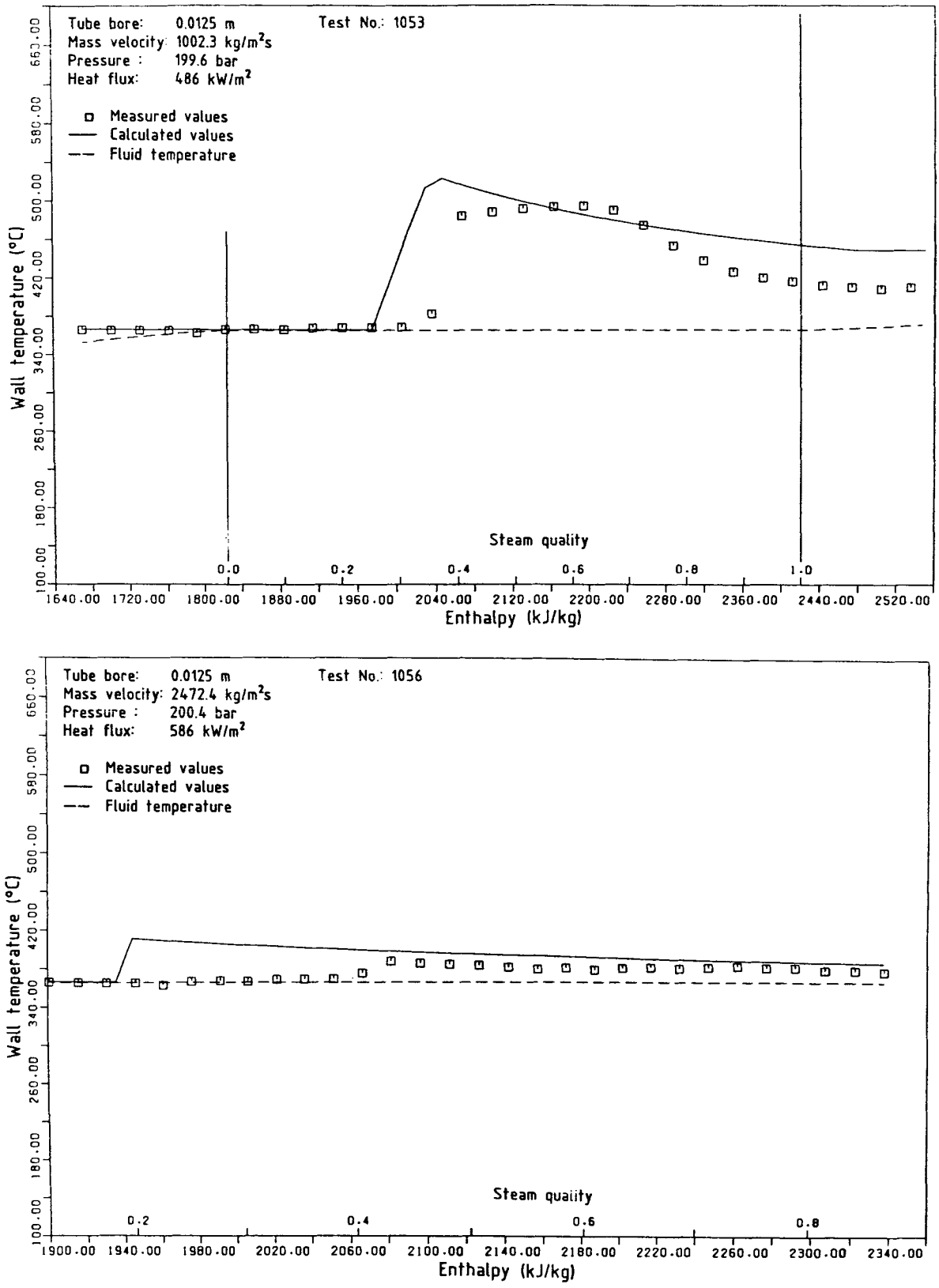


Figure 3-20 Calculated and measured wall temperature course with vertical flow

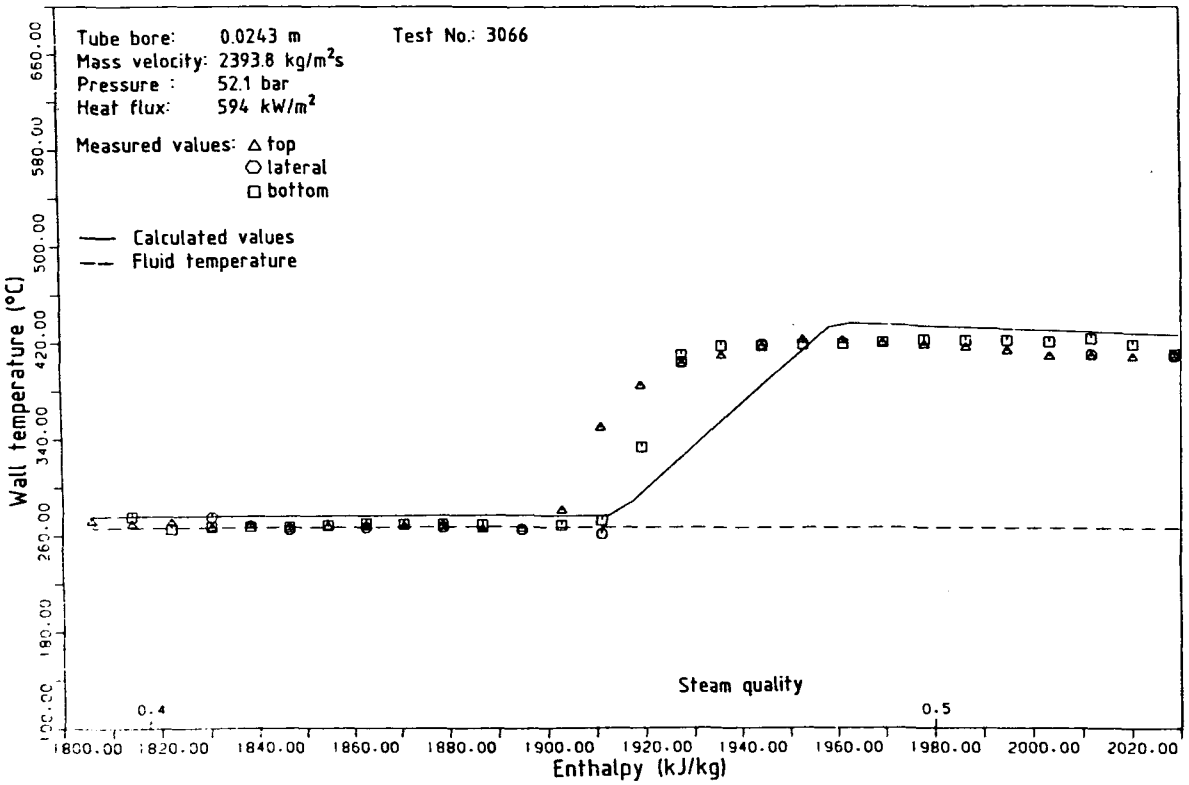


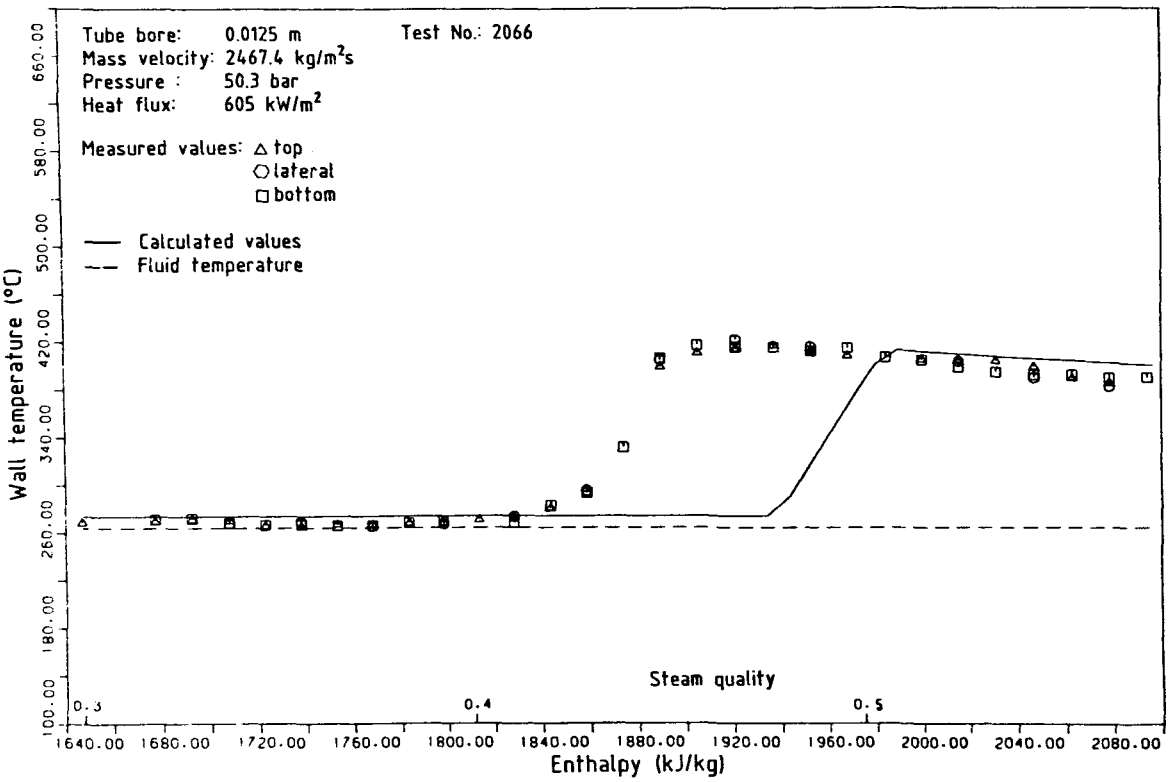


Figure 3-21 Calculated and measured wall temperature course horizontal flow

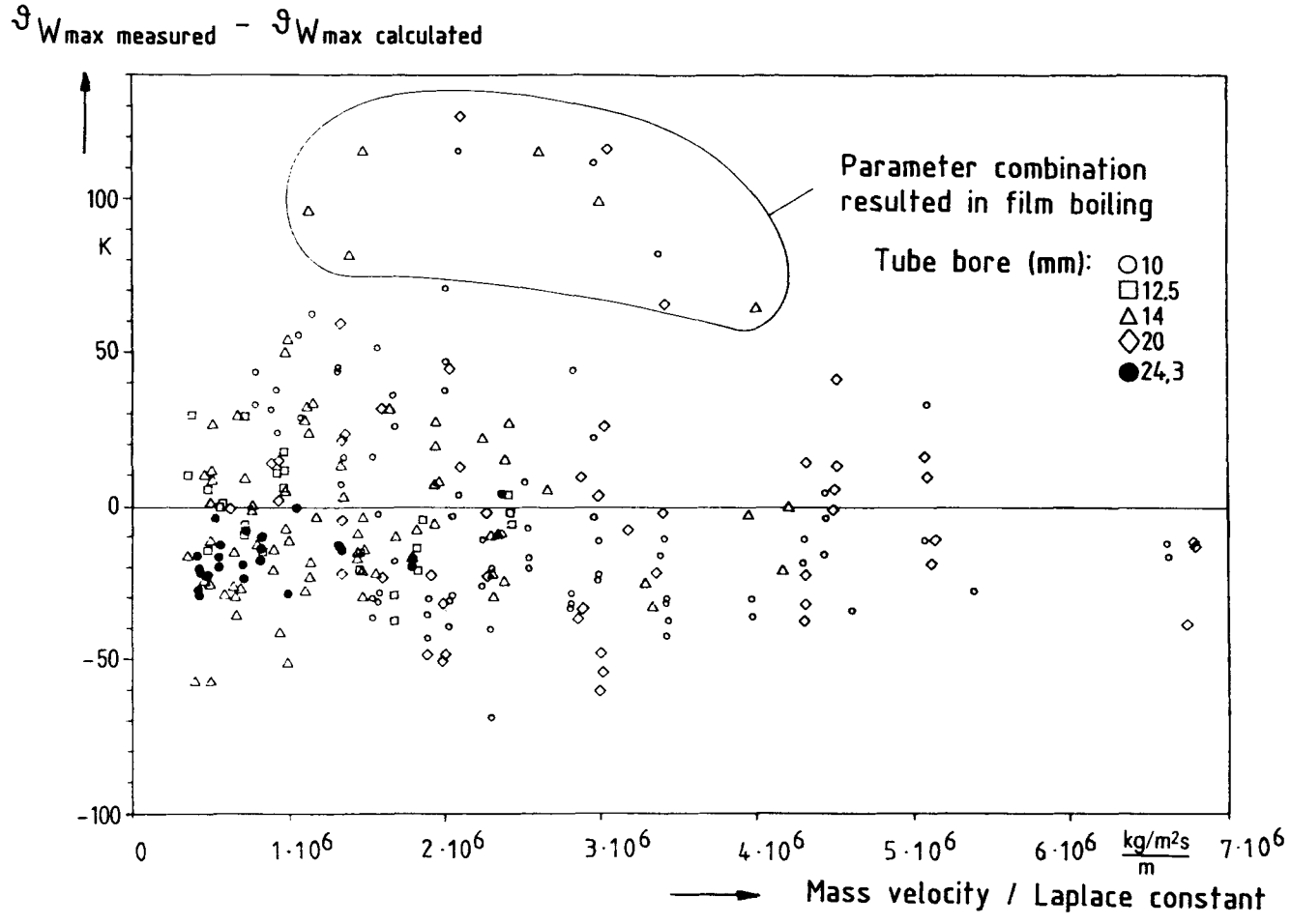


Figure 3-22 Comparison between calculated and measured maximum wall temperature in the post-dryout region

boiling occurred. The location of the boiling crisis shifts thereby to very low or even negative balance steam qualities, and parameter combinations are obtained which lie beyond possible operating conditions of a fossil-fired steam generator.

In view of the maximum wall temperature, 88% of all dryout tests of the calculation program are verified with an accuracy of ±40 K. The mean value of the deviations between the measured and calculated maximum wall temperature is 5.8 K. Standard deviation as well as the RMS error amount to 26K, and 27 K.

Figures 3-23 to 3-26 show examples for the course of the heat transfer coefficient as function of the flow enthalpy, calculated with the described model, respectively of the balance steam quality. In the region of the saturated nucleate boiling the JENS and LOTTES /38/ equation was used and in the single-phase region the GNIELINSKI equation /36/.

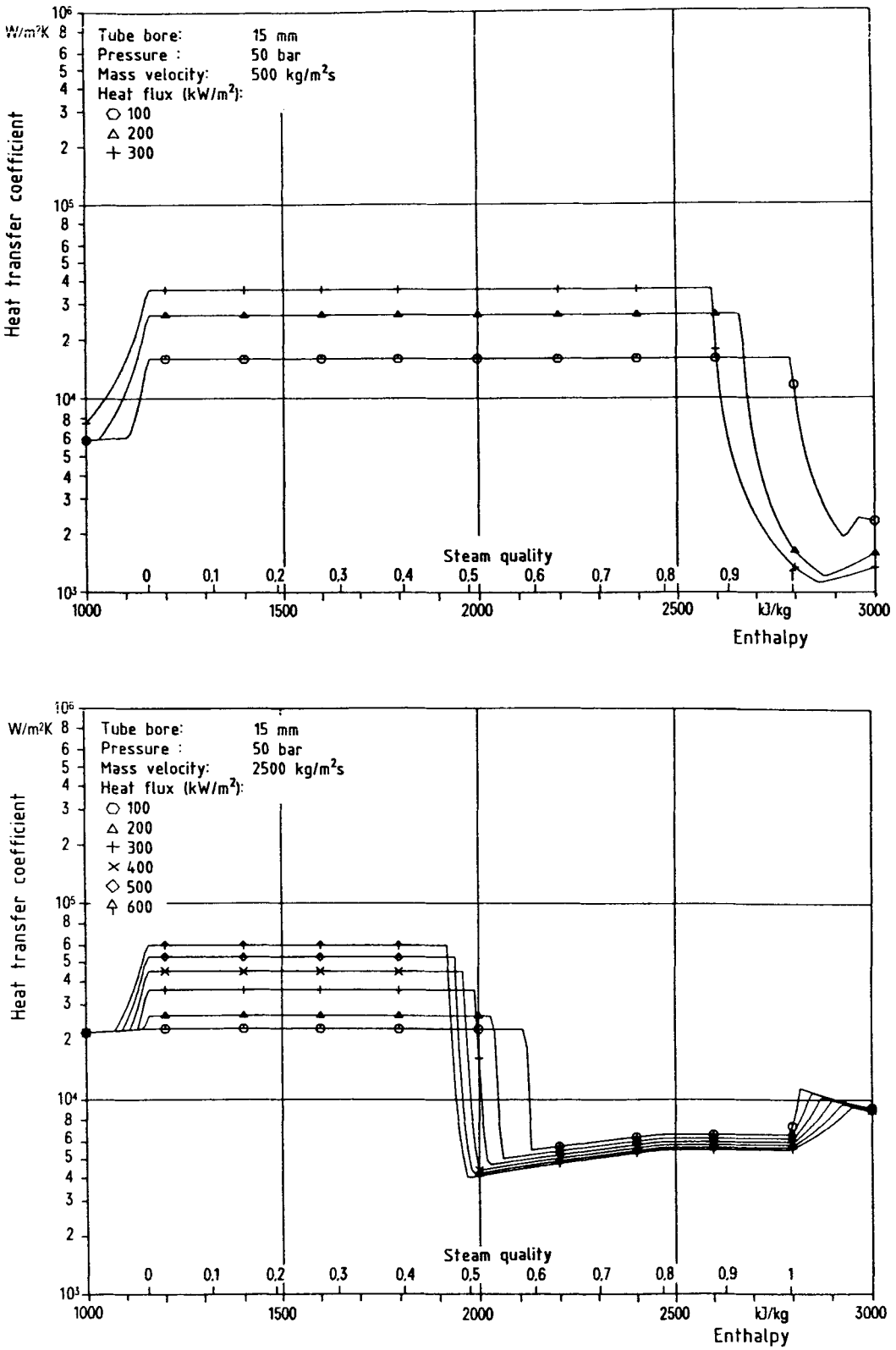


Figure 3-23 Calculated heat transfer coefficients

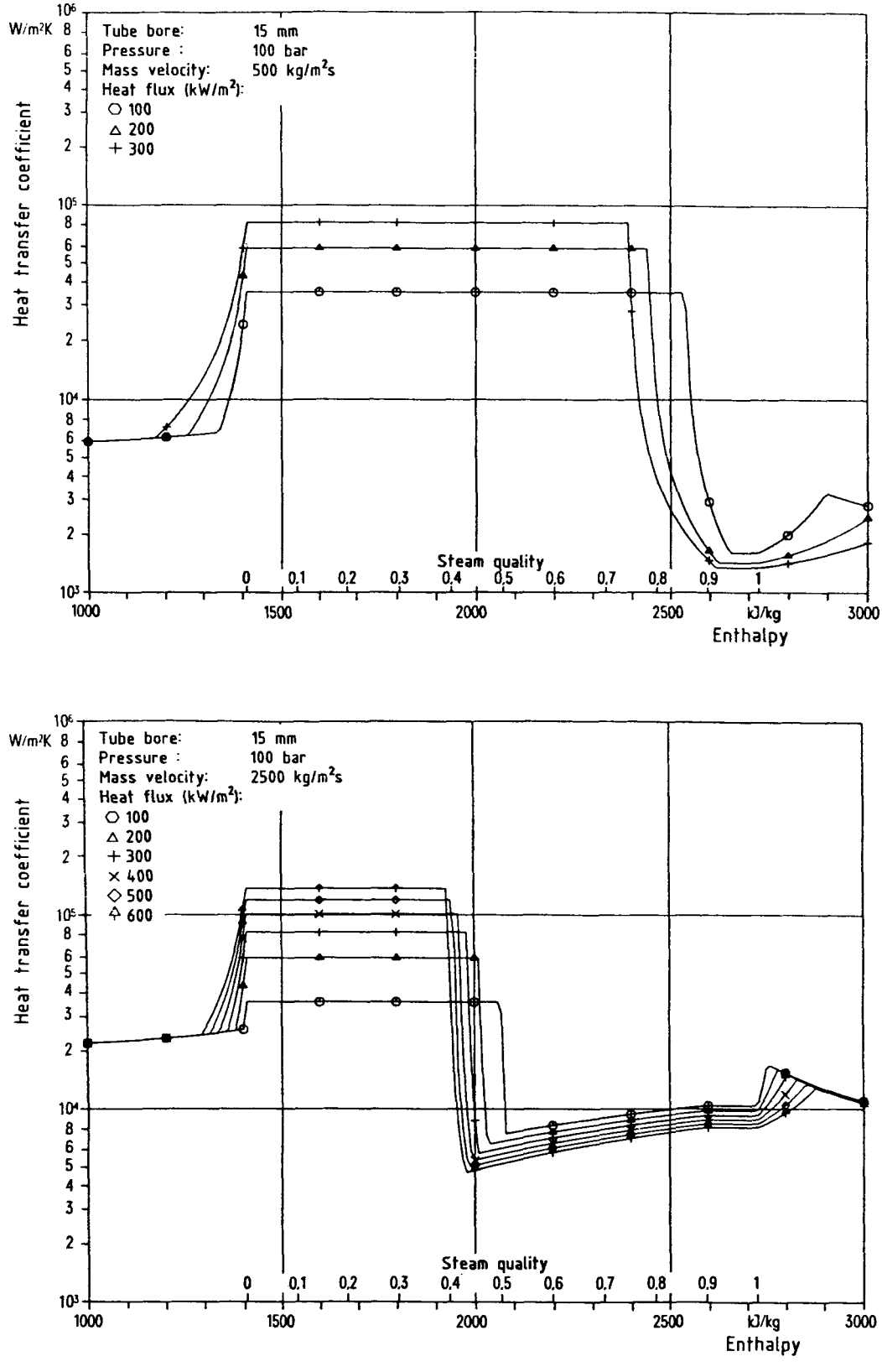


Figure 3-24 Calculated heat transfer coefficients

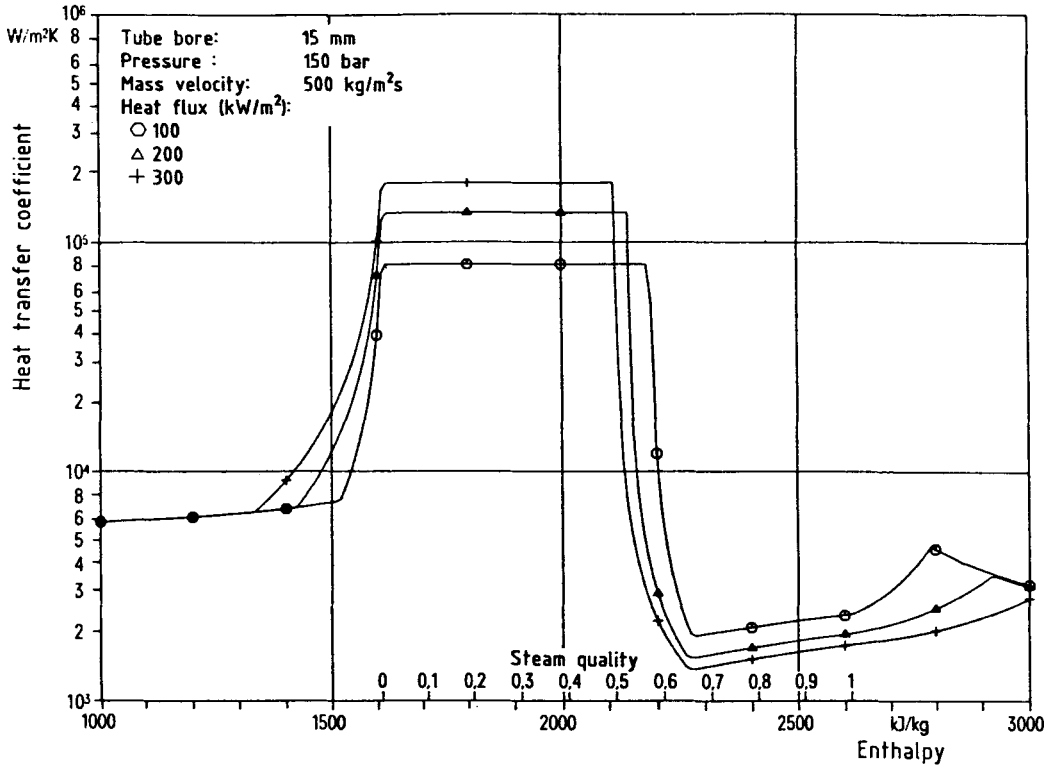


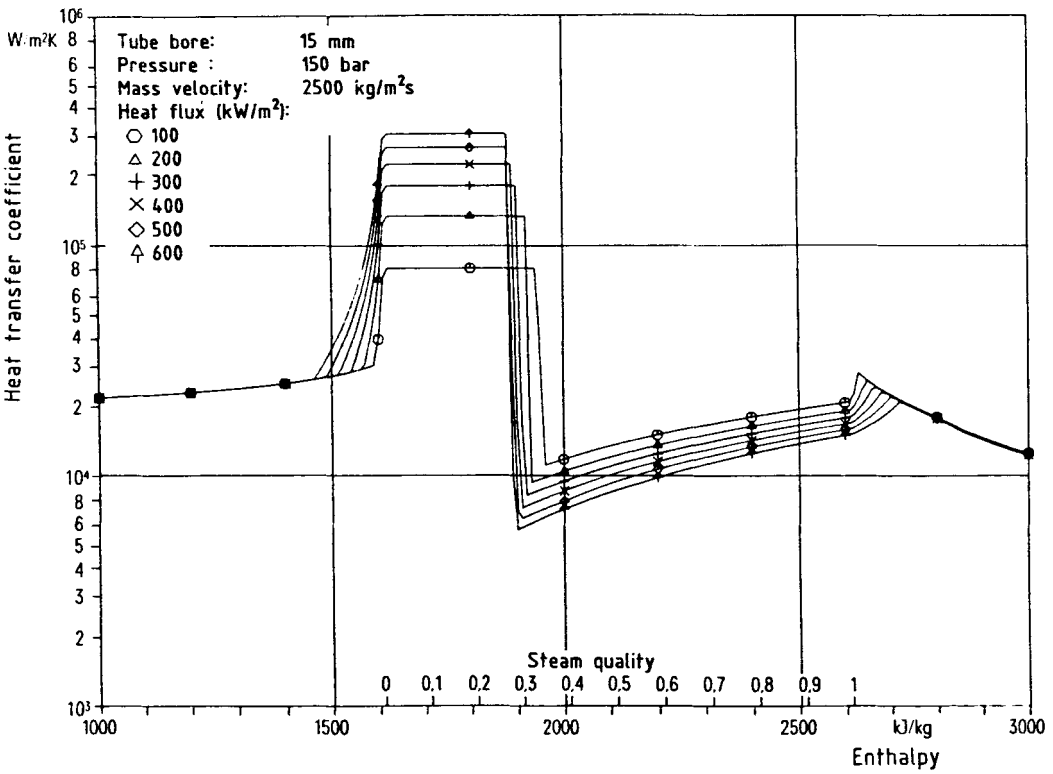


Figure 3-25 Calculated heat transfer coefficients

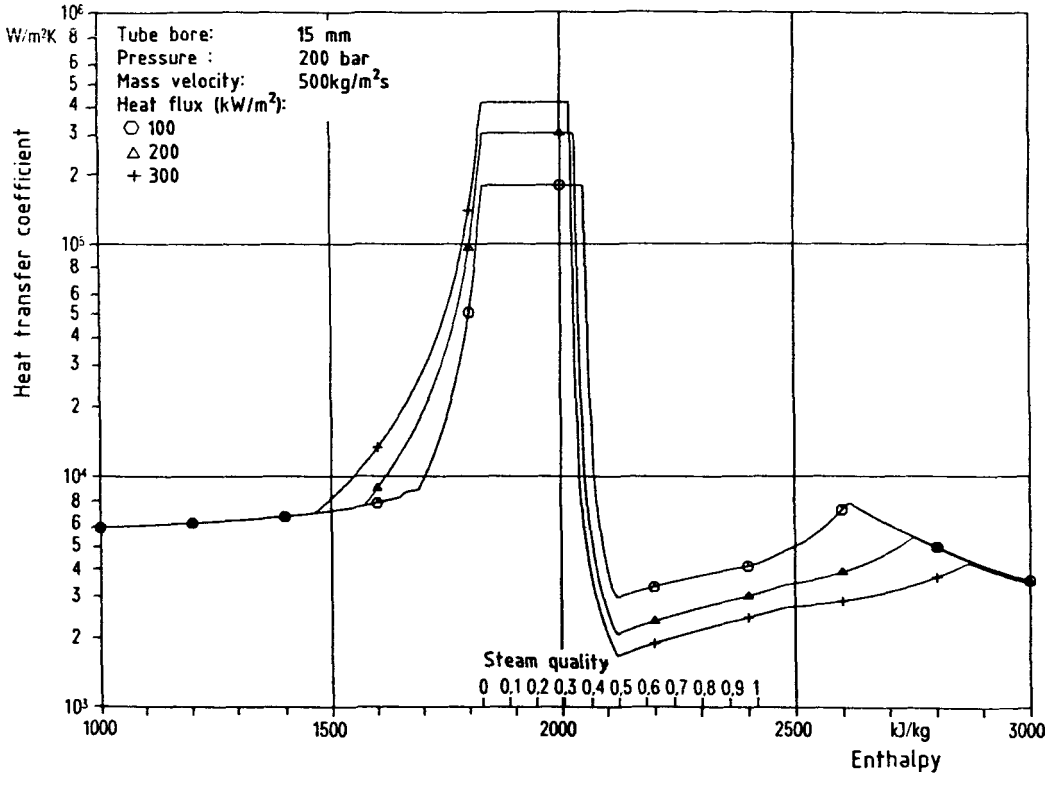


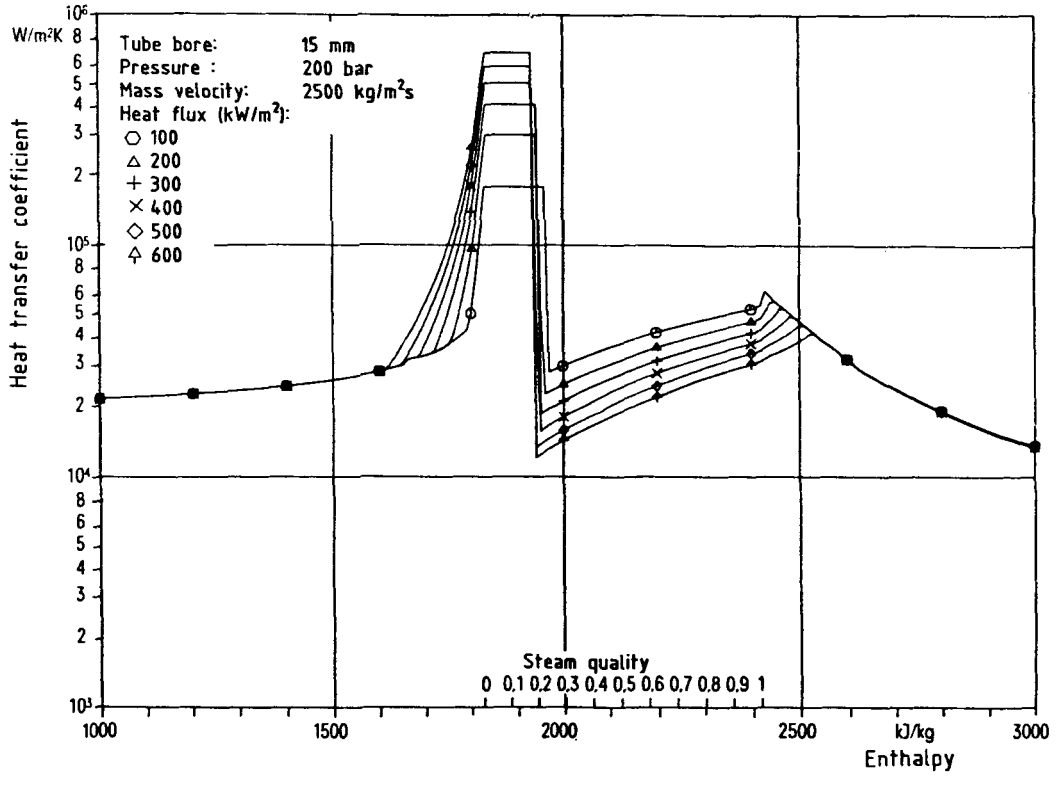


Figure 3-26 Calculated heat transfer coefficients

# 4 PRESSURE AND ENTHALPY TRANSIENTS

## 4.1 Transient Behavior of an Evaporator Tube

If a fluid in an evaporator tube is fully converted into steam by supplied heat, flow patterns and heat transfer regions are transversed from the simple-phase fluid flow via the various regions of the two-phase flow up to the simple-phase steam flow. Chapter 3.1 describes the flow patterns and heat transfer regions occurring in a vertical upflow evaporator tube uniformly heated along its length. Of special interest in connection with transient process is the location of the boiling crisis and the heat transfer in the post-dryout region.

During tests on the heat transfer in the post-dryout region it was observed, that during the transfer from one steady state to another one there could temporarily occur wall temperatures that are higher than expected according to the knowledge on the steady state heat transfer conditions. The expected steady state occurred only after a rather long period of time. This phenomenon was always observed when, due to the parameter for the newly developing state, the location of he boiling crisis had to be shifted toward the tube outlet, i.e., in a tube section which previously was unwetted. Tests were conducted for the analysis of this phenomenon, in which by a decrease of the pressure from the supercritical pressure region there had to be initiated a wetting process; of which, by decreasing the enthalpy of the flow at the test tube inlet, shifted the location of the boiling crisis farther to the tube outlet.

The transient processes were investigated with the BENSON test layout, described in Chapter 2. The test installation was somewhat modified for this purpose (Figure 4-1). The transients were simulated by the following measures:

1. Decrease of system pressure

   The pressure in the system was decreased in gradients of 5 to 20 bars per minute through the injection of cold water into the pressurizer.

   The other system parameters, such as the discharge flow of the pump and the heating of the measuring section were not modified.

2. Enthalpy decrease at the test tube inlet

   The enthalpy at the test tube inlet was reduced by 200 to 400 kJ/kg by reducing the preheating capacity. The discharge flow of the pump, the system pressure and the heating of the test tube were maintained constant.

In both transient processes could be observed a partially considerable worsening of the heat transfer in the post-dryout region. It was especially significant and present over an extended period of time when the pressure, respectively enthalpy, decrease occurred in the proximity of the critical pressure.

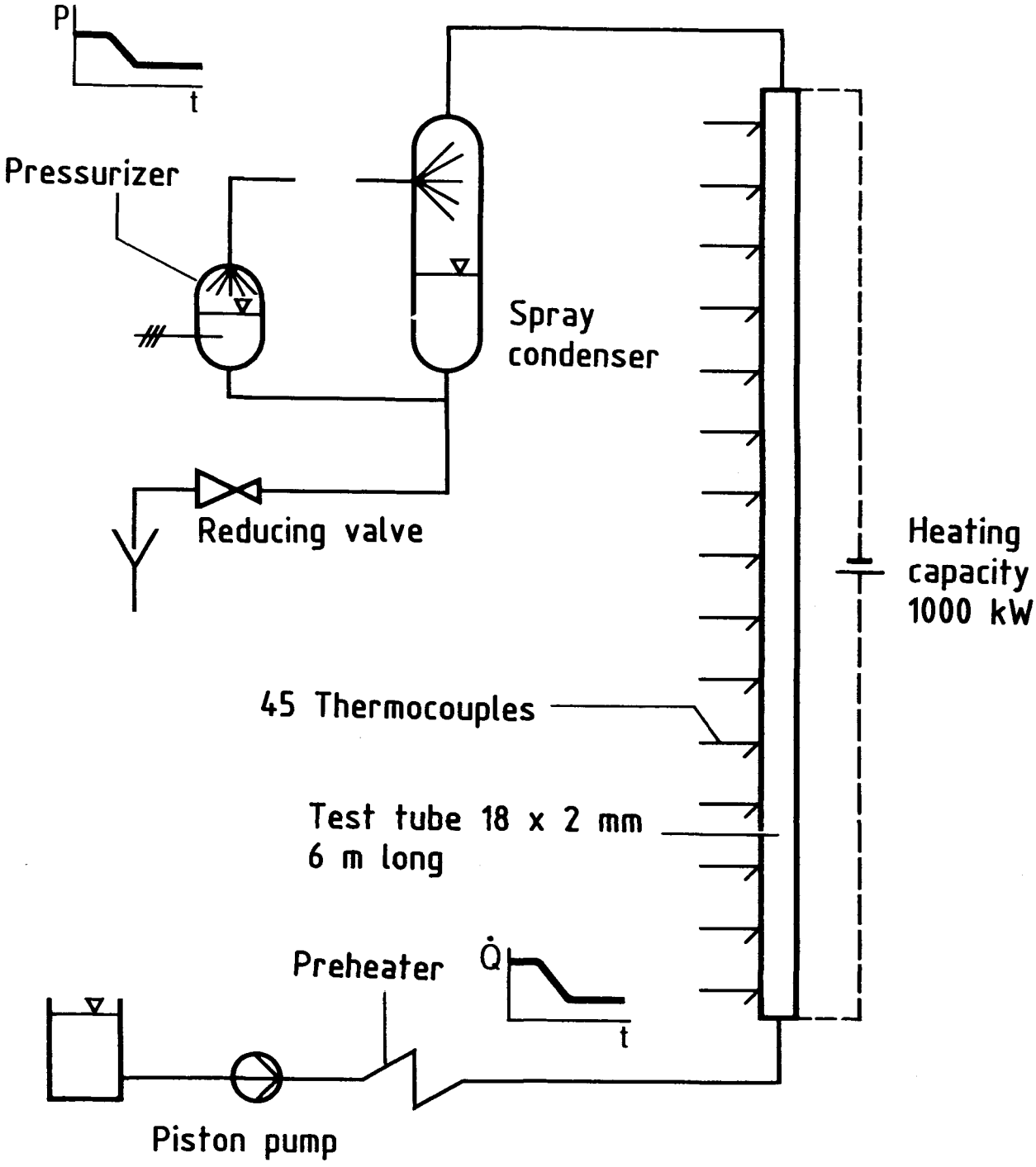


Figure 4-1 Test layout for the simulation of transient processes

Figure 4-2 presents a typical process of measured tube wall temperatures after a pressure decrease from the super critical pressure region. In its initial state at 247 bars, i.e., in the supercritical state, the tube has wall temperatures ranging from 380 to 400°C over its entire length. After 165 s, a temperature profile developed which, with an enthalpy of 1750 kJ/kg, presented a steep temperature increase as indication of the location of the boiling crisis. During the further course, the location of the boiling crisis shifted in flow direction, whereby the maximum temperature decreases again and after more than 600 s attains a steady state with a maximum temperature of about 430°C.

Figure 4-3 shows a detailed analysis of the test. In the diagrams, the measured values are compared with the calculated values which were obtained with the aid of a computer program /39/ for the simulation of dynamic processes in a steam generator. In the verification of the calculation it was assumed, however, that the transient process in respect to the heat transfer can be represented as a series of quasi-steady states. This means that although the conservation equations for mass, momentum and energy as well as the storage and release processes of the tube wall were taken into account, for the determination of the boiling crisis it was assumed that it can follow unimpeded the changing conditions in the tube.

In the initial state with supercritical pressure there is good agreement within the expected accuracy between the measured and calculated maximum wall temperature. Also the time slope of this maximum temperature is of similar course during the first 100 s. If the system pressure falls below the critical pressure the calculated maximum wall temperature increases to 440°C and maintains this value up to the end of the experiment. On the other hand, the maximum wall temperature rises to approximately 550°C in the experiment and attains the calculated value after about 600 s, when the new equilibrium condition sets in. The time slope of the enthalpy at the location of the boiling crisis, also shown in Figure 4-3, contributes to the understanding of this process. From the heat balance the enthalpy at the location of the boiling crisis which existed in the experiment was determined. While throughout the entire test time the calculation shows a constant value, which lies above the saturation enthalpy of the water, the enthalpy at the location of the boiling crisis increases constantly in the experiment and, in the time frame between 100 and 300 s, lies below the saturation enthalpy. Thus, in the case of a pressure reduction from the supercritical pressure region, tube sections with very low and even negative balance steam quality attain the unwetted state. This means that film boiling can occur and that the velocity of the two-phase flow at the location of the boiling crisis is considerably reduced in respect to the steady state, whereby the cooling effect is reduced and the wall temperature increases correspondingly.

Through the enthalpy decrease at the inlet of the test tube there is caused a temperature excursion of similiar effects. Figure 4-4 shows a typical course of the tube wall temperature after a sloping decrease of the inlet enthalpy. While in this case there could be expected a shifting of the temperature profile at the time 0 in the flow direction, the maximum temperature increases from about 400°C to about 480°C and it is only after 800 s that it approaches again the value of the initial state. During this period, the location of the boiling crisis shifts in the flow direction toward the tube outlet.

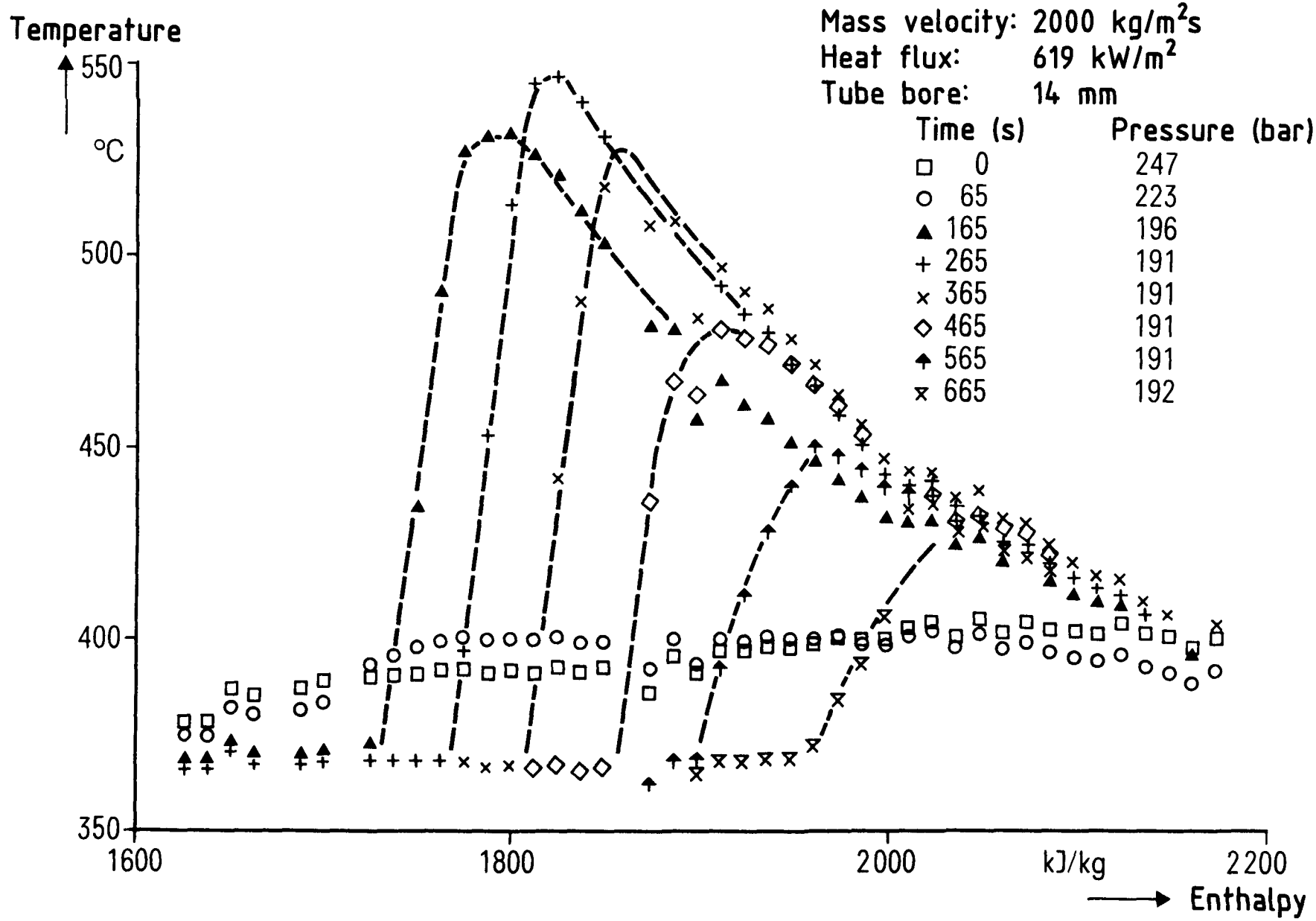


Figure 4-2 Course of the tube wall temperatures with pressure decrease

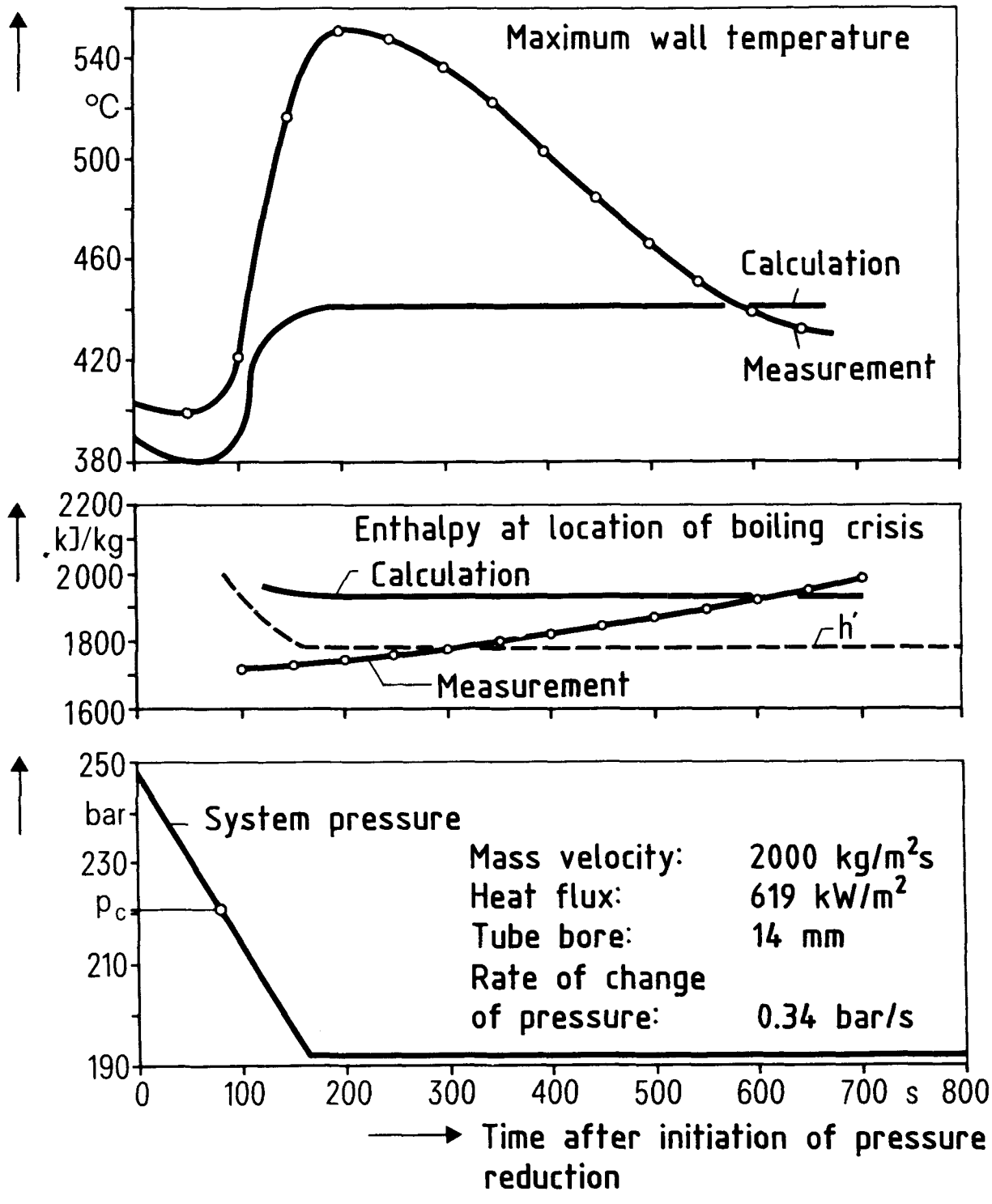


Figure 4-3 Course of thermal and fluid dynamic magnitudes with a pressure reduction in the proximity of the critical pressure

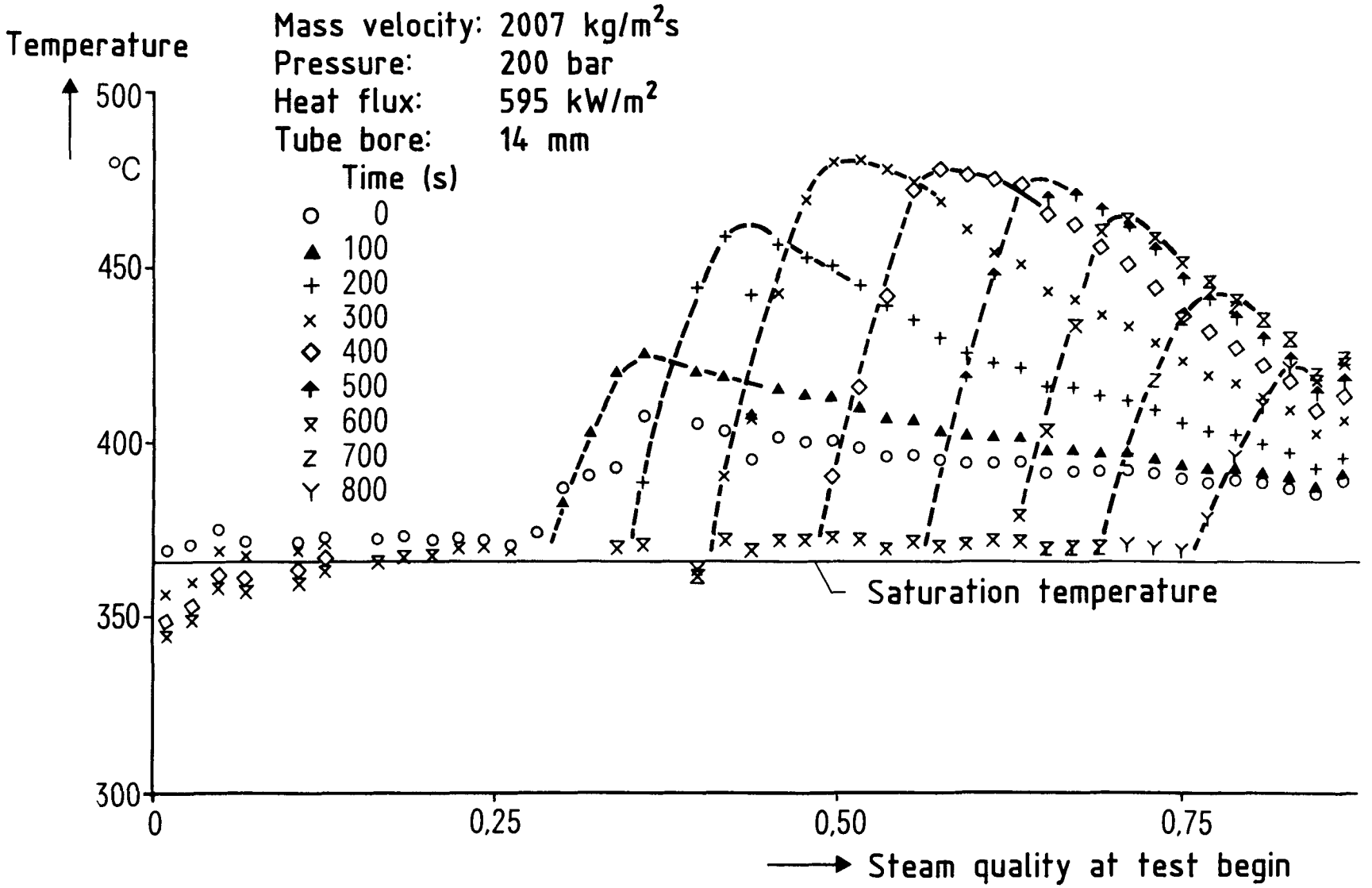


Figure 4-4 Course of the tube wall temperature with enthalpy decrease

Through a calculation with the described computer program in this case it is possible to separate the expected effects from the processes to be studied. Thus, it can be gathered from Figure 4-5 that, due to the enthalpy decrease during the time period of 0 to 200 s, there occurs a reduction of the mass flow in the test tube although the discharge flow of the pump remains constant. This temporary mass flow decrease can be attributed to a "filling process" because due to the throttling of the supplied heat in the preheating region the steam quality in the piping is reduced and thus the volume flow in the test tube decreases although the enthalpy at the inlet of the test tube has not yet decreased. This mass flow reduction causes in the calculation a corresponding increase of the maximum wall temperature during this period of time. In the experiment, however, the wall temperature reaches the maximum value only then, when the mass flow has again reached its initial value. Also in this case it can be deduced from the comparison of the enthalpies at the location of the boiling crisis, that the considerable increase of the wall temperature has to be attributed to the non-wetting of the heating surface, since the wetting process is delayed in respect to the steady state. The location of the boiling crisis does not shift in the tube outlet direction with the velocity which would correspond to the changed flow enthalpy. Therefore, the enthalpy at the location of the boiling crisis drops for a time range of 180 to 650 s below the saturation enthalpy of the water. It can be seen from Figure 4-4 that in this range the highest wall temperatures occur.

With the help of the course of the boiling curves of the heating element - fluid system there shall be interpreted the temperature excursions observed during the described transient processes.

## 4.2 Interpretation of the Transient Processes with Help of the Boiling Curve

For pool boiling NUKIYAMA /40/ presented for the first time the connection between heat flux and wall temperature for the various heat transfer regions in a curve. In contrast to the conditions in an evaporator tube, where the boiling crisis is brought about by dryout, with pool boiling film boiling occurs after the exceeding of the critical heat flux. However, the connection found by NUKIYAMA between heat flux and wall temperature can be qualitatively applied also to the forced convection conditions. Figure 4-6 shows the schematic course of the Nukiyama curve or boiling curve of the heating element - fluid system.

In the case of a wall temperature controlled system, the boiling curve can be traversed with increasing and decreasing wall temperatures in the same manner without hysteresis. If the wall temperature increases, boiling occurs on the heating surface after the convection region. Boiling crisis occurs it the critical heat flux is reached. The transferred heat flux decreases now with increasing wall temperature.

The heating surface is intermittently wetted and thus this heat transfer mechanism is characterized by unstable film boiling. Stable film boiling occurs if the Leidenfrost temperature is exceeded and a wetting is no longer possible. On the other hand, a decrease of the wall temperature below the Leidenfrost temperature leads to intermittent wetting processes until the heating surface is fully wetted.

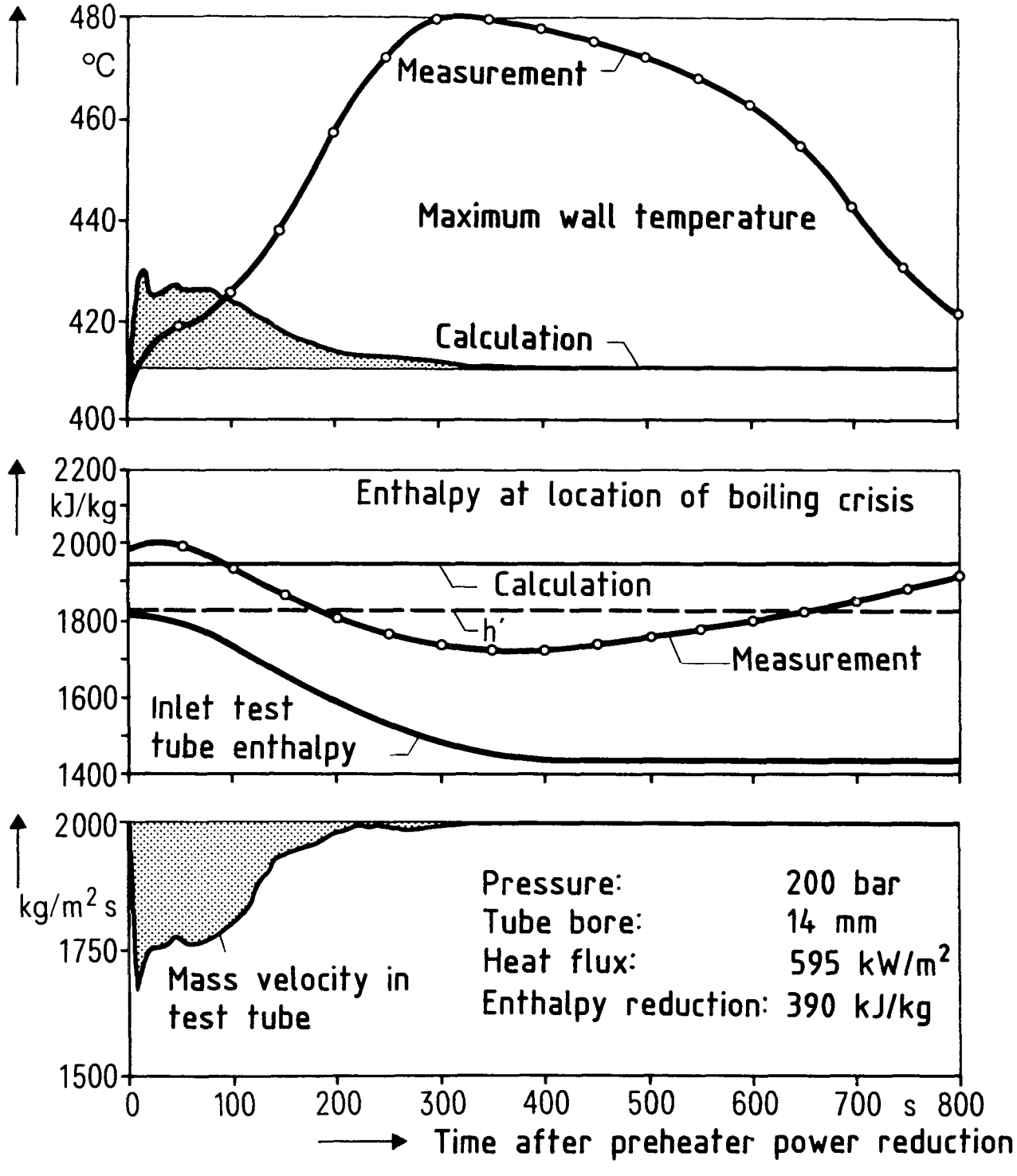


Figure 4-5 Course of thermal and fluid dynamic magnitudes with an enthalpy decrease in the proximity of the critical pressure

In contrast, the attaining of the critical heat flux in a heat flux controlled leads to a sudden temperature rise in the region of the stable film boiling and a fall below the Leidenfrost temperature leads to a sudden temperature drop with complete wetting of the heating surface. A cycle with heat flux increase and subsequent reduction leads thus to a marked hysteresis in the heat flux wall temperature course. However, also in a heat flux controlled system the only possible conditions are those that lie on the boiling curve. It has to be considered however that, when reaching the critical heat flux, the sudden rise of the heating surface temperature is connected with an energy storage in the heating element and that, when falling below the Leidenfrost temperature, the sudden decrease of the heating surface temperature is connected with an energy discharge from the heating element. The course for a heat flux controlled system, shown in Figure 4-6 by a broken line, can thus be characterized only as an apparent boiling curve.

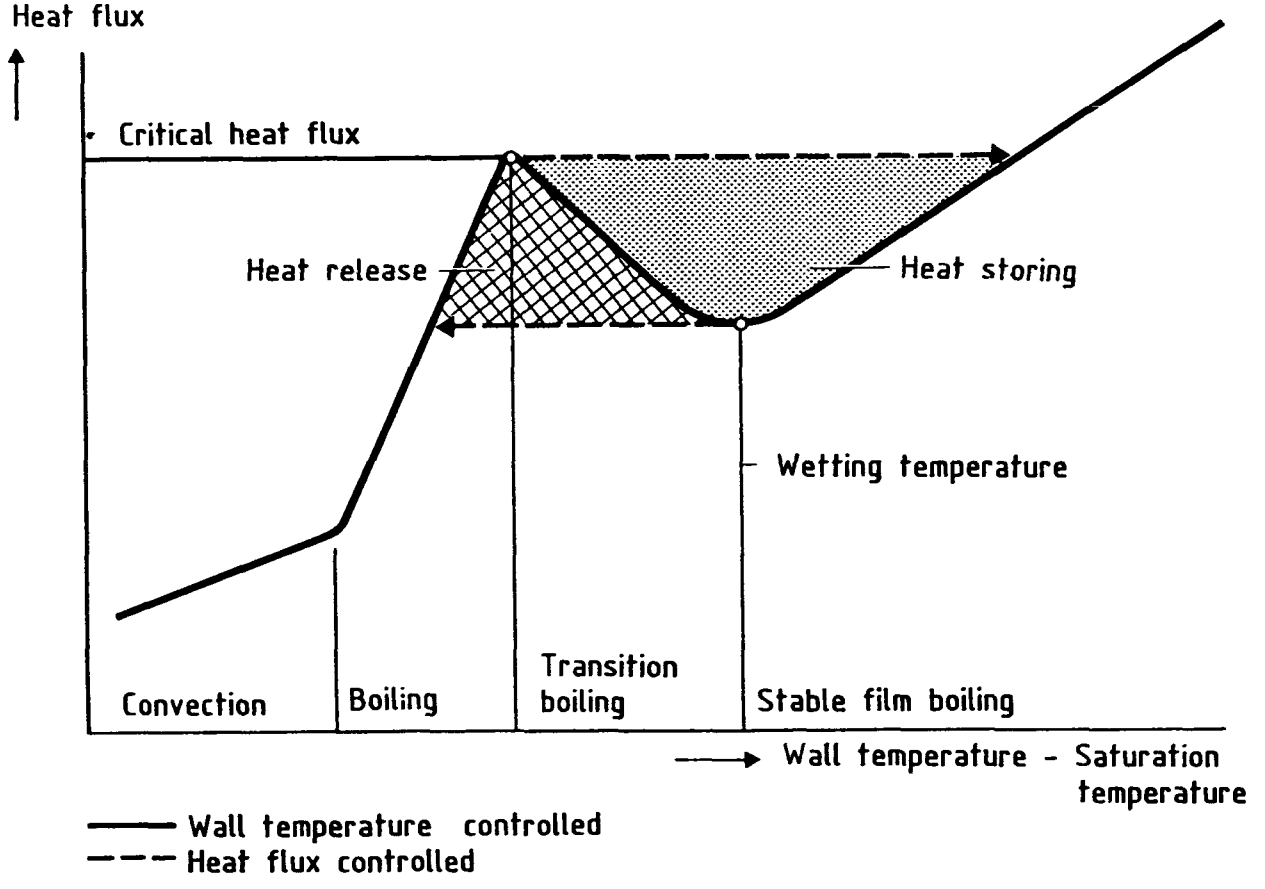


Figure 4-6 Connection between heat flux and wall temperature with pool boiling (boiling curve)

Additional influences occur for the determination of the boiling curve under forced convection conditions. Figure 4-7, which was taken from /41/, shows that in a uniformly heated evaporator tube there cannot be observed a

hysteresis in the heat flux-wall temperature course with an increase and a subsequent decrease of the heat flux. Quasi-steady state changes of operating parameters cause hereby a shifting of the location of the boiling crisis according to the thermal and fluid dynamic state of the heating surface-fluid system in the evaporator tube. The shifting of the location of the boiling crisis is made possible by axial heat conduction from the unwetted to the wetted tube wall, whereby an apparent boiling curve without hysteresis is simulated.

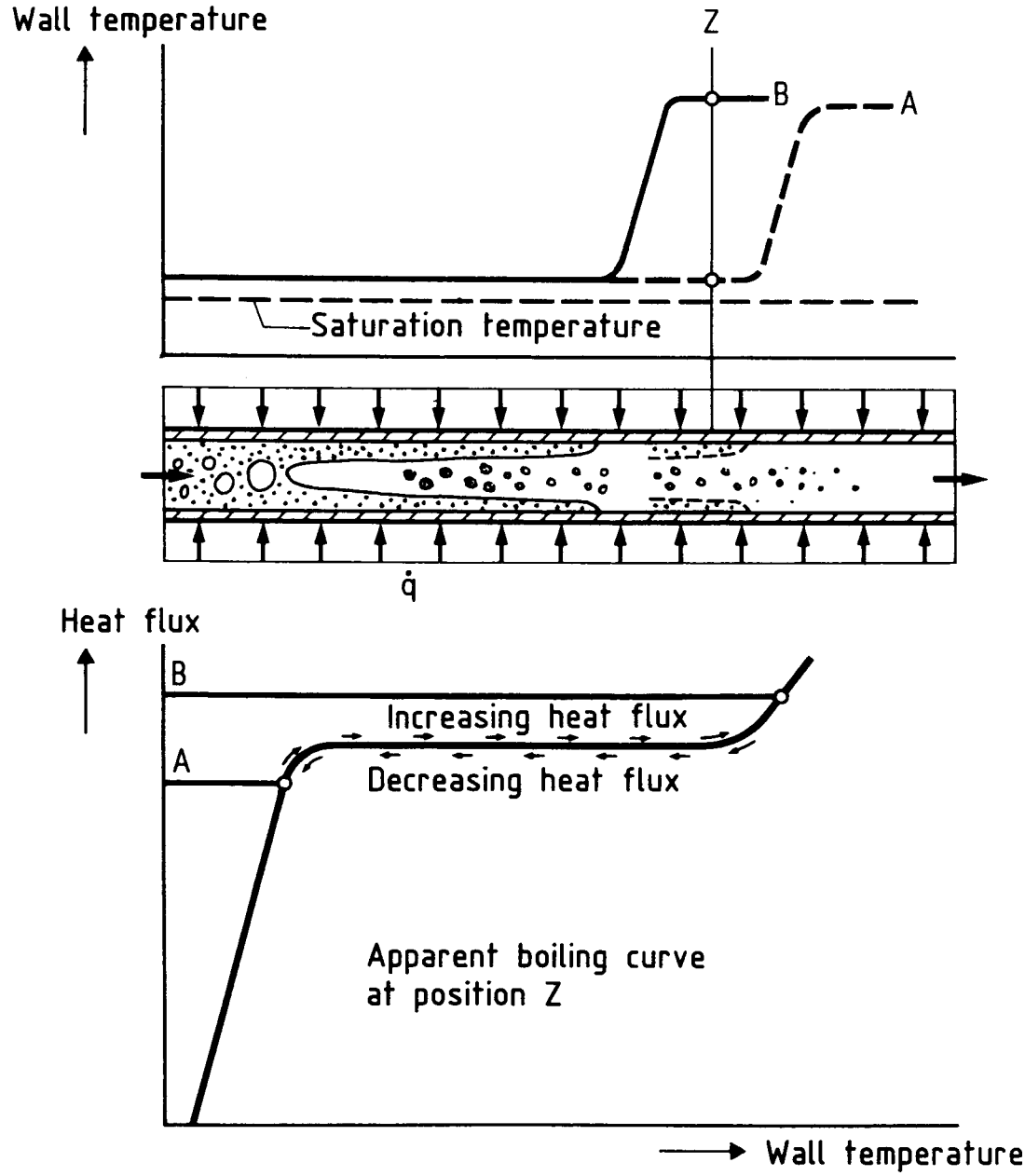


Figure 4-7 Boiling crisis in a uniformly heated evaporator tube

If the influence of the axial heat conduction is excluded, there can be observed a hysteresis in the heat flux wall temperature course also under forced convection conditions. Figure 4-8 (taken from /41/) shows the result of an experiment with a nonuniformly heated evaporator tube. At first, both tube sections are heated with the same heat flux ($\dot{q}_1 = \dot{q}_2$) in such a manner, that the boiling crisis occurs at the end of the first tube section and that the second tube section lies in the unwetted region. Through a reduction of

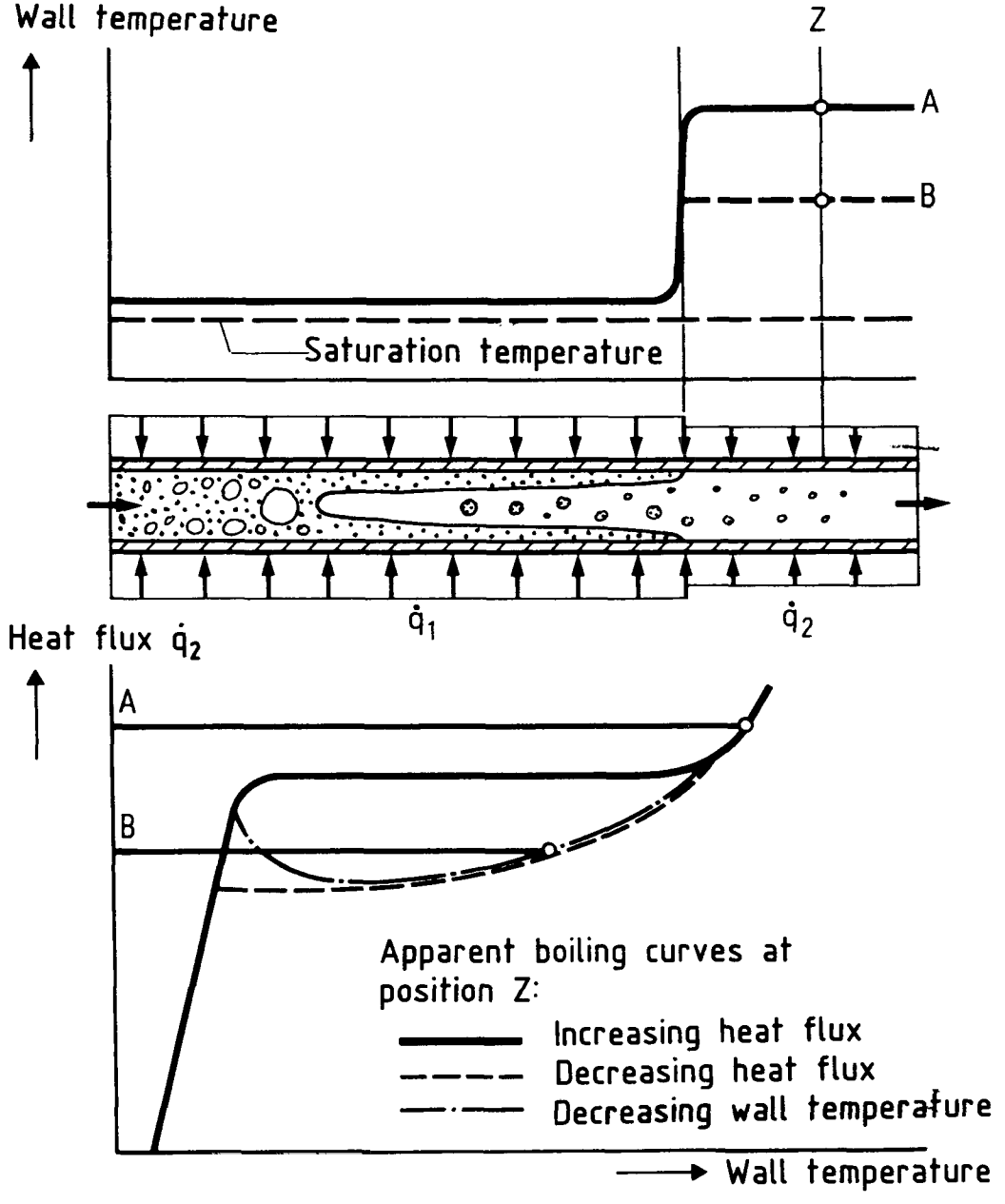


Figure 4-8 Boiling crisis in a nonuniformly heated evaporator tube

the heat flux of the second tube section ($\dot{q}_2 < \dot{q}_1$) there can be obtained the broken curve in the heat flux-wall temperature course, which is distinctly different from the solid line for increasing heat flux.

One obtains a similar result, if the second tube section is provided with a good heat-conducting storage mass and if after the superheating the second tube section is no longer heated. The released heat flux can be then determined from the rate of temperature drop of the storage mass and it shows a course (dot-dash line) which approaches very closely that of the boiling curve for pool boiling.

If one applies the findings from the course of the boiling curve under forced convection to transient processes, it is possible to present the pressure reduction from the super-critical pressure region according to Figure 4-9. In the initial state with supercritical pressure there will set-in the operating point A corresponding to the chosen heat flux. After the pressure reduction, the local boiling curve allows a stable operating point (B) for the position Z in the unwetted region and a stable operating point (C) in the wetted region. It depends on the temperature in the initial state which operating point occurs. If this temperature should be higher than the Leidenfrost temperature, at first there will not occur any wetting of the heating surface and in the opposite case wetting will occur. For the position Z shown in Figure 4-9, at first will occur film boiling after the pressure reduction. The steady state operating point C is finally attained by a wetting process, in which through axial heat conduction from the unwetted to the wetted heating surface there occurs a passing of the boiling curve from B to C.

Figure 4-10 shows the influence of an enthalpy reduction on the local boiling curve and the course of the wall temperature. To the axial position Z, which prior to the enthalpy decrease lies in the unwetted part of the evaporator and after the enthalpy decrease in the wetted part, can be assigned two boiling curves which indicate the possible operating points prior to and after the enthalpy decrease. In the initial state, at position Z the critical heat flux is exceeded and the operating point A lies in the unwetted region. If the local enthalpy is reduced, the boiling curve allows for position Z a stable operating point (B) in the unwetted region and a stable operating point (C) in the wetted region. Since, because of the reduced steam velocity, the cooling is worse after the enthalpy decrease than in the initial state, the heating surface temperature increases at first form A to B. The steady state operating point C is attained, same as after the pressure drop, through a wetting process whereby is made possible a passing of the boiling curve from B to C.

## 4.3 Influence of the Leidenfrost Temperature

Since the rise of the heating surface temperature has to be attributed to a delayed wetting of the heating surface in respect to steady state, an advancing of the wetting front, which separates the wetted from the unwetted tube section, has a strong influence on this process. The advancing of the wetting front, which is based on the axial heat conduction in the tube wall, can be calculated according to a model by YAMANOUCHI /42/.

Therein it is assumed, that for the determination of the velocity of the wetting front the heat transfer in the unwetted region can be neglected in

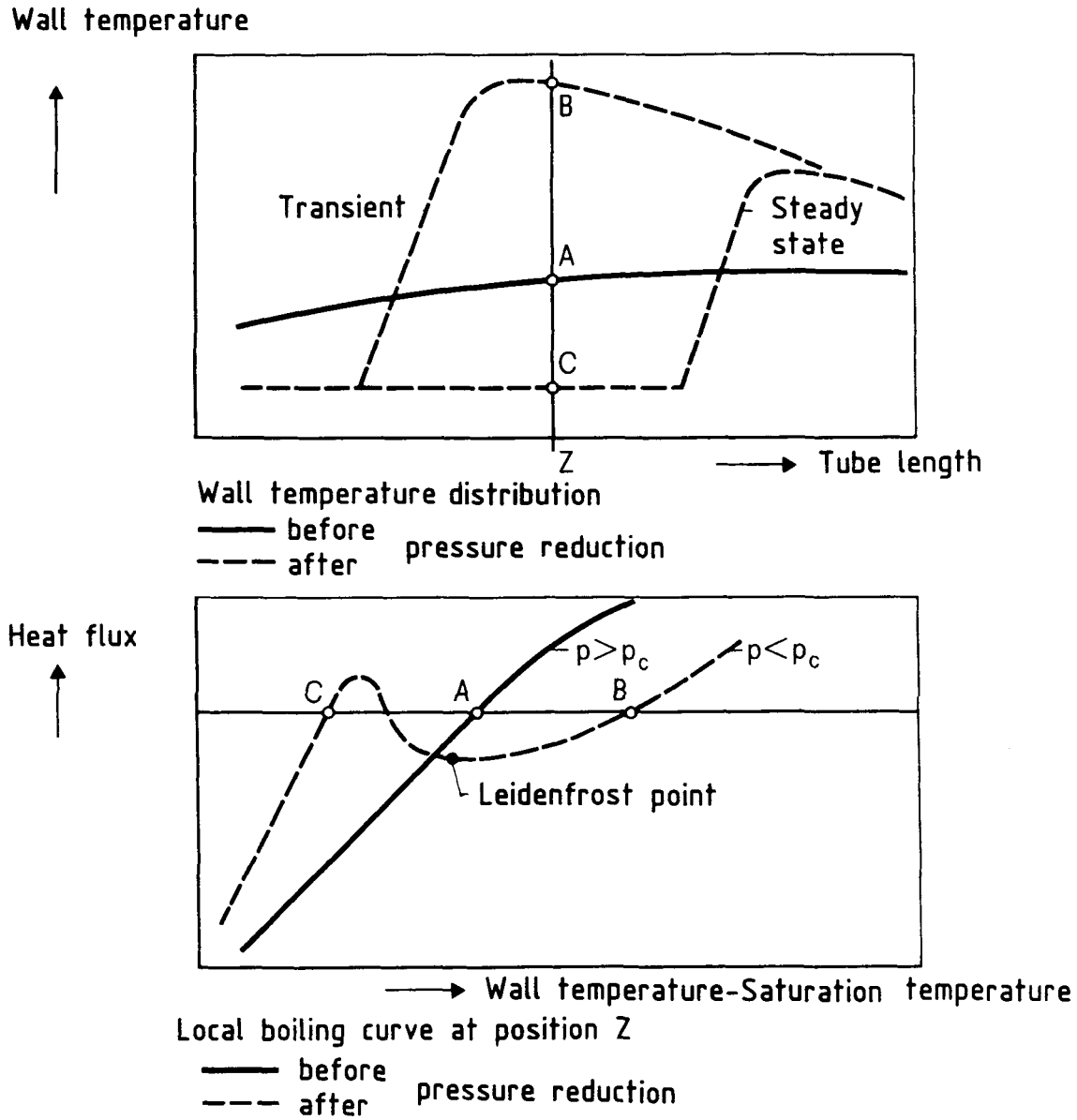


Figure 4-9 Influence of the pressure reduction on the course of the wall temperature and the local boiling curve

respect to that in the wetted region (Figure 4-11). By solving the one-dimensional, non-steady heat conduction equation, YAMANOUCHI obtains for the velocity of the wetting front

$$u = \frac{1}{\rho \cdot c}\sqrt{\frac{\alpha \cdot \lambda}{\delta}}\sqrt{\frac{(\vartheta_L - \vartheta_S)^2}{(\vartheta_\infty - \vartheta_S)(\vartheta_\infty - \vartheta_L)}} \qquad (4\text{-}1)$$

$\rho$, c and $\lambda$ are the values of the wall material, $\delta$ is the wall thickness of the tube and $\alpha$ is the heat transfer coefficient in the wetted region. $\vartheta_\infty$ is the temperature of the wall material in the unwetted region.

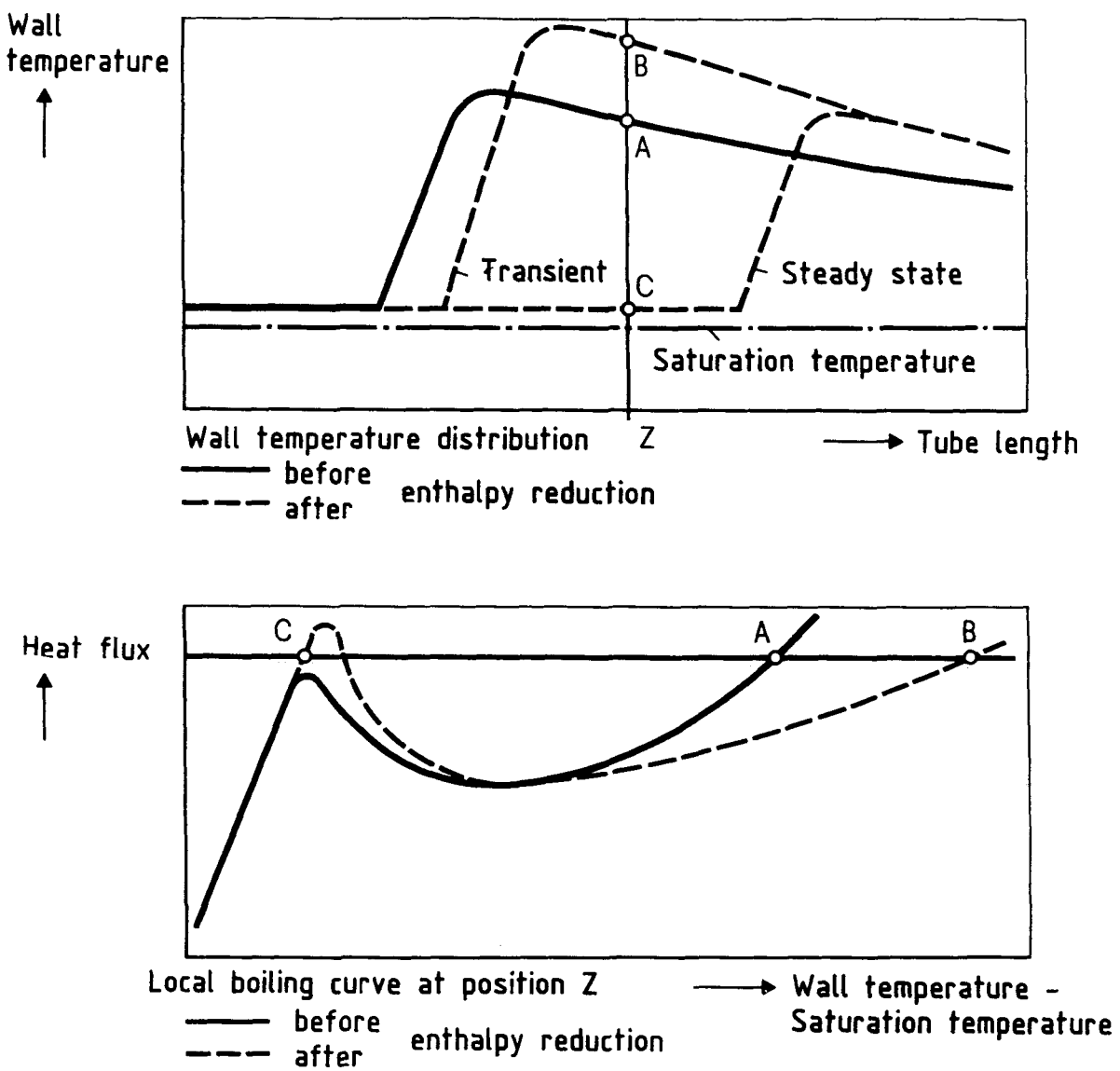


Figure 4-10 Influence of an enthalpy decrease on the course of the wall temperature and the local boiling curve

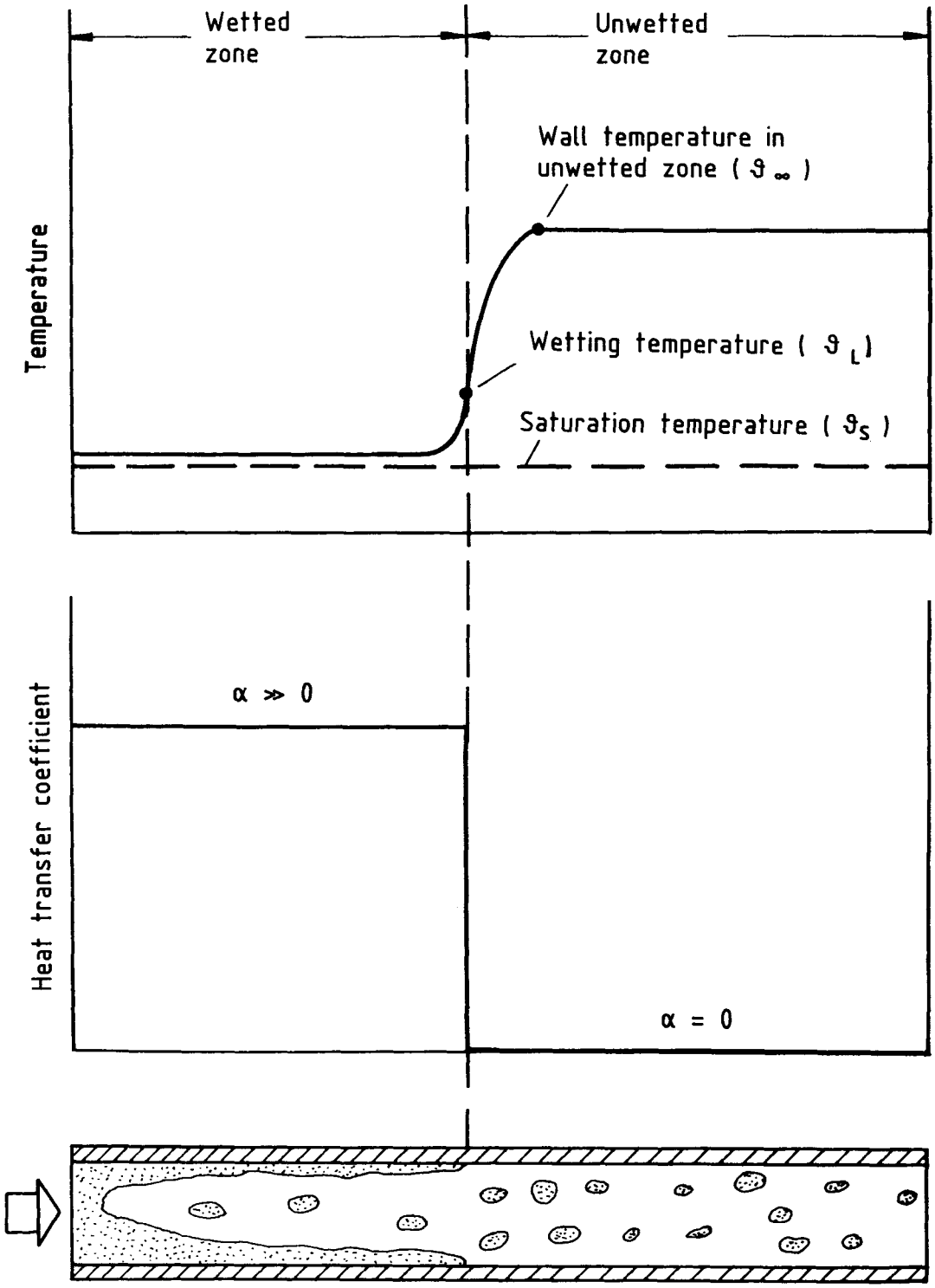


Figure 4-11 Wetting process according to the YAMANOUCHI model

Equation (4-1) shows that the velocity of the wetting front depends greatly on the difference between the Leidenfrost and the saturation temperatures.

If the Leidenfrost temperature is considerably higher than the saturation temperature of the fluid, the wetting front can follow the fluid-dynamic changes of the system and the transient process behaves quasi-steady in respect to the heat transfer. Otherwise, the wetting front velocity drops considerably.

The dependence of the Leidenfrost temperature on the pressure was experimentally determined by HEIN /43/ for water and the model medium R 12 based on the cooling curves of a submersible probe. While for R 12 it was possible to investigate the pressure dependence up to the critical pressure, due to the design limits it was possible to conduct the experiments with water only up to a reduced pressure of 0.32. From Figure 4-12 it can be gathered that in R 12 the Leidenfrost temperature in the lower pressure region lies approximately 30 to 50 K above the saturation temperature and in the high pressure region only approximately 4 K. Also, from the results presented in the same figure it can be seen, that with increasing pressure there occurs an approximation of the Leidenfrost temperature to the saturation temperature, and that in the high pressure region also for water there can be qualitatively started from a similar course of the Leidenfrost temperature as in the case of R 12.

Also measurements of the wetting temperature with forced convection, which were conducted by KEFER /44/ up to a pressure of 220 bars, show the approximation of the Leidenfrost temperature to the saturation temperature in the proximity of the critical pressure (Figure 4-13). Due to the higher turbulences, however, the measured wetting temperatures are herein higher than the values determined with a submersible probe.

The approximation of the Leidenfrost temperature to the saturation temperature in the proximity of the critical pressure is thus responsible for the observed wall temperature excursions. On the other hand, during transient processes in the low pressure region there were measured only rises of wall temperatures which, taking into account the mass dynamics or changes of the material values, can be attained by calculations.

## 4.4 Mathematical Model for the Determination of the Influence of Pressure and Enthalpy Transients on the Heat Transfer

As shown in the foregoing chapters, a decrease of the heat transfer takes place if the wetting front cannot follow the thermal and fluid-dynamic changes of the system during the transient.

While the system magnitudes, such as pressure-, enthalpy-and mass flow course can be determined with the aid of computer programs taking into consideration the storage processes, the location of the boiling crisis for the steady state can be calculated according to Chapter 3.2.

Equation (4-1) can be used in principle for the determination of the wetting front velocity. Therein there has to be known for each moment the temperature of the wall material in the unwetted region, the Leidenfrost temperature as well as the heat transfer coefficient in the wetted region. For the availability of these magnitudes there is required a numerical calculation method with accurate time and local discretization.

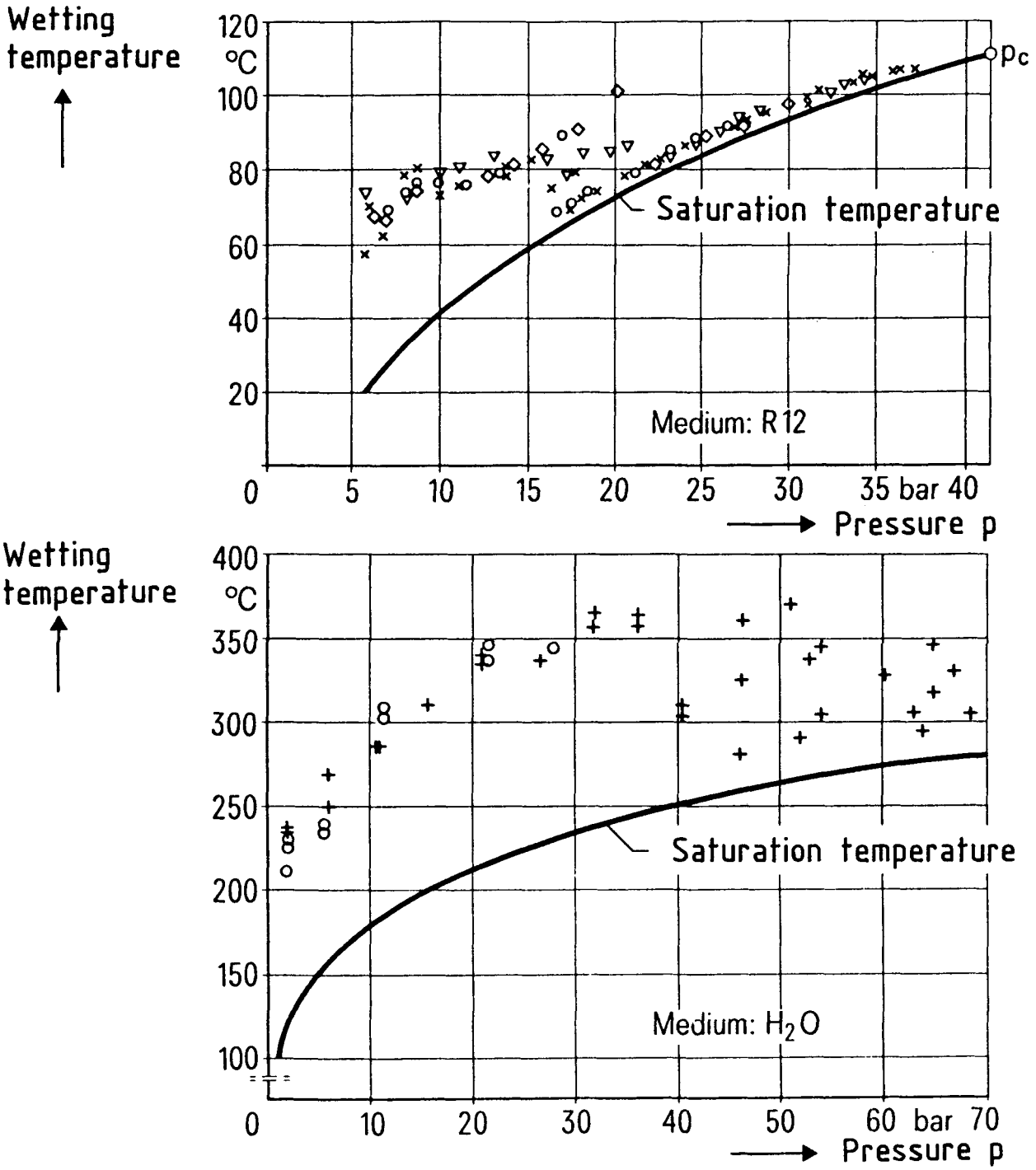


Figure 4-12 Dependence of Leidenfrost temperature on pressure

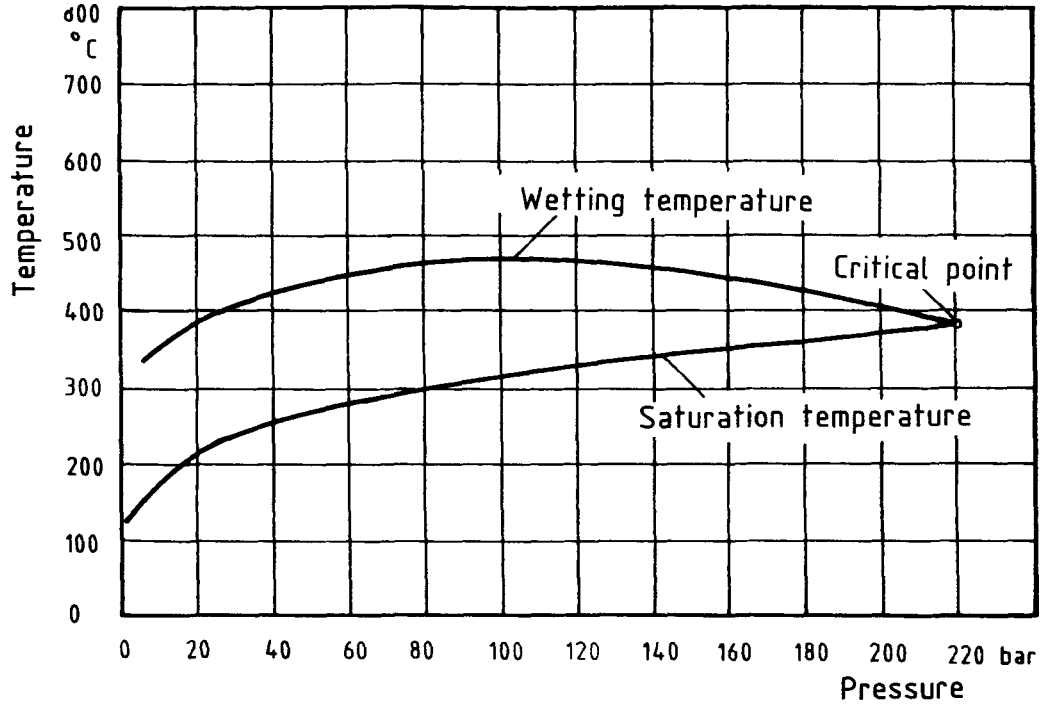


Figure 4-13 Course of the Leidenfrost temperature with forced convection

From the experimental values there was determined an empirical relationship for the progress of the wetting front. With the aid of the known magnitudes from equation (4-1) it is possible to apply the result to a tube geometry with different material values and different wall thickness.

From the measured wetting front velocities there can be derived the following statements:

1. The wetting front velocity is independent of the extent of the enthalpy or pressure decrease and it is also independent of how quickly this change takes place. However, the transient has to occur at least so quickly, that the wetting front cannot quasi-steady follow the process. Otherwise, the wetting front velocity can be determined from the locations of the boiling crisis for the intermediate states that are to be considered steady.

2. If the ratio of supplied heat flux to the mass flow remains constant, the wetting front velocity remains also constant. This can be attributed to the fact that the wall temperature in the unwetted region remains constant at the first approximation if the ratio of the heat flux to the mass flow is not changed. If one assumed that the Leidenfrost temperature and the heat transfer coefficient is the wetted region remain unchanged for the considered parameter change, from equation (4-1) it can be gathered that

the wetting front velocity cannot change if the wall temperature in the unwetted region is of a constant value.

3. In a semilogarithmical plot it is possible to represent the influence of the pressure on the wetting front velocity as a straight line. The wetting front velocity drops considerably with increasing pressure, which is caused by the approximation of the Leidenfrost temperature to the saturation temperature.

Taking into account these statement and the material value and geometry influence of equation (4-1) there was formulated the semi-empirical equation (4-2) for the determination of the wetting front velocity:

$$u = 27.35 \cdot \frac{1}{\rho \cdot c} \cdot \sqrt{\lambda/\delta} \cdot (\dot{m}/\dot{q})^2 \cdot e^{-0.019 \cdot p} \qquad (4\text{-}2)$$

Herein $\rho$, $c$ and $\lambda$ are the values of the wall material and $\delta$ the wall thickness of the evaporator tube. $\dot{m}$, $\dot{q}$ and $p$ are the operating parameters mass velocity, heat flux and pressure.

The influence of the values of the wall material ($\rho$, $c$ and $\lambda$) as well as the wall thickness $\delta$ of the evaporator tube were taken from the YAMANOUCHI model (equation 4-1).

The factor $(\dot{m}/\dot{q})^2$ in equation (4-2) was empirically determined. If one assumes, that the wall temperature in the unwetted region is considerably higher than the saturation temperature and the Leidenfrost temperature, according to equation (4-1) the wetting front velocity becomes approximately inversely proportional to the difference between wall and saturation temperature in the unwetted region.

$$u \sim 1/(\vartheta_\infty - \vartheta_S) \qquad (4\text{-}3)$$

If, as with single-phase flow, the heat transfer coefficient in the unwettd region were approximately proportional to the mass flow and independent of the heat flux, according to equation (4-3) it follows

$$u \sim \dot{m}/\dot{q} \qquad (4\text{-}4)$$

However, in the post-dryout region the heat transfer coefficient increases more than proportionally with increasing mass flow and decreases with increasing heat flux. This can be attributed to the thermal non-equilibrium between steam and water droplets (cf. Chapter 3) and explains the dependence of the wetting front velocity on the mass and heat flux, as determined by equation (4-2).

Also the influence of the pressure was empirically determined by equation (4-2) with

$$u \sim e^{-0.019 \cdot p} \qquad (4\text{-}5)$$

According to YAMANOUCHI (equation (4-1)) the wetting front velocity is approximately proportional to the difference between Leidenfrost and saturation temperature

$$u \sim \vartheta_L - \vartheta_S \qquad (4\text{-}6)$$

This difference decreases with increasing pressure. This is taken into account in equation (4-2) by the described pressure dependence.

As shown by Figures 4-14 and 4-15 it is possible to verify the measured wetting front velocities with sufficient accuracy by equation (4-2). The comparison was based on experiments with a stainless steel tube with a wall thickness of $\delta = 2 \cdot 10^{-3}$m.

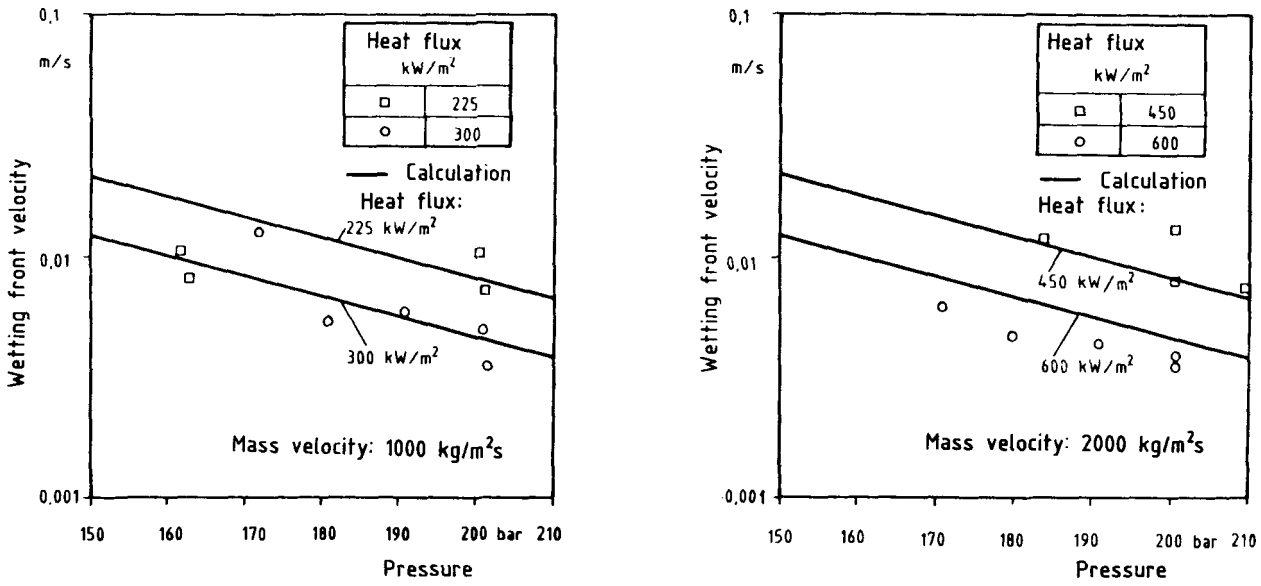


Figure 4-14 Wetting front velocity with a pressure drop

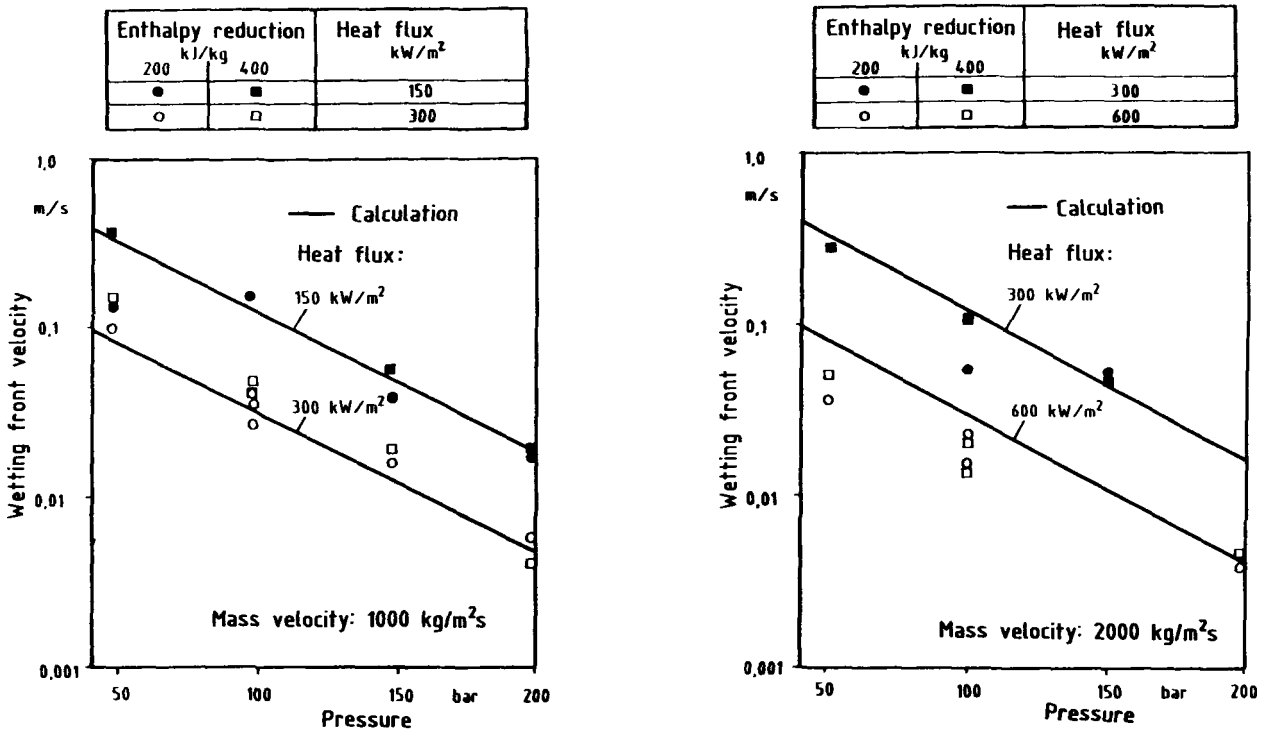


Figure 4-15 Wetting front velocity with an enthalpy reduction

# 5 INFLUENCE OF THE TUBE ORIENTATION ON THE HEAT TRANSFER

## 5.1 Flow Patterns and Heat Transfer Regions

While in a vertical tube flow there is present a symmetrical distribution of the steam and water phase over the cross-section, in the case of a tube with horizontal flow there occurs a more or less distinct phase separation due to the gravity effect. The heavier medium (water) flows preferably in the lower tube region while the lighter steam flows above it. The greater the ratio of the buoyant forces to the turbulent mixed forces of the flow, the greater the difference to the vertical tube flow. This is the case with decreasing specific mass flow or increasing tube diameter.

Figure 5-1 shows typical flow configurations in a horizontal tube. With increasing steam quality the shown flow configurations traverse not always an evaporator tube. With the help of flow pattern charts /45/ to /47/ it is possible to determine which flow patterns are possible in a horizontal tube with a determined parameter combination.

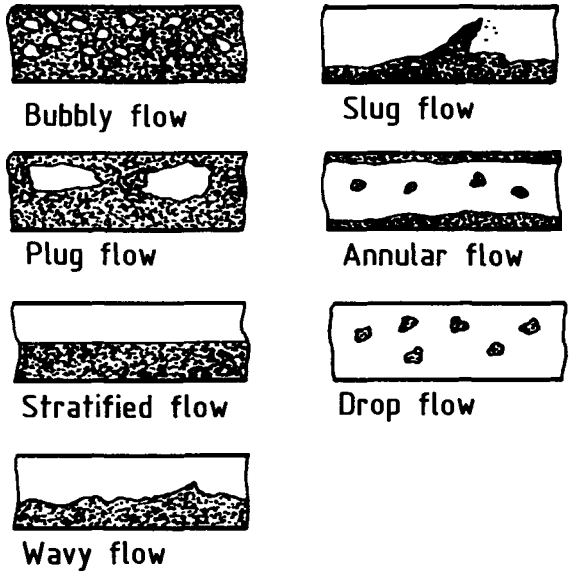


Figure 5-1 Flow patterns in horizontal tube

Since the flow pattern also influences the heat transfer it has to be expected that, if the flow patterns differ greatly with vertical and horizontal tube orientations, there will also occur different heat transfer regions. Figure 5-2 shows a typical wall temperature course for a horizontal tube with strong influence of the tube orientation on the heat transfer. Therein can be observed the following developments with increasing flow enthalpy:

Caused by a thermal convection flow occurring in a heated, horizontally flow-traversed tube, which is superposed over the forced convection flow, the fluid temperature, and thus also the wall temperature, rises higher on the upper side than on the bottom side of the tube. Boiling occurs correspondingly earlier on the upper side. Due to the force of gravity, the originating steam collects in the upper tube part. Stratified flow occurs and dryout of the heating surface takes place on the upper side of the tube. Boiling was not even attained at the tube bottom at the same axial tube position.

With increasing enthalpy the void fraction in the flow and thus the mixture velocity increases. Slug or annual flow occurs and the upper side of the tube is rewetted. Finally, with a further heat supply the water film breaks off, and dries out, at first at the upper side and with a much higher enthalpy also at the bottom side.

From the shown example it can be seen, that in a horizontal evaporator tube a dryout of the heating surface on the upper side can occur already in the subcooled region, while the bottom side remains wetted up to the complete evaporation of the fluid.

If the mass velocity is greatly increased, the turbulent mixture forces of the flow prevail and cause a symmetrical distribution of the steam and water

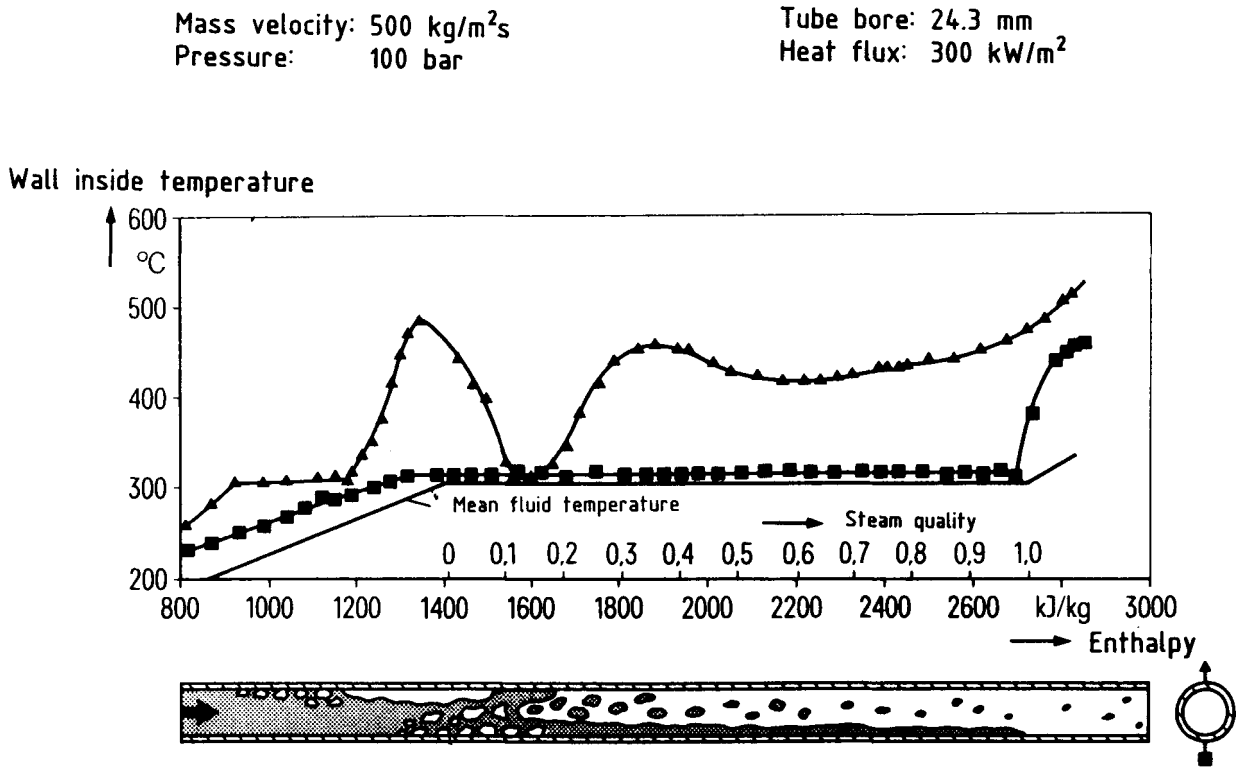


Figure 5-2 Influence of gravity on the heat transfer in horizontal tubes

phase. Thus, the wall temperature on the upper and the bottom sides of the tube have the same course. Figure 3-21 is an example of this. The heat transfer regions are therein identical with those in the vertical tube.

## 5.2 Heat Transfer in the Wetted Region

In the horizontal tube, with certain parameter combinations, there were measured great temperature differences between the upper and the bottom sides of the tube in the region of the water flow. From Figure 5-3 it can be gathered that, with a mass velocity of 500 kg/m$^2$s and a heat flux of 300 kW/m$^2$, these temperature differences amount to approximately 40 K. The measured wall temperatures with vertical flow, which were also entered in the Figure, lie between the temperatures of the upper and bottom sides. They are however shifted toward the temperatures on the bottom side of the horizontal tube. Also the temperatures which were measured along a lateral surface line on the horizontal tube do not

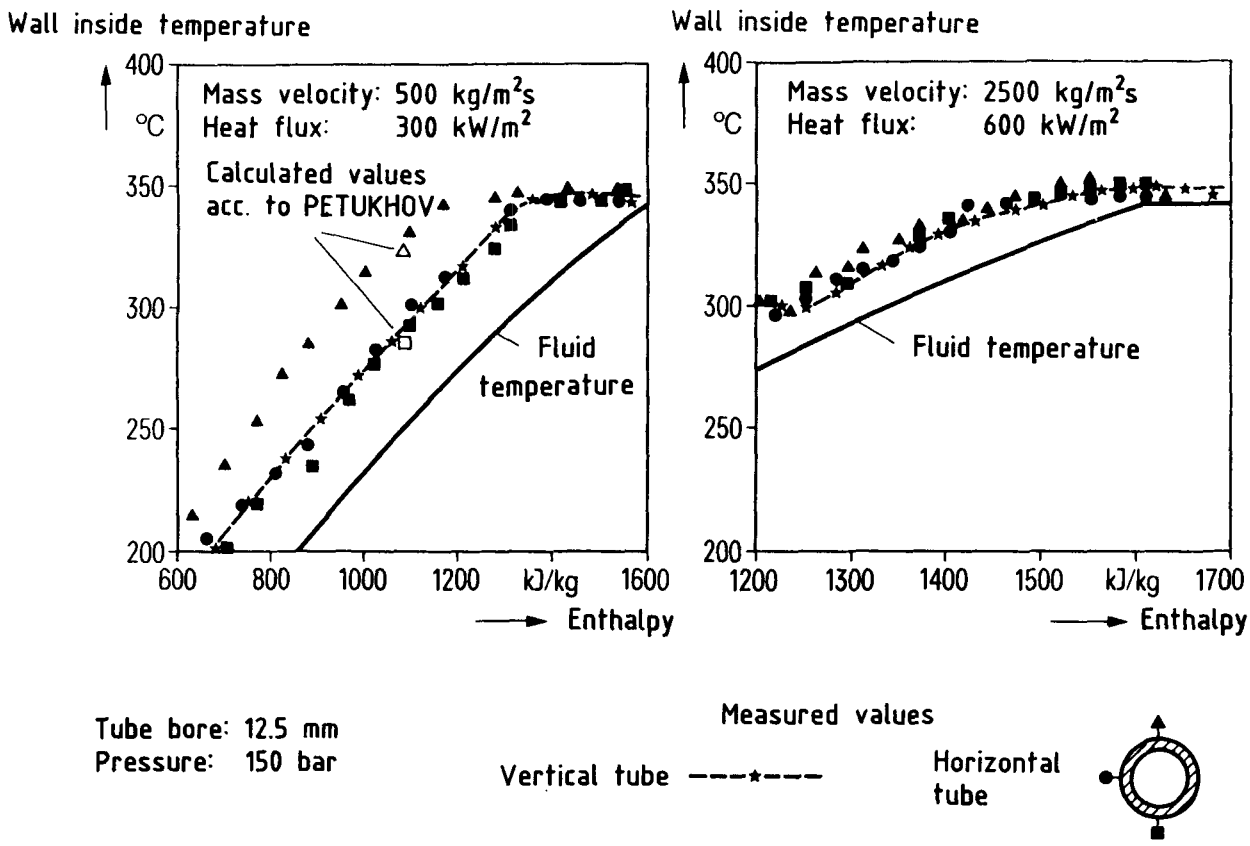


Figure 5-3 Influence of the tube orientation on the heat transfer with one-phase water flow and with subcooled boiling

lie in the middle between the values on the upper side, and bottom side. They are also shifted toward the temperatures on the bottom side. From Figure 5-3 can also be gathered, that the temperature differences disappear when the mass flow is increased.

The temperature differences between the upper and the bottom side of the horizontal tube are caused by a thermal convection flow, which is superposed over the forced convection flow. Thereby, the heated fluid rises upward in the proximity of the wall. Figure 5-4 presents typical wall temperatures, measured on the outside of the heated tube. If one conceives the gravity-dependent thermal convection flow in the shown manner, on the upper side of the tube there is created a stagnation zone which the thermal convection flow takes in only to a limited extent. The fluid is there considerably quicker heated-up than in the rest of the tube, whereby the wall temperature rises correspondingly. It is of interest that the turbulent fluctuations, which should be already very distinct with a Reynolds number of 96000, does not lead to a greater reduction of the temperature differences.

For the verification of the temperature differences there was used the PETUYKHOV /48/ model, which covers the thermal convection flow and allows thus to calculate the wall temperatures as a function of the peripheral angle. According to this model, the local Nusselt number has the following form:

$$\frac{Nu}{\overline{Nu}} = 1 - \frac{340 \cdot Gr \cdot \cos\Psi}{Re^{2.75} \cdot Pr^{0.5}} \cdot \frac{1}{1 + 2.4\ Re^{-1/8} \cdot (Pr^{2/3} - 1)} \qquad (5\text{-}1)$$

is the mean Nusselt number and, according to PETUKHOV, is calculated as

$$\overline{Nu} = \frac{(\xi/8) \cdot Re \cdot Pr}{1.07 + 12.7 \cdot \xi/8 \cdot (Pr^{2/3} - 1)} \qquad (5\text{-}2)$$

where $\xi = (1.82 \cdot \log_{10} Re - 1.64)^{-2}$ Tube friction coefficient

$Gr = \frac{g \cdot \beta \cdot \dot{q} \cdot d^4}{\lambda \cdot \nu^2}$ *Grashof number*

$Re = \frac{\dot{m} \cdot d}{\eta}$ Reynolds number

$Pr = \frac{\eta \cdot c}{\lambda}$ Prandtl number

$\Psi$ = peripheral angle (upper side $\Psi = 0$, bottom side $\Psi = \pi$)

As it can be gathered from Figure 5-3, the model renders sufficiently well the test values with a mass velocity of 500 kg/m$^2$s. If the mass velocity is increased to 2500 kg/m$^2$s, with the chosen parameters for the model, as well as in the experiment, there cannot be observed an influence of the thermal convection.

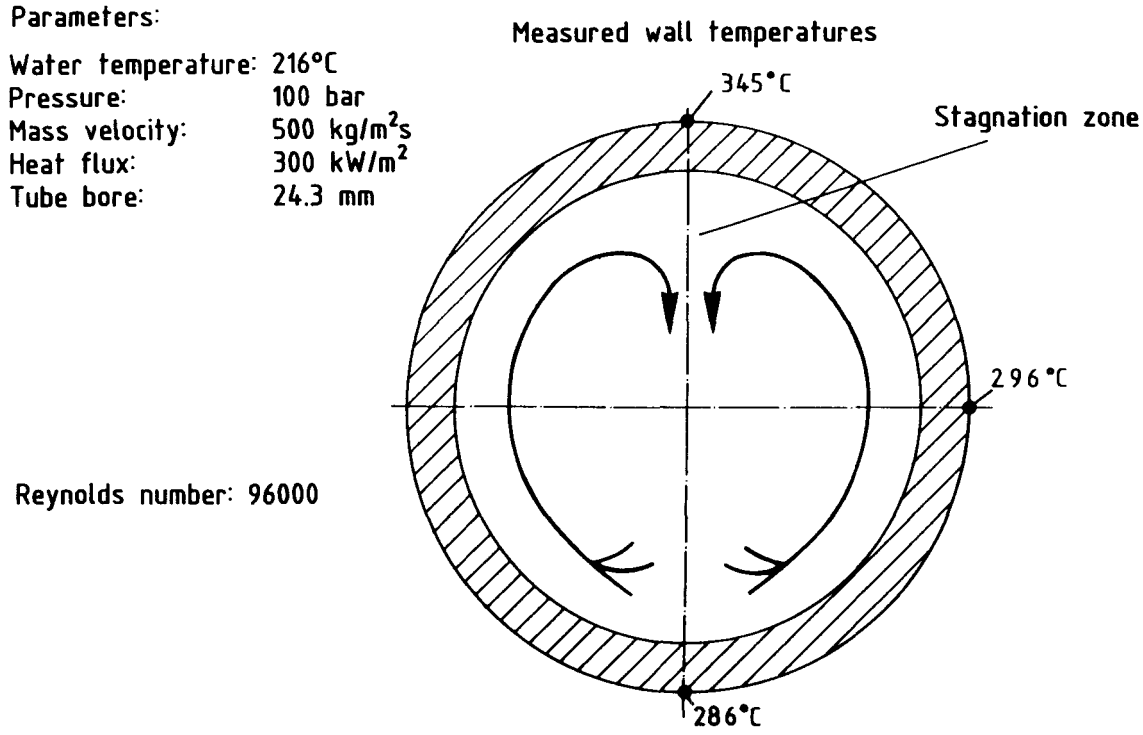


Figure 5-4 Influence of the thermal convection on the wall temperature course with horizontal flow

In the case of the extreme conditions, which is the case with a high ratio from the Grashof to the Reynolds number, the PETUKHOV model can fail and even calculate negative Nusselt numbers on the upper side of the tube. Thus, the model furnishes, e.g., for the parameters in Figure 5-2, excessively high temperatures on the upper side of the tube.

The temperature differences between the upper and the bottom sides of the horizontal tube disappear, or they cannot be detected with the measuring technique used if boiling sets in over the entire tube circumference (cf. Figure 5-3).

## 5.3 Critical Boiling States

As already shown by Figure 5-2, in the horizontal tube transfer from the wetted to the unwetted heating surface state does not take place in an axial position. The course of the critical heat flux as function of the steam quality can be of entirely different shape on the upper side of the tube than on the bottom side (cf. Figure 5-5). In a limited region of the heat flux it is also possible to record several times the boiling crisis on the upper side of the tube. However, for the evaluation of the heat transfer in the region of the boiling crisis it suffices to know the locations of the first occurrence of the boiling crisis (on the upper side of the tube) and of the last one (one the bottom side of the tube).

Figures 5-6 to 5-11 show measured critical heat flux as function of the steam quality. The values for the first occurrence of the boiling crisis (Δ) are connected with the values for the last occurrence (□) by horizontal lines. Therefrom can be seen the steam quality region, in which has to be expected the boiling crisis in the tube. If the boiling crisis on the upper side was recorded several times (as, e.g., in the example shown in Figure 5-2), several triangles are entered on one line. If the boiling crisis could not be measured on the bottom side up to the outlet of the tube, there is no square entered and the horizontal line is drawn up to the steam quality at the outlet of the tube.

The steam qualities, calculated according to KON'KOV (cf. equation (3-2)) and measured on a vertical upflow tube, lie frequently between the values of the upper and bottom sides of the horizontal tube. With increasing tube diameter (Figures 5-9 to 5-11), increases the difference of the critical steam quality between the upper side and the bottom one.

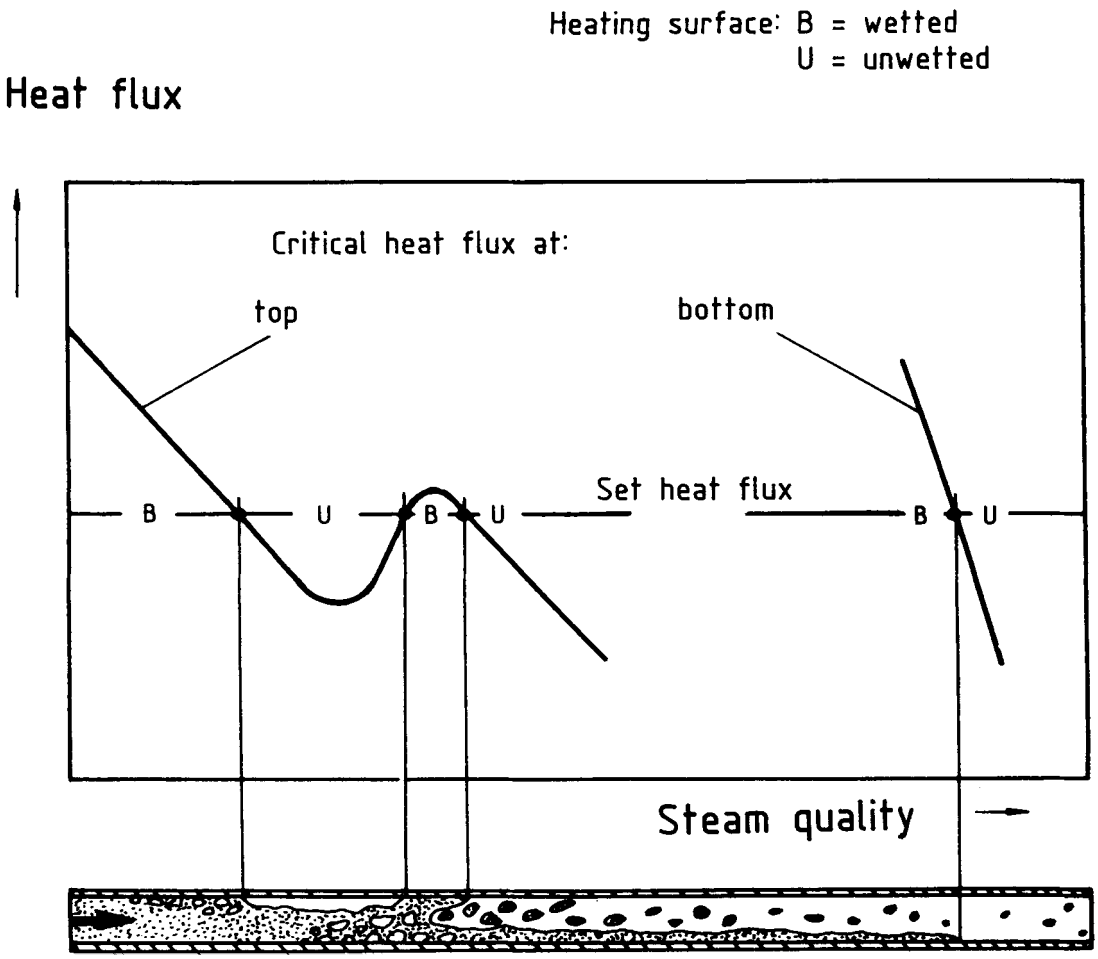


Figure 5-5 Course of the critical heat flux density with horizontal flow

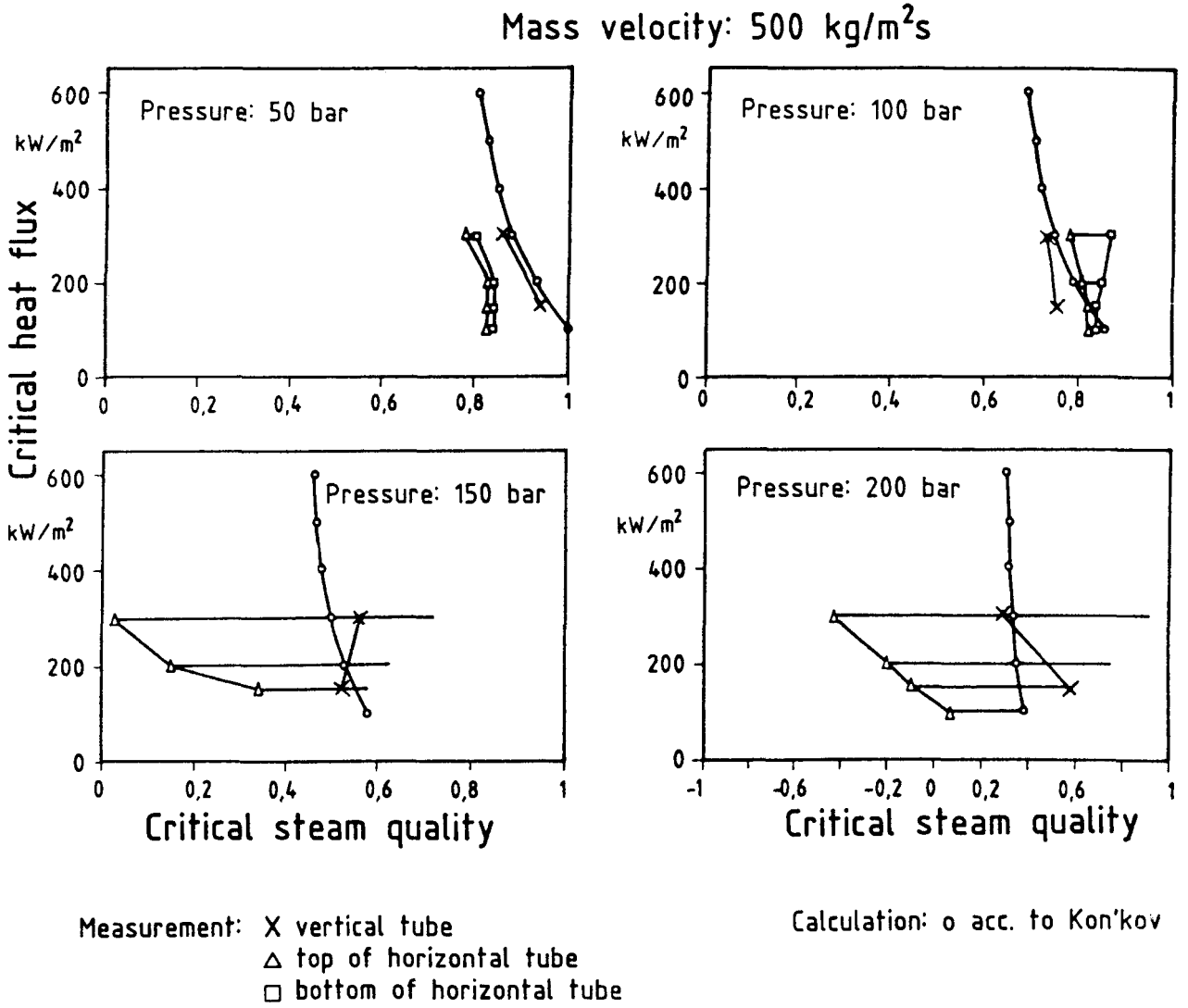


Figure 5-6 Critical heat flux as function of the steam quality (tube bore 12.5mm)

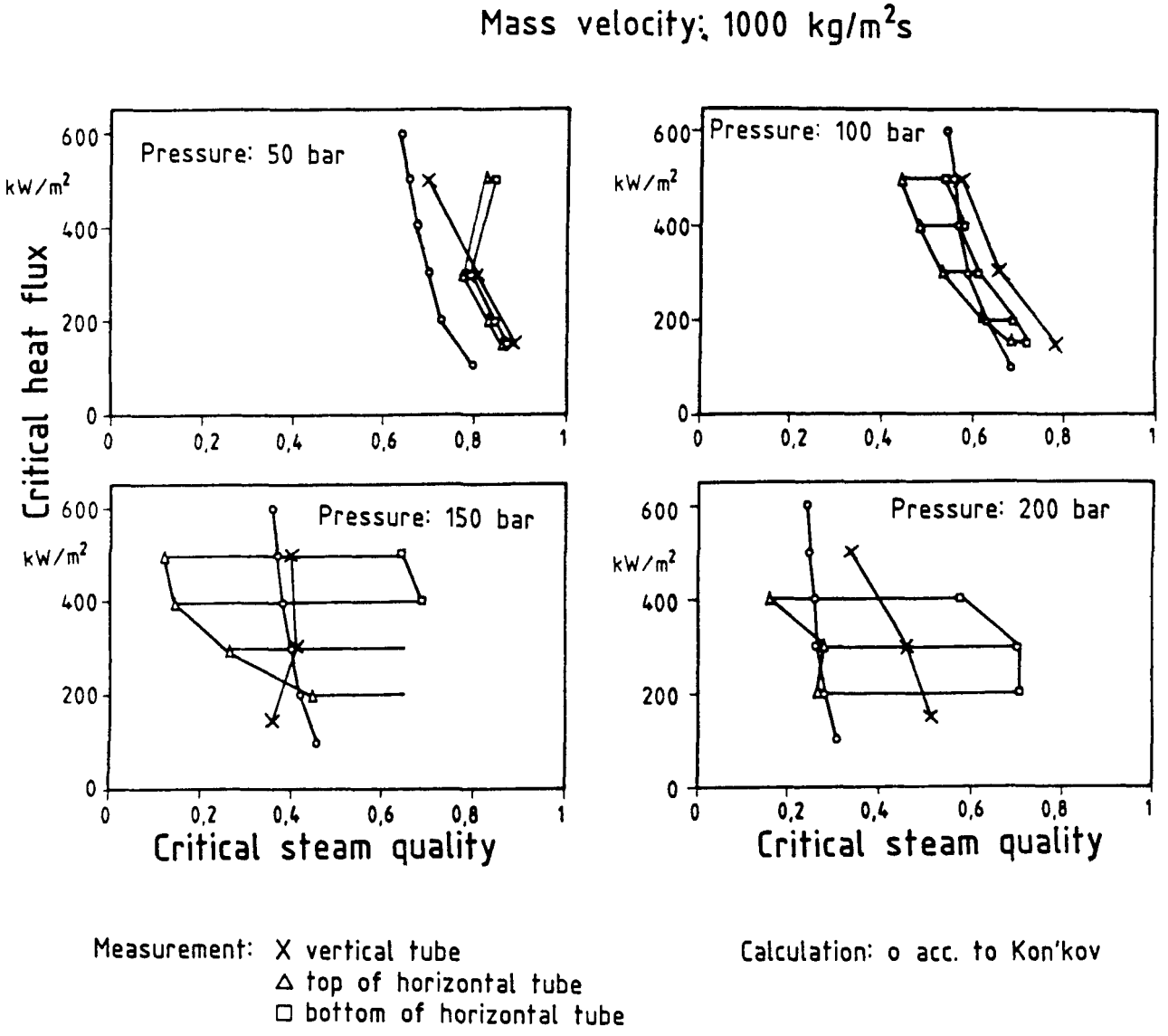


Figure 5-7 Critical heat flux as function of the steam quality (tube bore 12.5 mm)

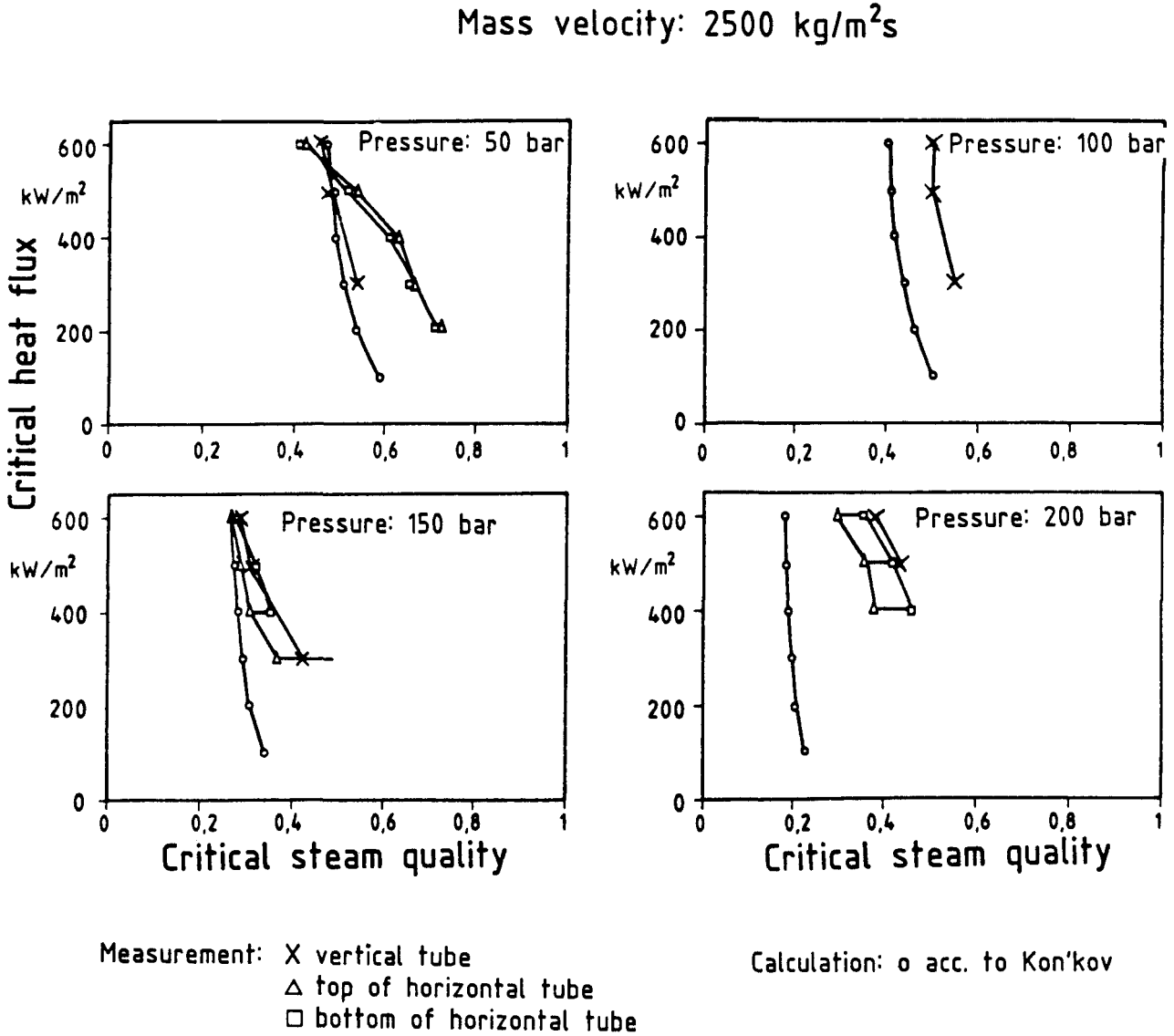


Figure 5-8 Critical heat flux as function of the steam quality (tube bore 12.5 mm)

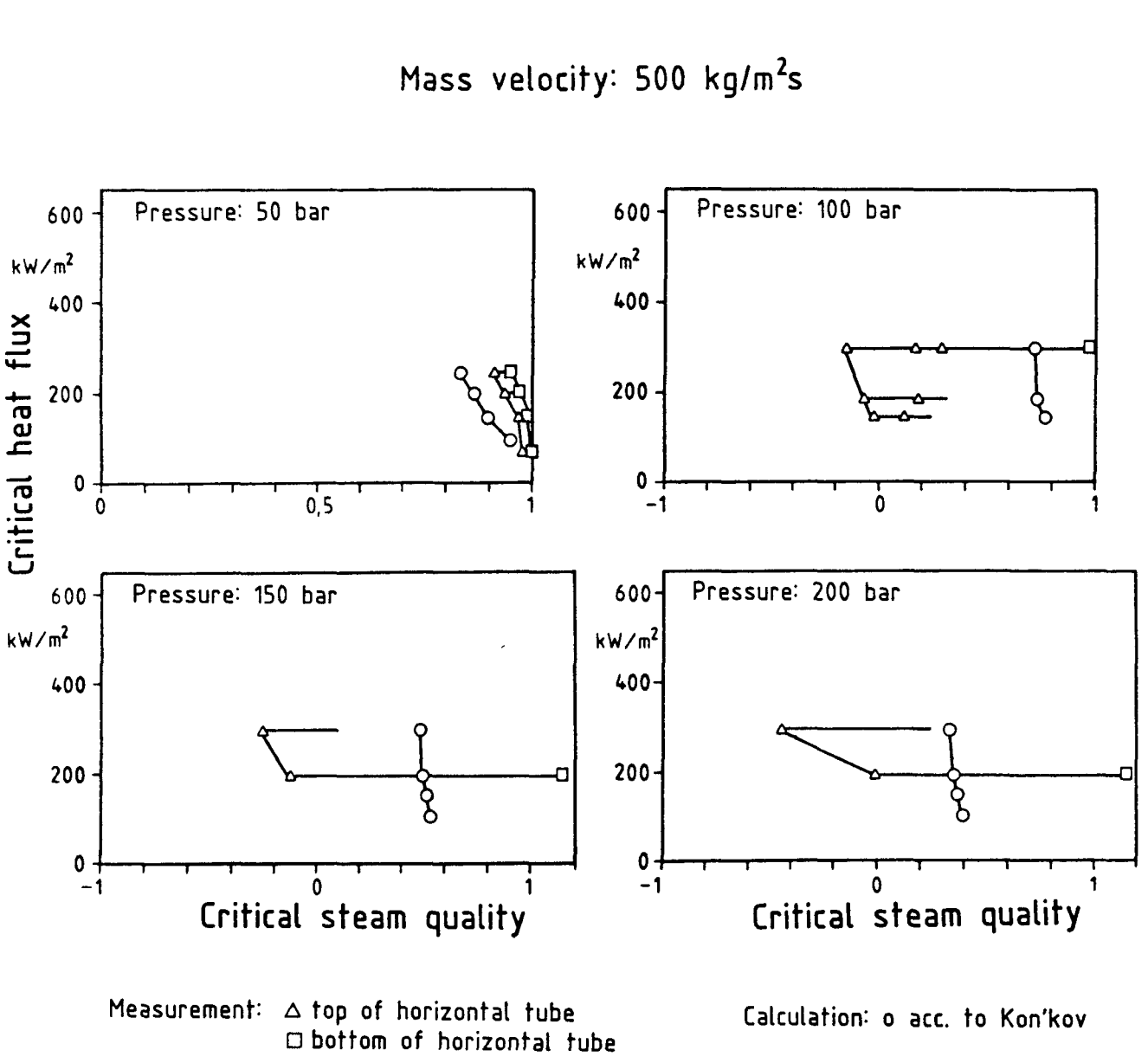


Figure 5-9 Critical heat flux as function of the steam quality (tube bore 24.3 mm)

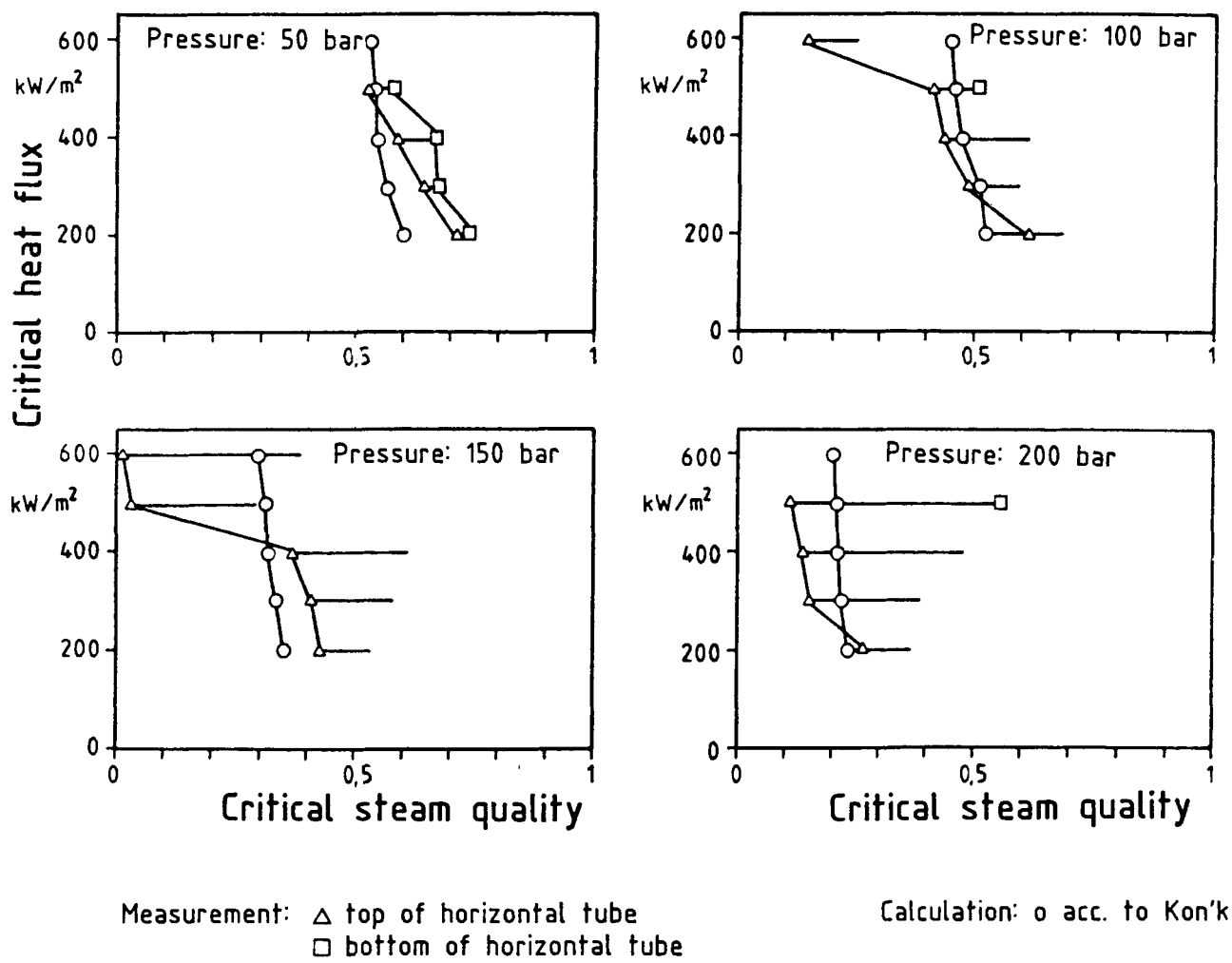


Figure 5-10 Critical heat flux as function of the steam quality (tube bore 24.3 mm)

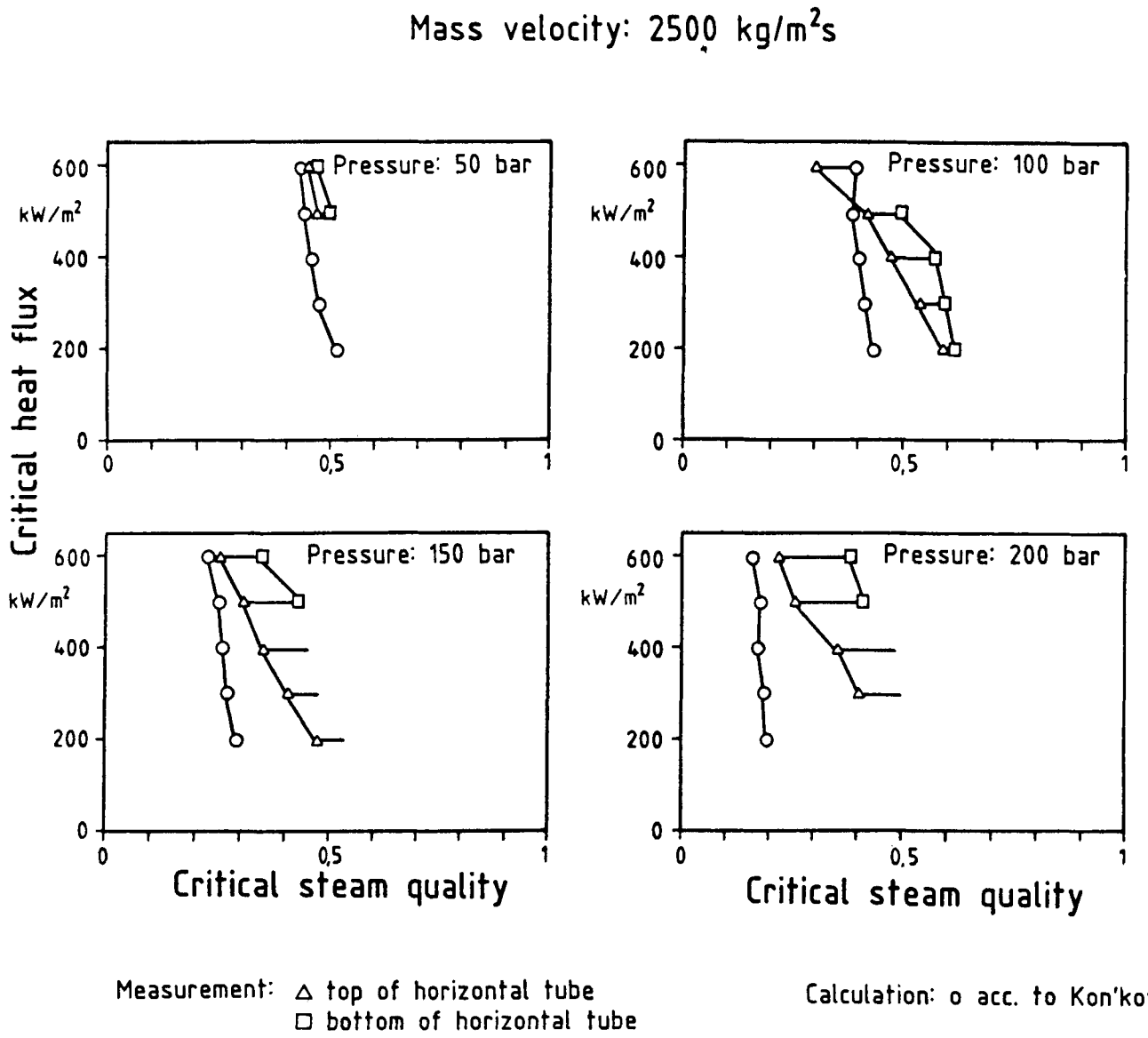


Figure 5-11 Critical heat flux as function of the steam quality (tube bore 24.3 mm)

Figure 5-12 shows, by way of example, the course of the critical heat flux for various mass velocities with a pressure of 100 bars. In contrast to the vertical tube, where a monotonic decrease of the critical heat flux can be expected with increasing steam quality, the relationships in Figure 5-12 are considerably more complicated.

The difference of the critical steam quality between the upper and the bottom sides of a tube with horizontal flow is shown in Figure 5-13. Within the measured heat flux region there was determined an average critical steam quality region for each of the parameters mass velocity, pressure and tube diameter. The difference of the critical steam quality decreases with increasing mass flow and increases with rising pressure.

An increasing mass flow leads to increased turbulent fluctuations in the flow and thus to a decrease of the influence of gravity. On the other hand, if one compares experiments with the same mass velocity, the velocity of the two-phase mixture decreases with rising pressure as a consequence of the increasing steam density. With higher pressure the velocity effect prevails evidently over the influence of the decreased buoyance of the steam phase. A larger tube diameter causes an increase of the gravitational influence.

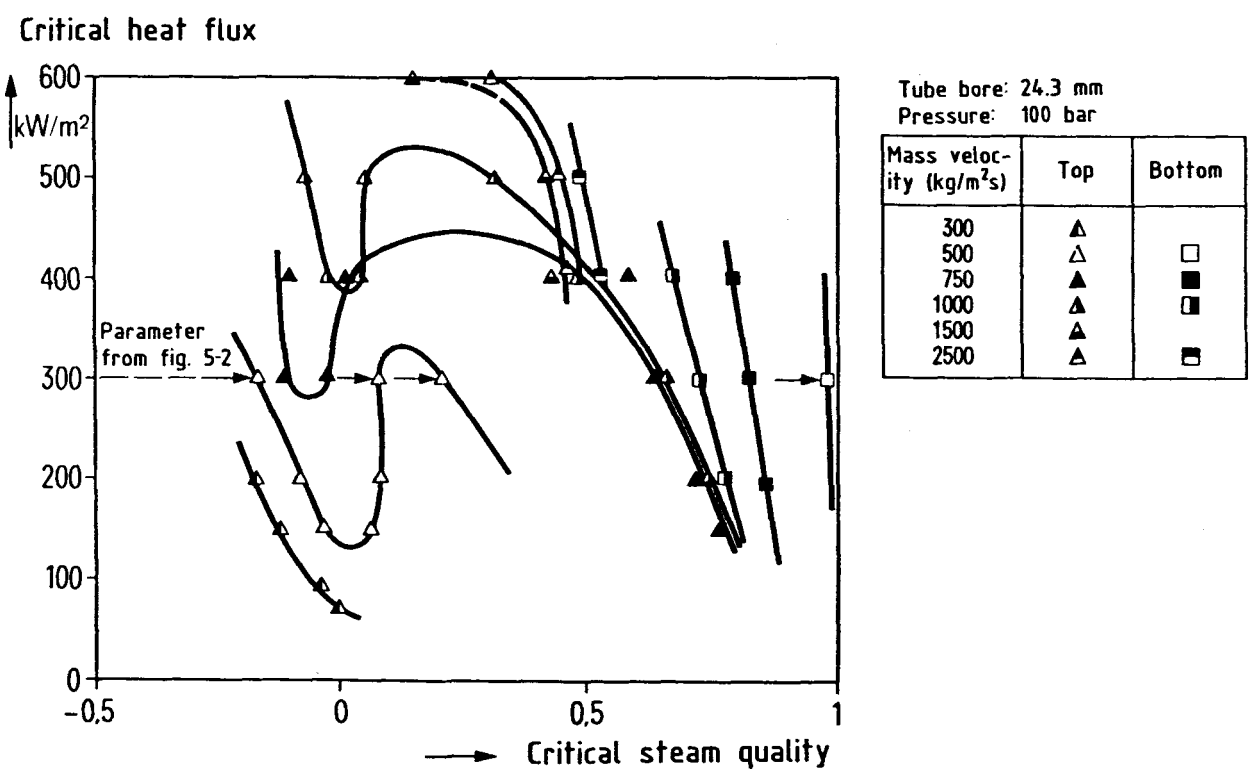


Figure 5-12 Course of the critical heat flux with horizontal flow

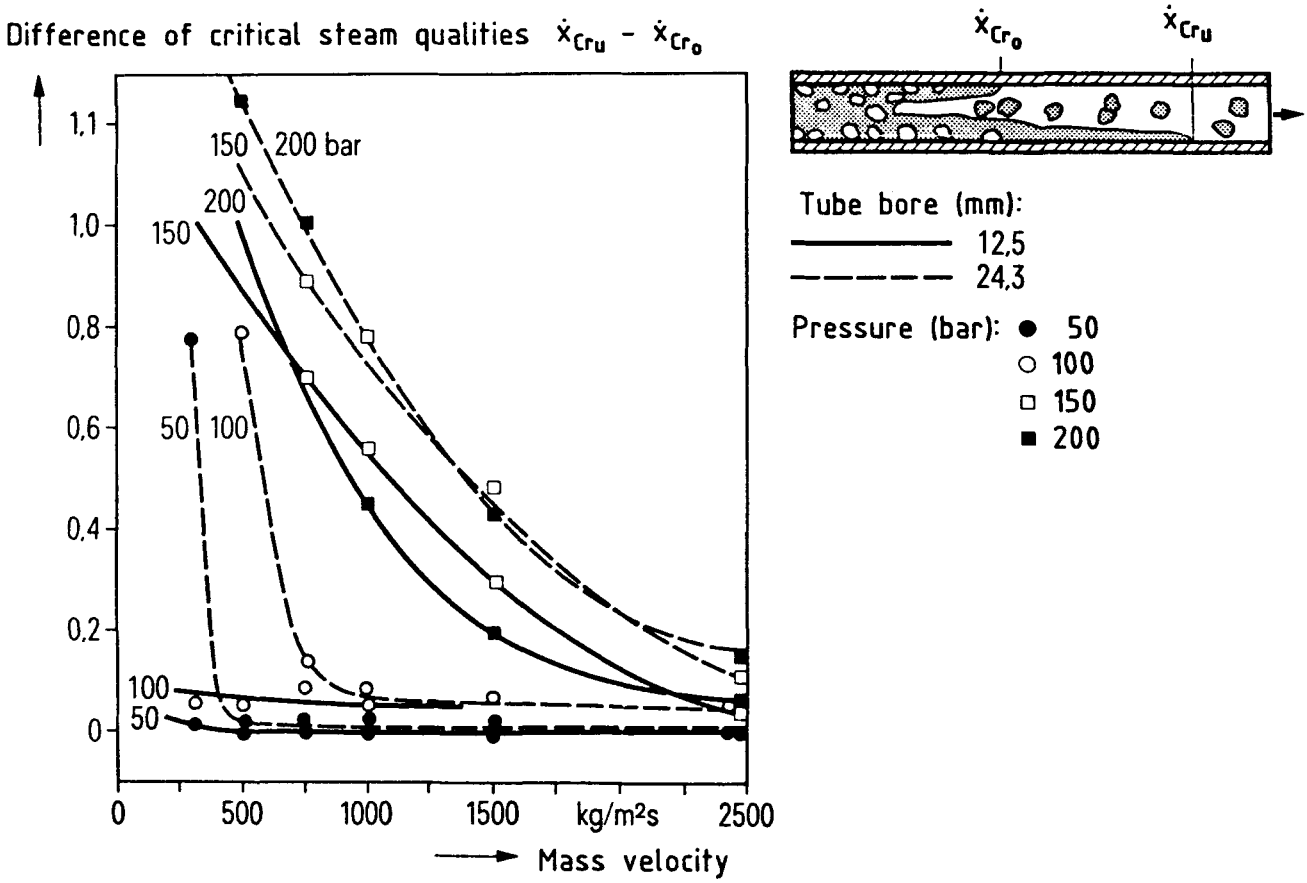


Figure 5-13 Critical steam quality region with horizontal flow

Frequently it is of interest if for the chosen parameters the tube orientation has any influence at all on the location of the boiling crisis and, thus, on the heat transfer in the post-dryout region. The Froude number seems to be an adequate quantity for such an evaluation. It represents the relation of the inertia to the buoyant force of a flow.

CUMO /49/ formed a Froude number with the kinetic energy of the water flow in saturation state and could thus furnish a criterium about the parameter combination with which one has to reckon with an influence of the tube orientation on the location of the boiling crisis. For

$$Fr = \frac{(\dot{m}/\rho') \cdot \cos\Theta}{\sqrt{g \cdot d \cdot (\rho' - \rho'')/\rho'}} \geqq 6 \text{ to } 7 \qquad (5\text{-}3)$$

according to CUMO, the location of the boiling crisis is no longer influenced by the tube orientation.

Equation (5-3) was verified through heat transfer experiments in the pressure range of 50 - 200 bars. In Figure 5-14 there is entered as abscissa the Froude number determined by equation (5-3) and as ordinate the difference of the critical steam quality between the upper and the bottom sides of the horizontal tube. It can be seen that the thus formed Froude number does not render an accurate statement about the anticipated influence of the tube orientation on the location of the boiling crisis. Apparently, this relation, which is based on experiments with a pressure of 180 bars, cannot be applied to other pressures.

The following method was studied by a second step:

According to a modelling by WALLIS /50/, it is possible to evaluate stratification effects of a two-phase flow in the horizontal tube through a dimensionless group, which has the inertia force of the steam in the numerator and the buoyant force in the denominator. This is again a Froude number

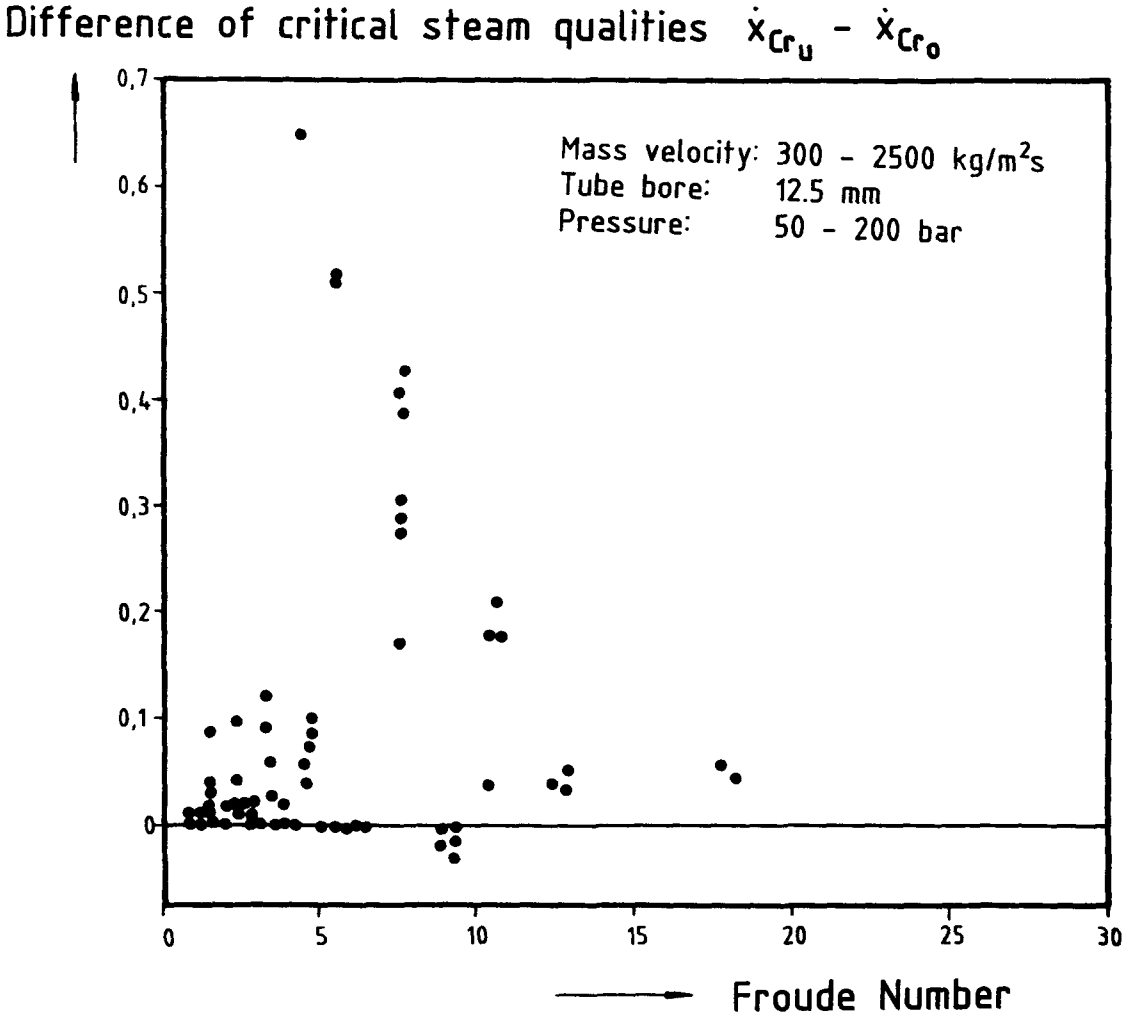


Figure 5-14 Difference of the critical steam quality as function of the Froude number according to euation (5-3)

which, however, is in respect to the steam quality of the flow. The inertia force is therein formed with the superficial velocity of the steam. Since the steam velocity depends greatly on the steam quality, the latter has to be known at the location of the boiling crisis. The critical steam quality with vertical flow was taken as reference magnitude for this. It is known with sufficient accuracy and it can be determined, e.g., according to the method described in Chapter 3.

The stratification effects were thus evaluated by a Froude number as follows:

$$Fr = \frac{(\dot{x}_{Kr} \cdot \dot{m})/\rho''}{\sqrt{g \cdot d \cdot (\rho' - \rho'')/\rho''}} \qquad (5\text{-}4)$$

From Figure 5-15 it can be gathered that, according to equation (5-4), for Froude numbers higher than 7 the tube orientation has practically no influence on the location of the boiling crisis. The difference of the critical steam quality between the upper and the bottom sides of the tube is below 0.1. On the other hand, with Froude numbers below 3 one has to reckon with strong stratification effects. In the case of horizontal tubes, the boiling crisis occurs already at very low steam qualities on the upper side while the bottom side remains wetted almost up to the point of complete evaporation.

## 5.4 Heat Transfer in the Post-Dryout Region

The heat transfer in the post-dryout region of vertical tubes can be calculated with the method described in Chapter 3, which considers the thermal non-equilibrium between the steam and the water droplets. In order to investigate the applicability of such a model to tubes with horizontal flow, information is required on the influence of the tube orientation on the heat transfer in the post-dryout region.

Figure 5-16 shows a typical wall temperature-enthalpy course. The boiling crisis in the case of a tube with horizontal flow sets-in on the upper side with considerably lower enthalpy than in a vertical tube, while on the bottom side it sets-in at a higher enthalpy. The rise of the wall temperature after the occurring of the boiling crisis on the upper side is however lower in the horizontal than in the vertical tube. This has to be attributed to the heat flux in peripheral direction from the unwetted upper side to the wetted bottom side of the tube. Figure 5-17 shows this influence on the wall temperature distribution. If the heat conduction in peripheral direction were neglected, there could be expected a wall temperature course ($\vartheta'_0$) on the upper side, which lies considerably above the measured wall temperature course ($\vartheta_0$). In the case of the horizontal tube there could thus occur, that the wall temperatures in the post-dryout region are lower than in a vertical tube although the location of the first boiling crisis is present at considerably lower steam quality and thus in the region with reduced steam cooling.

The influence of the heat conduction in peripheral direction depends on the ratio of the heat flows in radial direction and in peripheral direction and, thus, on the heat conductivity of the wall material as well as on the wall thickness. Thus, boundaries are set for an accurate but not too cumbersome calculation of the post-dryout heat transfer with horizontal flow. No models can be developed which, as in the case of the vertical tube, calculate the

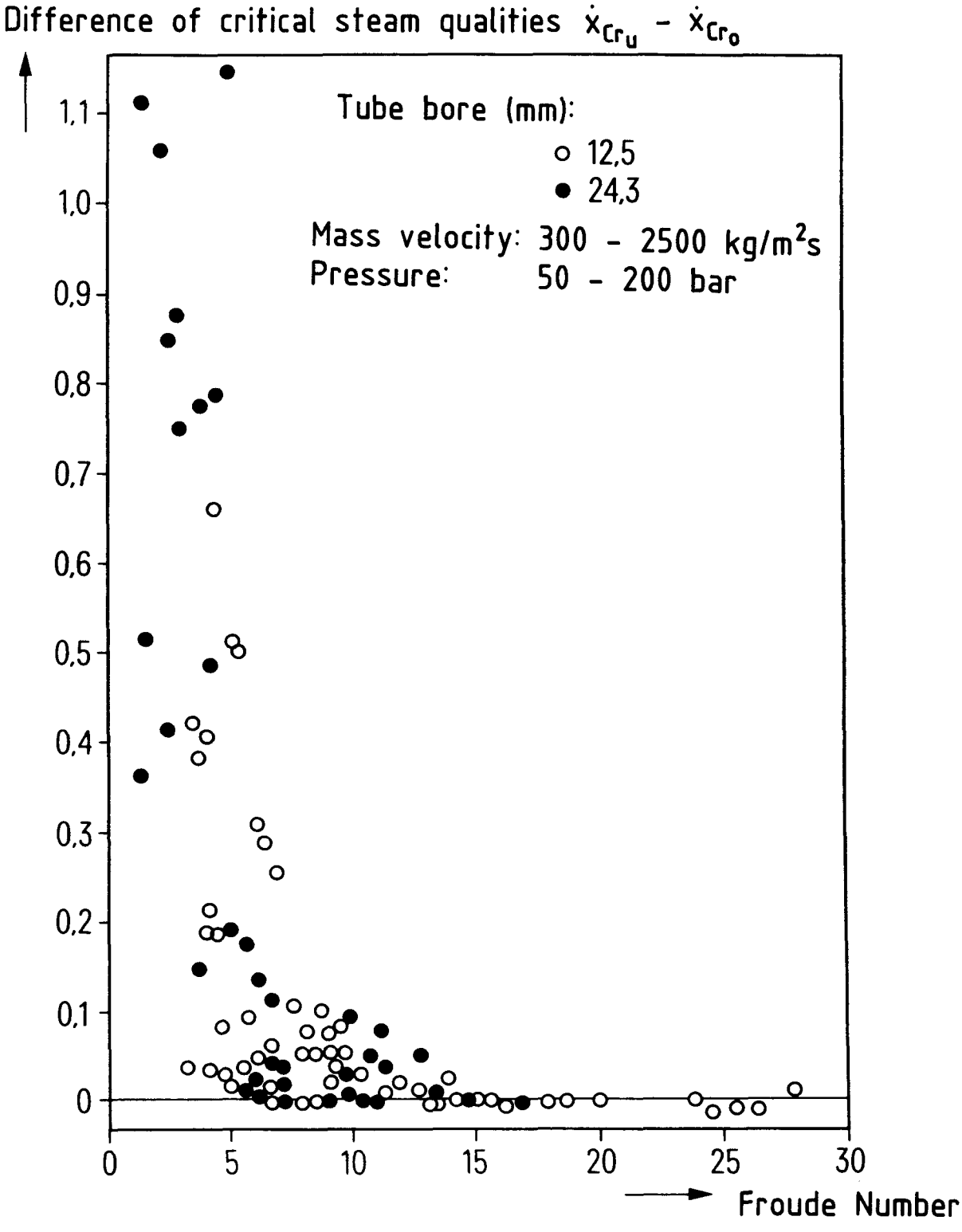


Figure 5-15 Difference of the critical steam quality as function of the Froude number according to equation (5-4)

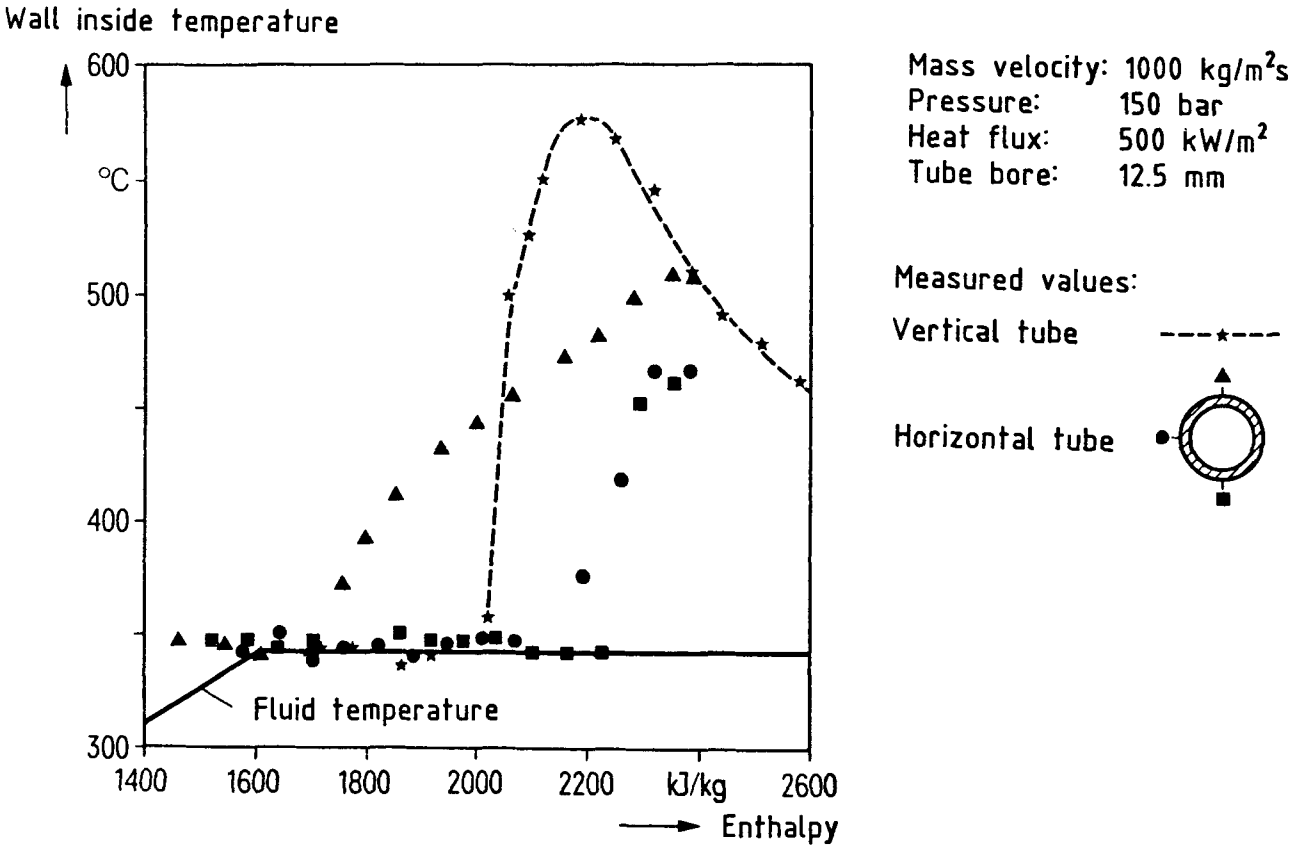


Figure 5-16 Influence of the tube orientation on the heat transfer in the post-dryout region

temperature unaffected by the dimensions and properties of the tube. In the transfer of the test results it has to be further considered that most of the ferritic steels used in steam generators have a heat conductivity which is approximately double than that of the test tubes out of austenitic steel. Thus, the influence of the heat conductivity from the unwetted upper side to the wetted bottom side increases even more.

From the experiments it can be gathered that at the moment when in the horizontal tube the boiling crisis on the upper and on the bottom sides occurs at the same axial position, the heat transfer in the post-dryout region is equal to that in the vertical tube (Figures 5-18 and 5-19). In Figure 5-19, the wall temperature course of the vertical tube is shifted on the enthalpy axis by about 150 kJ/kg in respect to the horizontal one. This value lies still within a deviation of 6% with which, according to CUMO /21/, one has to reckon in reproducibility tests.

With a larger tube diameter there is an increase of the temperature difference between the upper and bottom sides of the tube in the post-dryout region

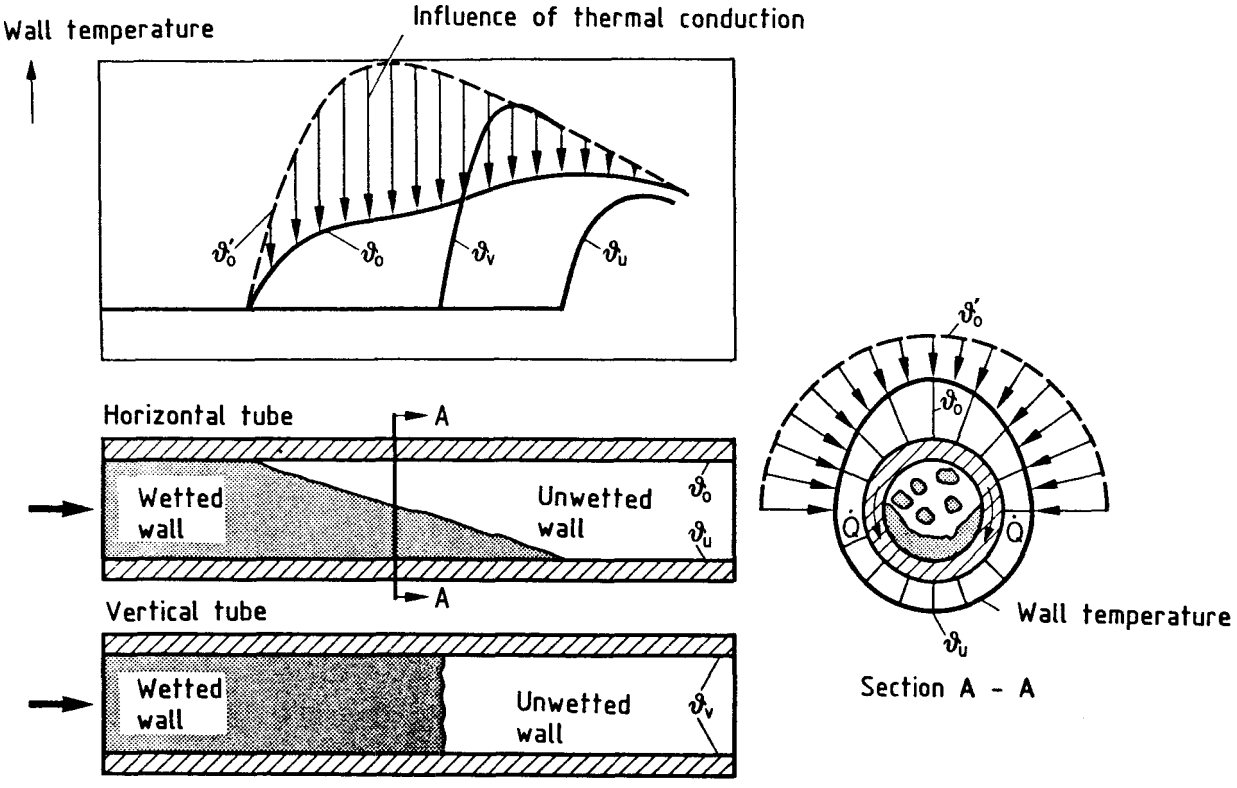


Figure 5-17 Heat conductivity from the unwetted upper side to the wetted bottom side of the tube

(Figure 5-20). From the figure it can be gathered that this temperature difference is still present, if the critical heat flux is exceeded over the entire tube circumference. Since in the post-dryout region is present steam flow with water droplets and thus the steam is the continuous phase, it was studied if also in this case - analogous to the water region - the temperature differences are caused by a thermal convection flow of the steam, which have calculated according to the PETUKHOV model. It was evidenced, however, that the thermal convection flow in this region has practically no influence on the wall temperatures. The statement by SCHNITTGER and MAYINGER /51/ is more plausible, that the water droplets concentrate in the lower tube region. Thus, the thermal non-equilibrium in it is reduced while it increases in the upper tube region.

An indicative value for the expected temperature differences between the upper and the bottom sides of the tube in the post-dryout region is the temperature

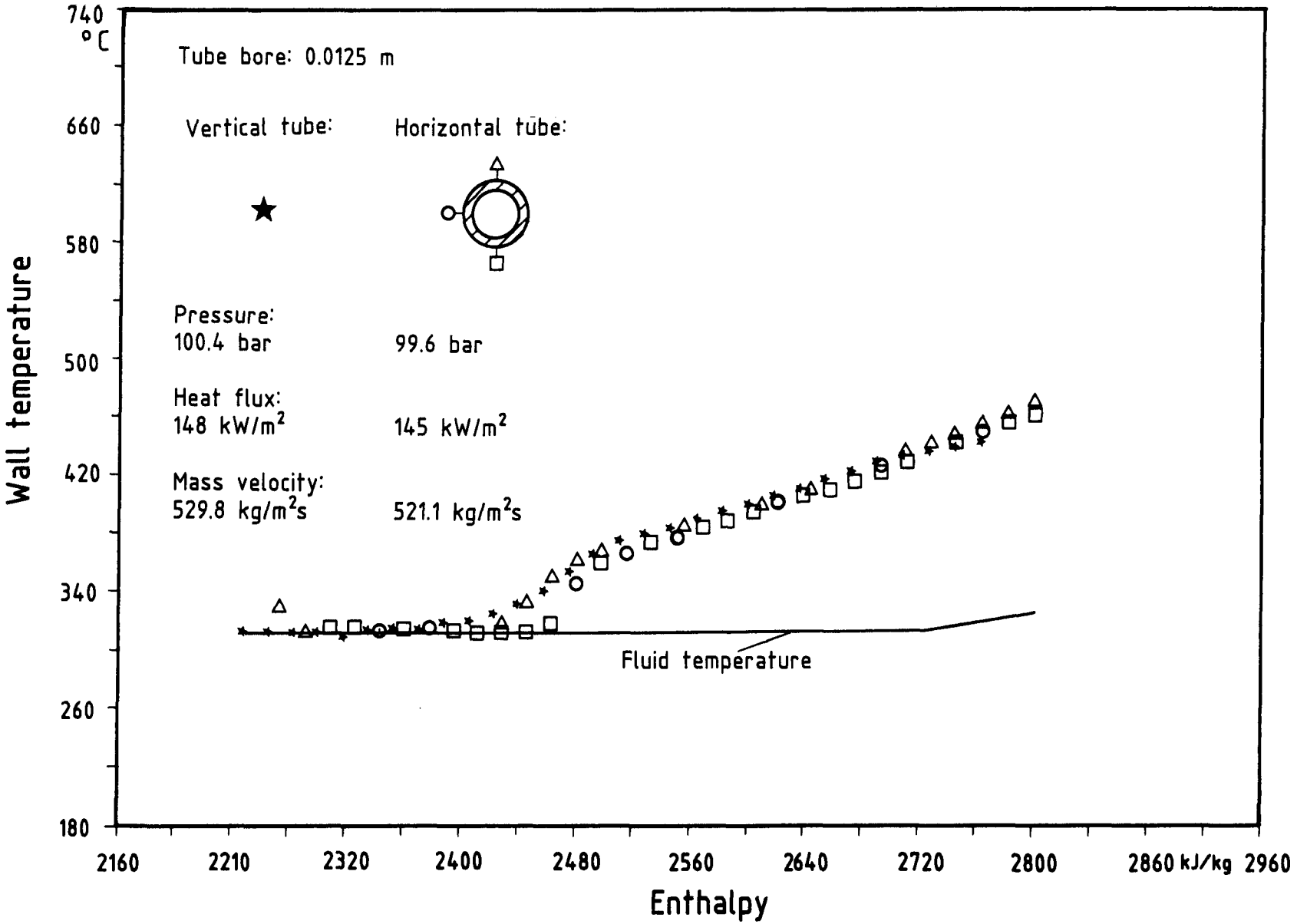


Figure 5-18 Influence of the tube orientation on the heat transfer in the post-dryout region

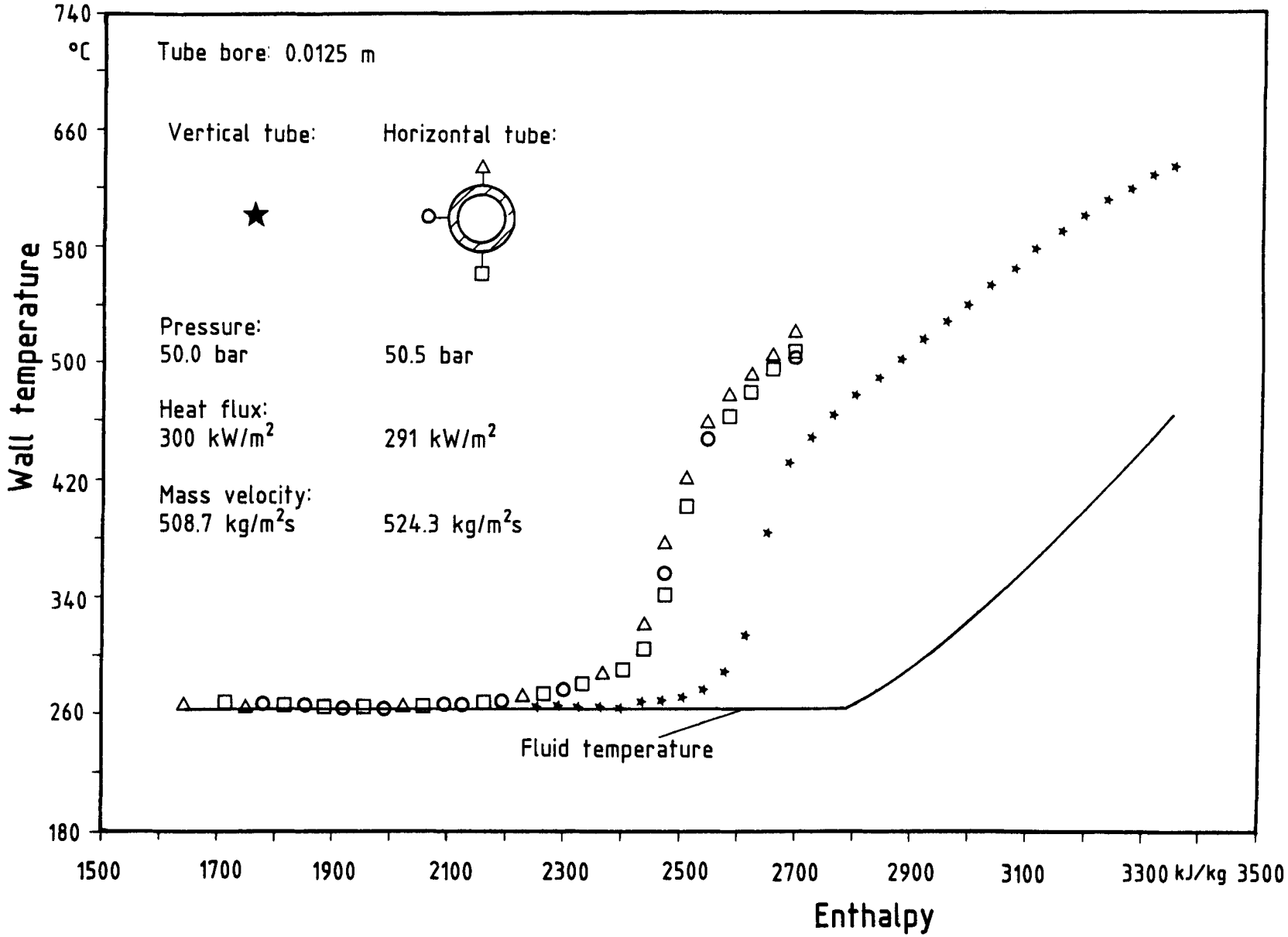


Figure 5-19 Influence of the tube orientation on the heat transfer in the post-dryout region

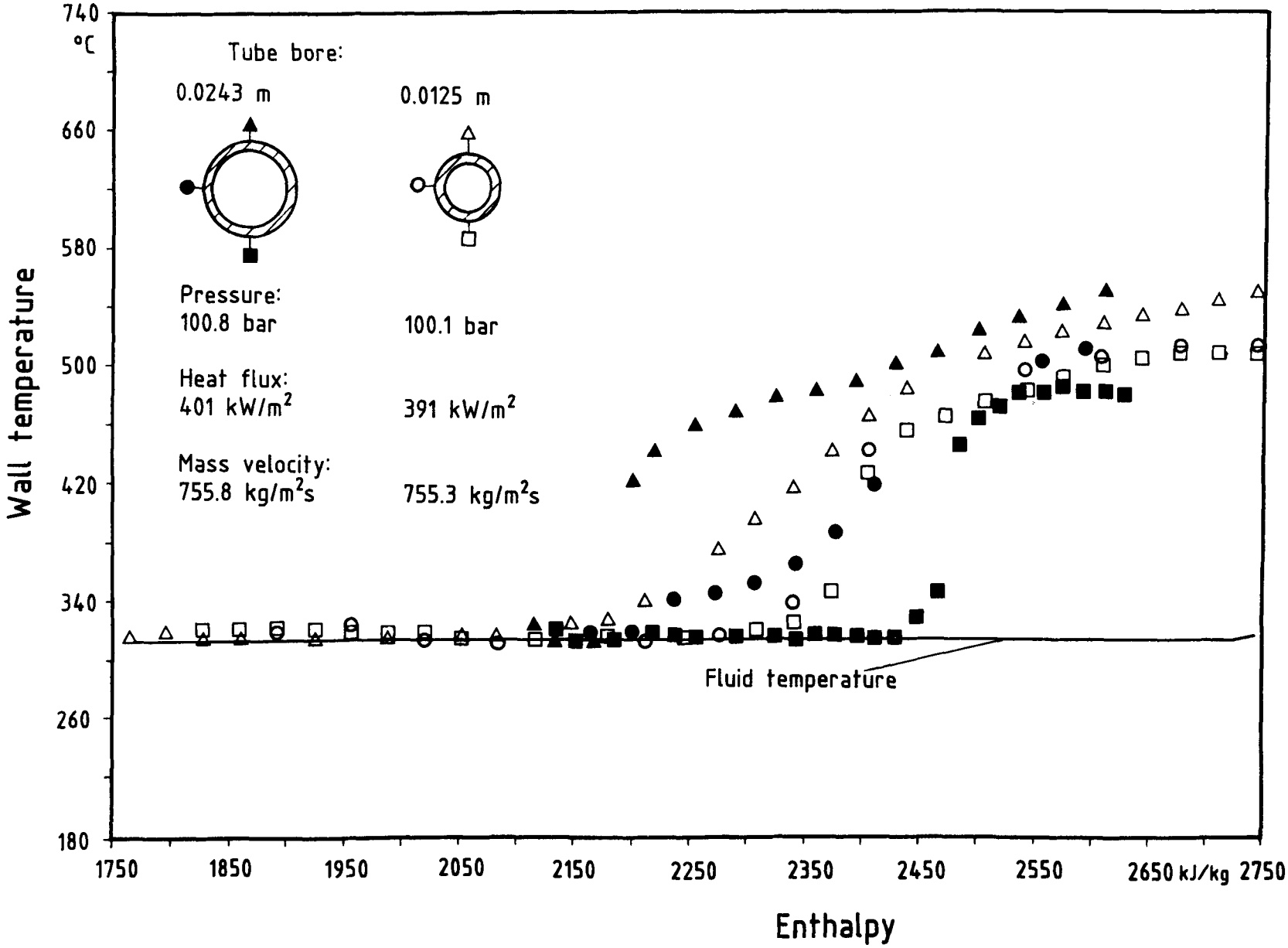


Figure 5-20 Influence of the tube diameter on the heat transfer in the post-dryout region

difference between steam and water droplets (thermal non-equilibrium) in a vertical tube. It can be determined according to the model of Chapter 3. A prerequisite for this procedure is that, based on the parameters, there has to be reckoned with an influence of the tube orientation on the heat transfer (cf. Chapter 5.3). Otherwise, there cannot be expected any temperature differences around the tube circumference.

Figure 5-21 shows that an increased tube diameter leads to a considerable rise of the wall temperatures if the boiling crisis on the upper side of the tube occurs at very low steam quality - apparently in the region of the stratified flow. If, on the other hand, the tube orientation does not have any influence on the heat transfer, a diameter change influences only very slightly the wall temperatures in the post-dryout region (Figure 5-22).

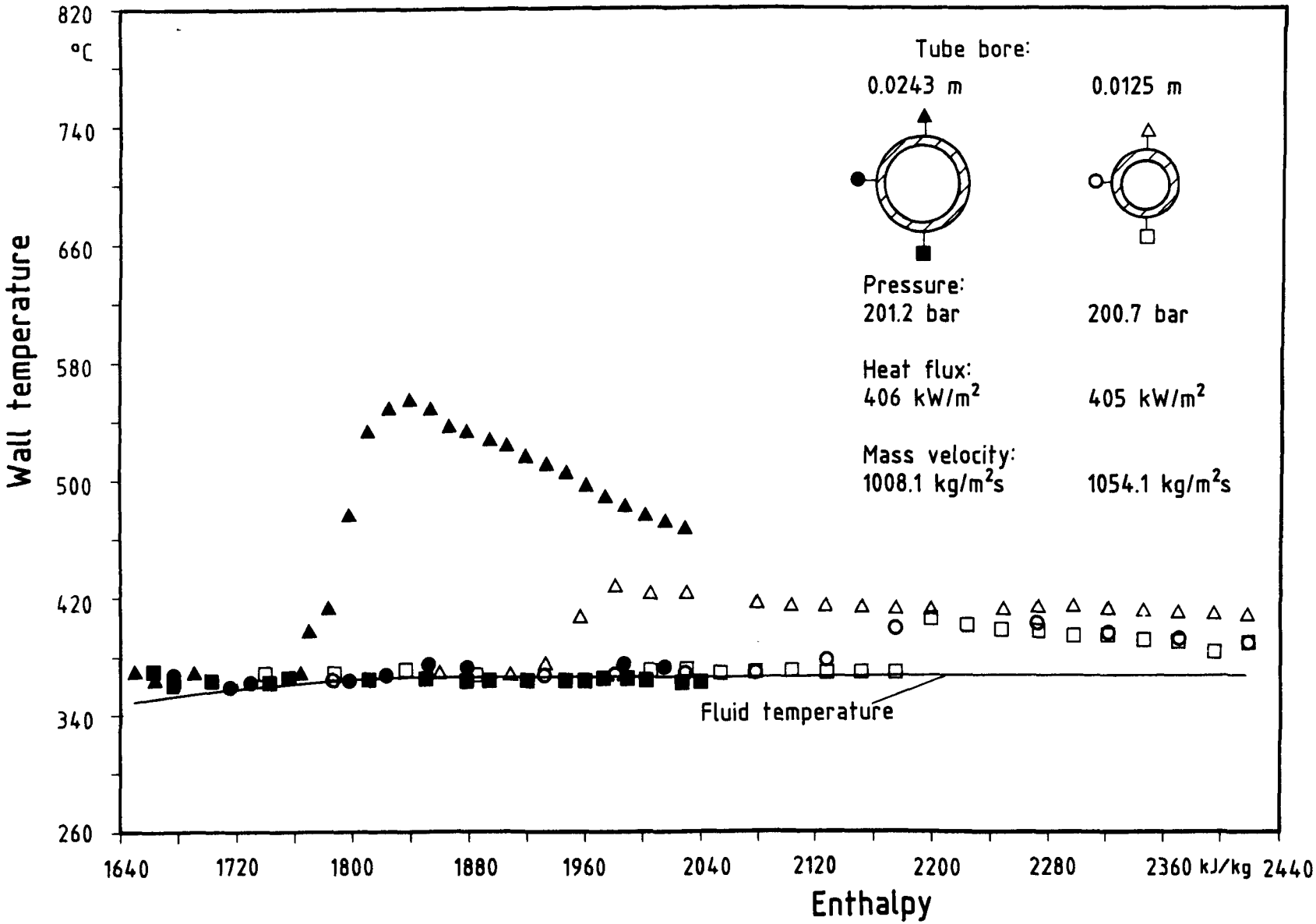


Figure 5-21 Influence of the tube diameter on the heat transfer in the post-dryout region

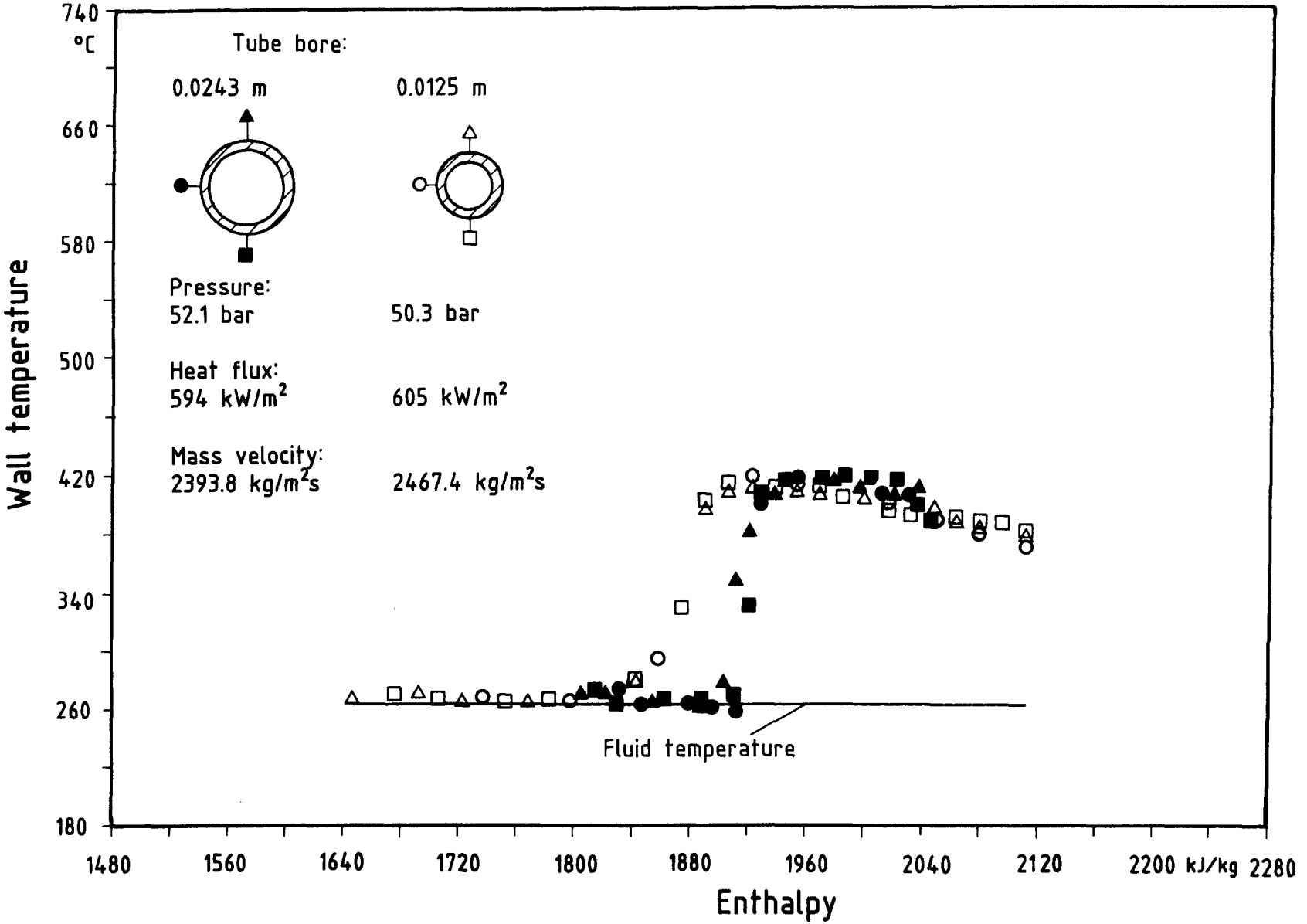


Figure 5-22 Influence of the tube diameter on the heat transfer in the post-dryout region

# 6 PRESSURE DROP

## 6.1 Pressure Drop Components in an Evaporator Tube

The total pressure drop in an evaporator tube is composed of the terms for friction, acceleration and gravity.

$$\Delta P_{Ges} = \Delta P_R + \Delta P_B + \Delta P_G \qquad (6\text{-}1)$$

| Total pressure drop | = | Friction pressure loss | + | Acceleration pressure drop | + | Hydrostatic pressure drop |
|---|---|---|---|---|---|---|

Depending on the parameter combination and on the tube orientation one or more of these fractions dominate in a particular case.

The greatest uncertainties exist always in the determination of the friction pressure loss. Even the verification of a correlation for the friction pressure loss with the help of measured values is not always possible to be accurate since it is always the total pressure drop that is measured and the friction fraction has to be determined according to equation (6-1). While in a single-phase flow there can be determined the acceleration and the hydrostatic pressure drop merely from the parameters and properties of the fluid, for a two-phase flow there is still required data on the phase velocities and/or phase distribution, on the flow cross-section, since this flow has additional degrees of freedom. Flow models (homogeneous or heterogeneous) /50/, which agree sufficiently well with reality in certain parameter regions, were developed for the mathematical handling of this. The most accurate statement about the friction pressure loss is possible with an unheated and horizontal two-phase flow since in this case the friction pressure loss corresponds approximately to the measured total pressure drop. Since, however, the investigations below correspond mostly to heated and not always horizontal flows, it is necessary to study closer all occurring fractions.

The friction pressure loss of the two-phase flow is in respect to the friction pressure loss which occurs, when the entire mass would flow as liquid in the saturation state. This is the magnitude for the two-phase pressure loss most frequently used in the literature and leads to the following definition of the two-phase multiplier:

$$R = \frac{(\Delta P_R)_{2ph}}{(\Delta P_R)_{1ph,w}} \qquad (6\text{-}2)$$

wherein

$$(\Delta P_R)_{1ph,w} = \xi \cdot \frac{L}{d} \cdot \frac{\dot{m}^2}{2 \cdot \rho'} \qquad (6\text{-}3)$$

with

$$\xi = \left[0.86859 \cdot \ln[Re'/(1.964 \cdot \ln Re' - 3.8215)]\right]^{-2} \qquad (6\text{-}4)$$

(according to Friedel /52/ for $Re' > 1055$)

and

$$Re' = \frac{\dot{m} \cdot d}{\eta'} \tag{6-5}$$

The acceleration pressure drop is caused by the change of the flow momentum, e.g., through evaporation of the liquid. If the flow cross-section remains constant, the acceleration pressure drop for a tube section in which the steam quality changes from $\dot{x}_1$ to $\dot{x}_2$ and the void fraction from $\varepsilon_1$ to $\varepsilon_2$ becomes:

$$\Delta P_B = \dot{m}^2 \cdot \left[ \frac{\dot{x}_2^2}{\varepsilon_2 \cdot \rho_2''} + \frac{(1 - \dot{x}_2)^2}{(1_2 - \varepsilon_2)\rho_2'} - \frac{\dot{x}_1^2}{\varepsilon_1 \cdot \rho_1''} - \frac{(1 - \dot{x}_1)^2}{(1 - \varepsilon_1)\rho_1'} \right] \tag{6-6}$$

The hydrostatic pressure drop is caused by the change of the potential energy of the fluid.

$$\Delta P_G = \Delta H \cdot g \cdot \bar{\rho} \tag{6-7}$$

$\Delta H$ is the difference in the height between the start and the end of the considered tube section and $\bar{\rho}$ is the mean density of the fluid in this region and is calculated by

$$\bar{\rho} = \frac{1}{\Delta H} \int_0^{\Delta H} \rho \cdot dH \tag{6-8}$$

The densities to be entered into equations (6-6) and (6-8) also depend on the velocity ratio of both phases. If one assumes the same velocity for water and steam, the mixture density can be calculated as follows:

$$\frac{1}{\rho_h} = \frac{\dot{x}}{\rho''} + \frac{1 - \dot{x}}{\rho'} \tag{6-9}$$

## 6.2 Friction Pressure Loss in the Wetted and Unwetted Regions

### 6.2.1 Experimental Observations and Their Interpretation

The heating surface of an evaporator tube in which the liquid is completely evaporated lies partially in the wetted and partially in the unwetted region. In order to investigate the influence of the wetting state of the heating surface on the pressure loss, in the experiments on the heat transfer in the post-dryout region there was measured the pressure loss in three equally long tube sections (instrumentation layout, cf. Chapter 2). The location of the boiling crisis was therein shifted to the boundary between two tube sections, so that one of them was completely in the wetted region and the other two in the unwetted region. Figure 6-1 shows a typical wall temperature course with one wetted and two unwetted tube sections. The two-phase multiplier for the three tube

sections, calculated from the measurement, was also entered in the figure. It can be seen, that the pressure loss in the wetted region lies distinctly higher than in the unwetted one. This effect was observed in almost all experiments.

For the first time, TARASOVA and LEONTIEV /53/ and /54/ described the reduction of the friction pressure loss in the unwetted region. They attribute the effect to a "pressure loss crisis" and compare this process with the occurrence of the boiling crisis during heat transfer. Quantitative values for the friction pressure loss in the unwetted region were published by BEATTIE /55/ and /56/ based on boundary layer analysis which, however are not expounded in more details in any of the two articles. WHITCUTT and CHOJNOWSKY /57/ conducted extensive measurements of the two-phase pressure loss at vertical upflow evaporator tubes.

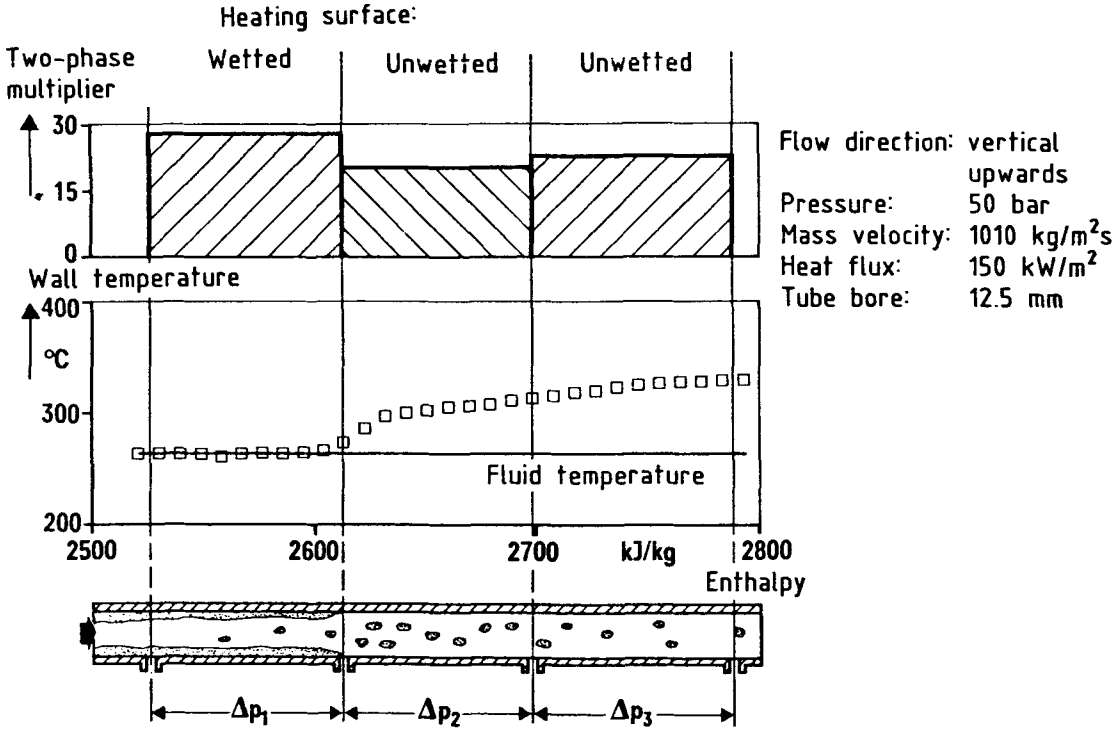


Figure 6-1 Two-phase multiplier in the wetted and the unwetted region of a heated tube flow

The boiling crisis occurred therein mostly at the outlet of the tube, so that the pressure loss was measured in the wetted region. The comparison of the measured values with the homogeneous model in the OWENS /58/ formulation showed only an average deviation of 9% between calculation and measurement. The mass velocity was varied between 400 and 3500 kg/m²s in these experiments, the pressure between 110 and 205 bars and the steam quality between 0 and 80%. According to OWENS expressions, the viscosity of the liquid phase was used - independently of the steam quality - for the determination of the friction coefficient of the tube.

For the evaluation of the measurements of the two-phase pressure loss there were used the OWENS model and the BEATTIE model for the friction pressure loss.

According to the homogeneous model, the pressure loss of a two-phase flow is calculated according to equation (6-3) whereby instead of the fluid density $\rho'$ there has to be entered the mixture density, determined by equation (6-9):

$$(\Delta P_R)_h = \xi \cdot \frac{L}{d} \cdot \frac{\dot{m}^2}{2 \cdot \rho_h} \qquad (6\text{-}10)$$

The friction coefficient $\xi$ is - same as in the single-phase region - dependent on the Reynolds number (equations (6-4) and (6-5)), wherein exist many expressions for the "representative" viscosity in the two-phase region (cf. /41/ and /59/). Since according to the OWENS model the viscosity of the liquid phase is used for the two-phase region, also the tube friction coefficient $\xi$ becomes independent of the steam quality and the two-phase multiplier becomes very simple by using the equations (6-2), (6-3), (6-9), and (6-10):

$$R_{OWENS} = 1 + \dot{x} \left( \frac{\rho'}{\rho''} - 1 \right) \qquad (6\text{-}11)$$

The two-phase multiplier for the unwetted region is calculated according to BEATTIE by

$$R_{BEATTIE} = \left( \frac{\eta''}{\eta'} \right)^{0.2} \cdot \left( \frac{\rho''}{\rho'} \right)^{0.8} \cdot \left( 1 + \dot{x} \; \frac{\rho'}{\rho''} - 1 \right)^{1.8} \qquad (6\text{-}12)$$

The verifications of the experiments carried out with the equations (6-11) and (6-12) are shown in Figure 6-2 to 6-4 for the horizontal tube and in 6-5 to 6-6 for the vertical upflow tube. In the Figures was identified the wetting state of the heating surface, which was determined from the course of the wall temperatures. It can be noted, that the friction pressure loss in the wetted region is covered sufficiently well, on the average, by the OWENS homogeneous model and well in the unwetted region by the BEATTIE model. It is peculiar that the scattering of the two-phase multiplier in the wetted region is considerably higher than in the unwetted one.

From the Figures 6-2 to 6-6 it can be deduced that in the investigated parameter range there is obtained a high accuracy in the calculation of the two-phase pressure loss, if in the wetted region the calculation is made according to OWENS and in the unwetted one according to BEATTIE. Figure 6-7 shows a comparison between the measured two-phase multiplier and the one calculated according to this procedure. The pressure loss for the entire parameter range is sufficiently well determined both for the horizontal as well as for the vertical upflow tube.

### 6.2.2 Comparison of Various Pressure Loss Correlations

For the design of evaporator tubes there are frequently proposed correlations which were obtained from experiments on adiabatic two-phase flows. In order to check their applicability for this purpose, measured two-phase multipliers

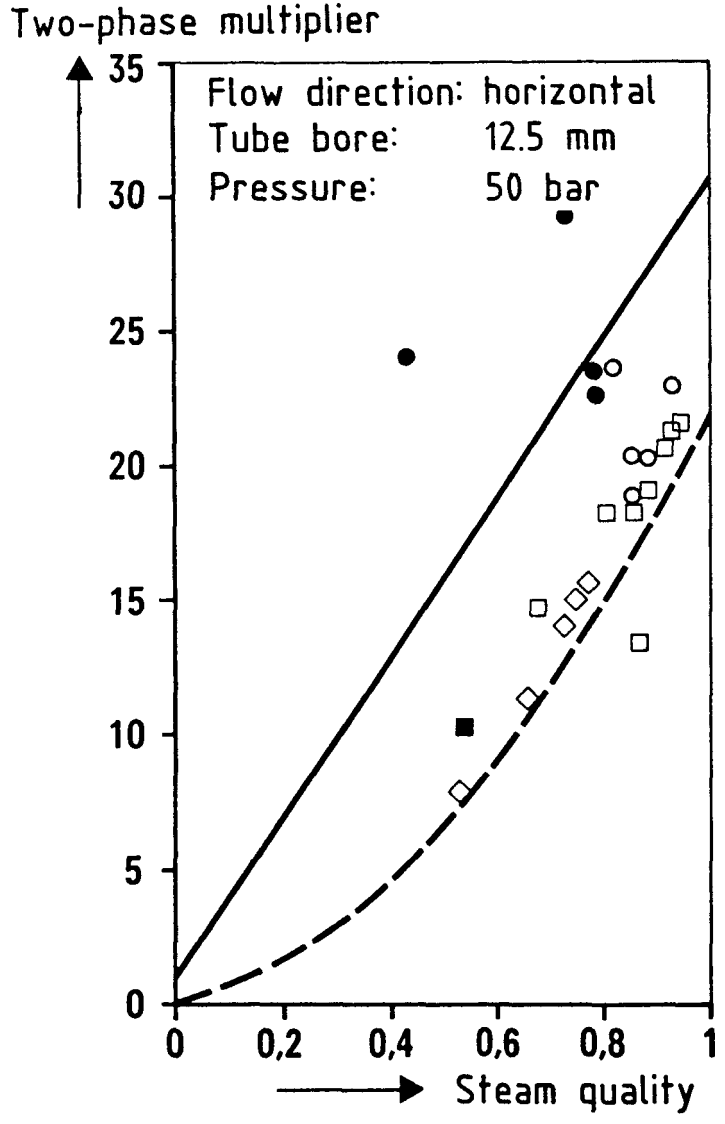


Measured values:

| Heating surface | | Wetted | Unwetted |
|---|---|---|---|
| Mass velocity ($kg/m^2s$) | 500 | ● | ○ |
| | 1000 | ■ | □ |
| | 2500 | ◆ | ◇ |

Calculated values:

——— Homogeneous model acc. to OWENS

– – – – BEATTIE Model

Figure 6-2 Influence of the wetting state of the heating surface on the two-phase multiplier

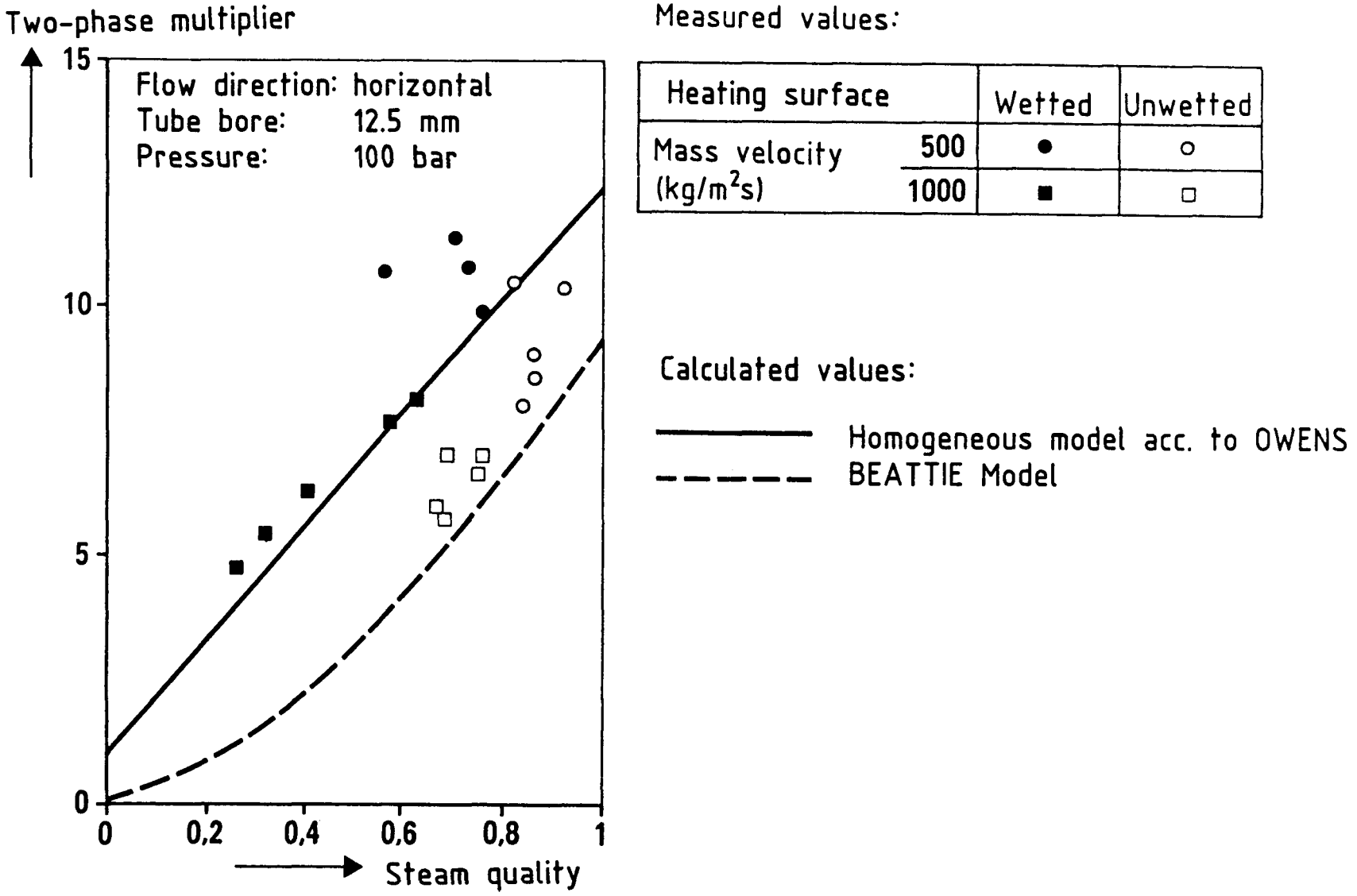


Figure 6-3 Influence of the wetting state of the heating surface on the two-phase multiplier

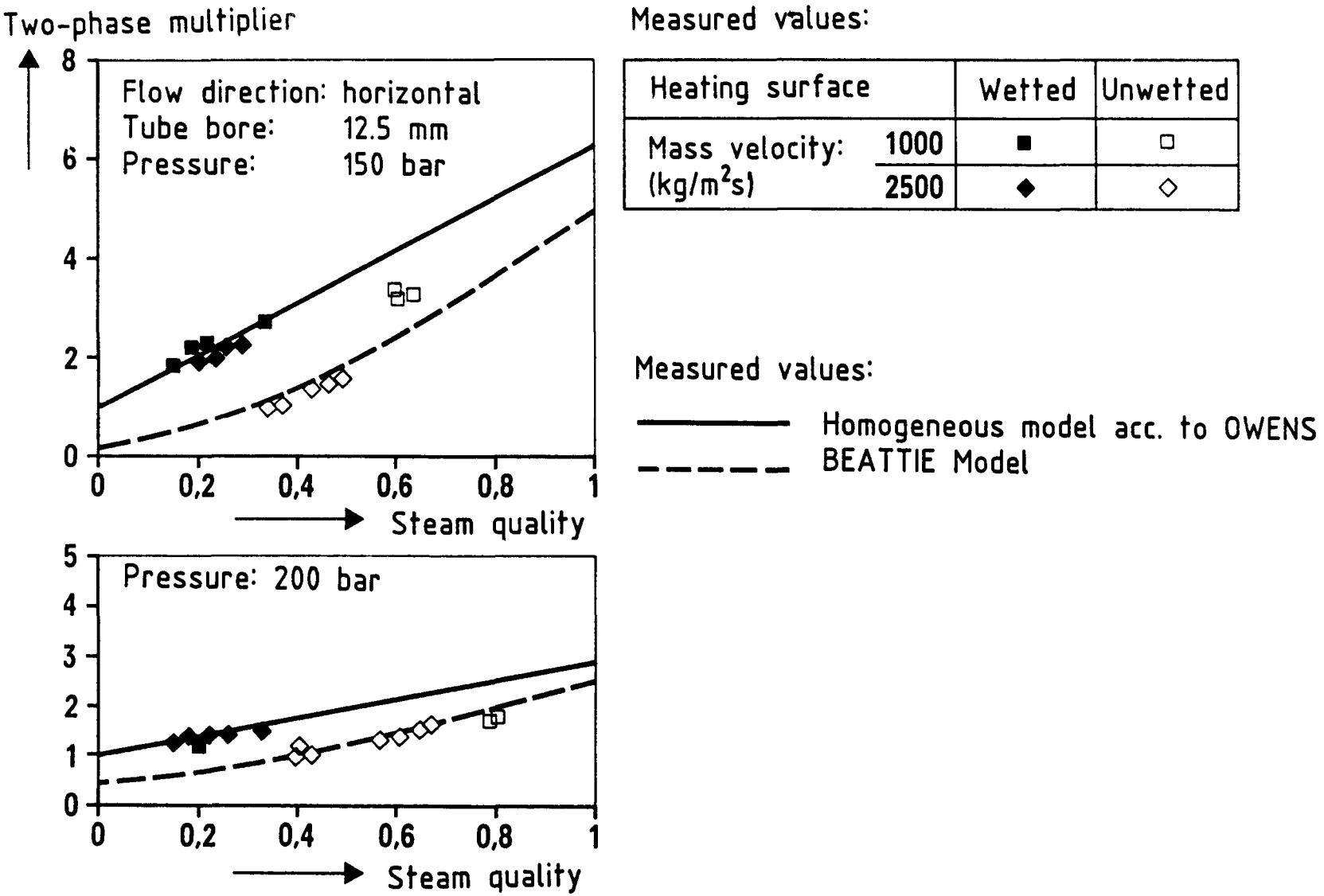


Figure 6-4 Influence of the wetting state of the heating surface on the two-phase multiplier

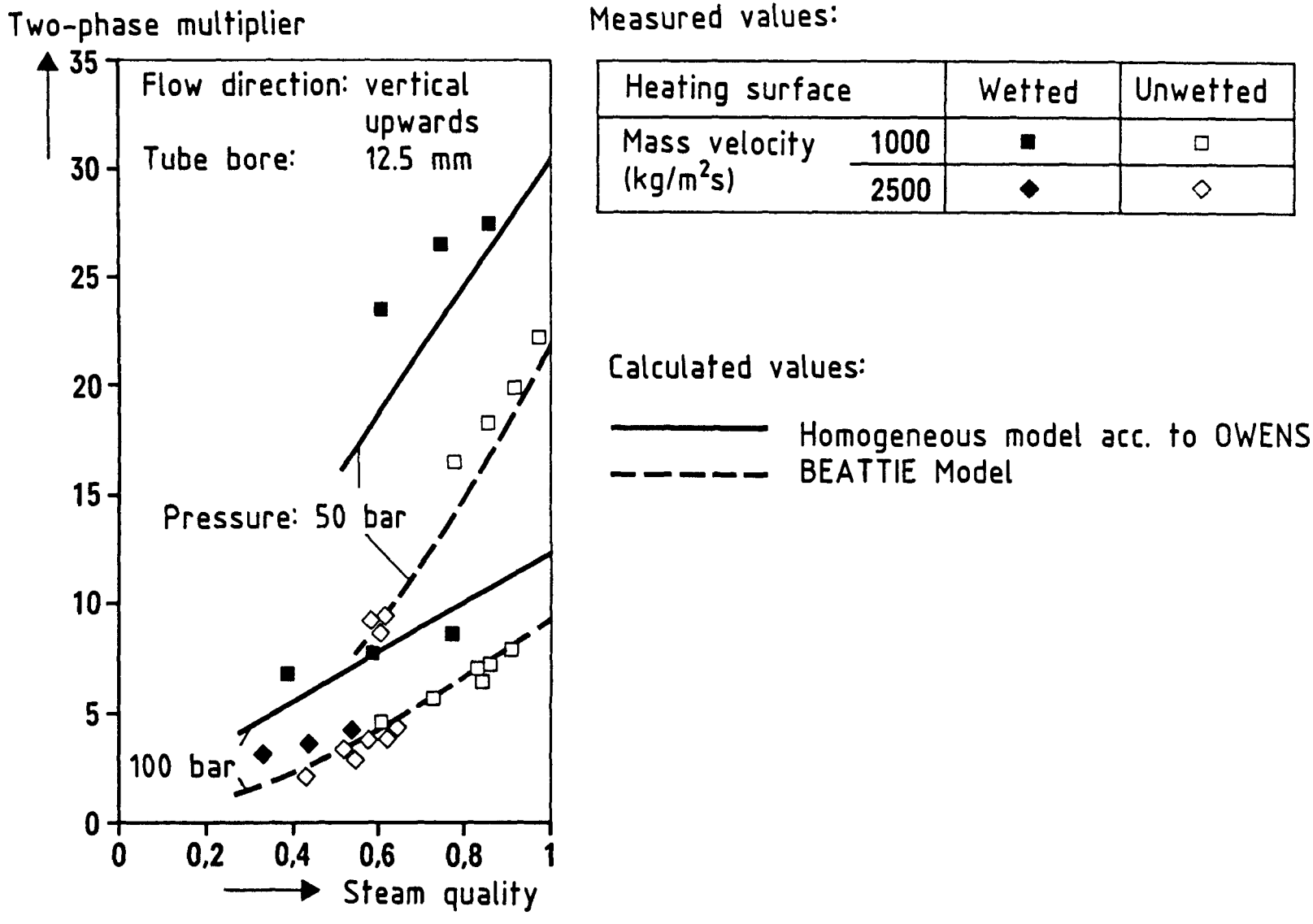


Figure 6-5 Influence of the wetting state of the heating surface on the two-phase multiplier

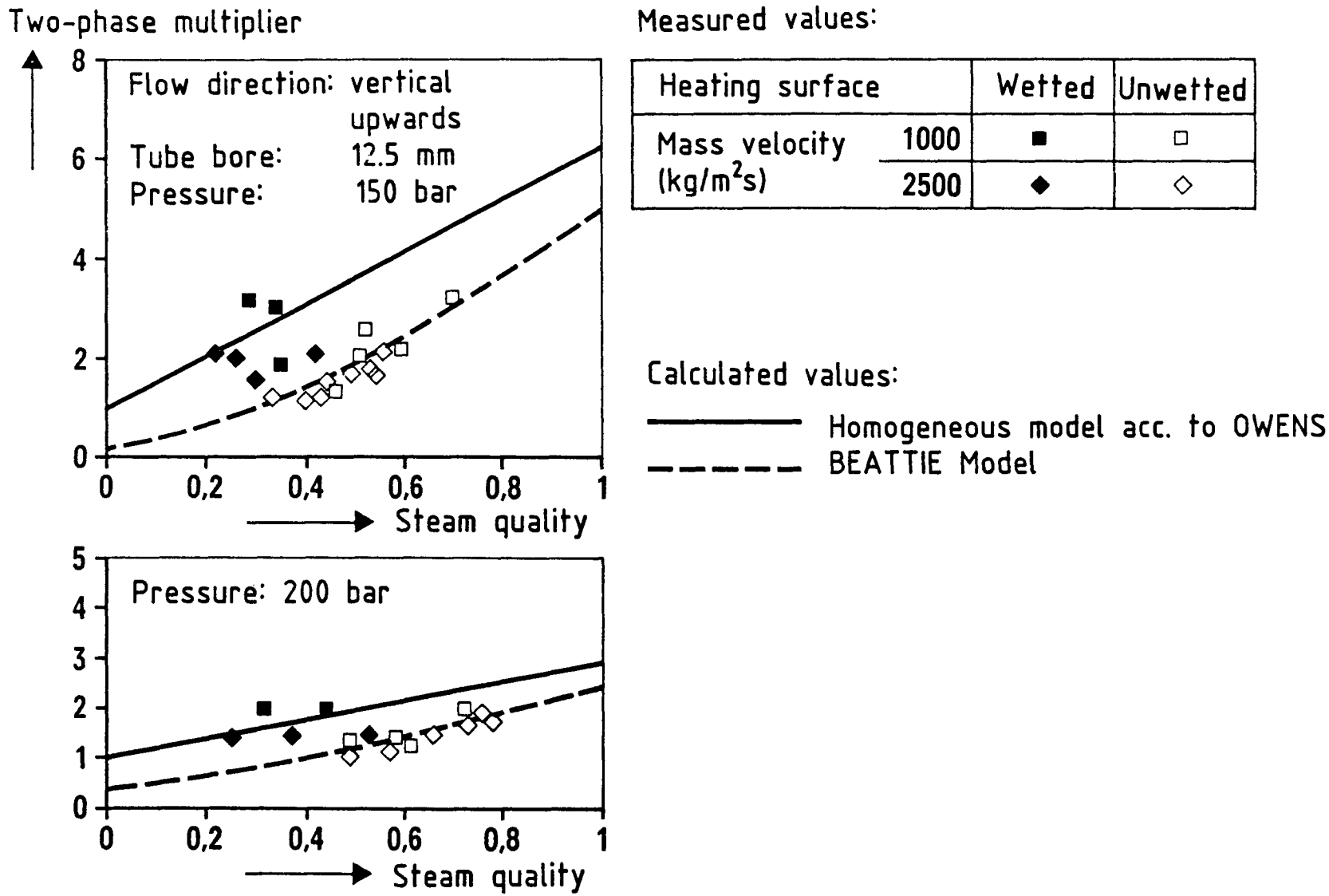


Figure 6-6 Influence of the wetting state of the heating surface on the two-phase multiplier

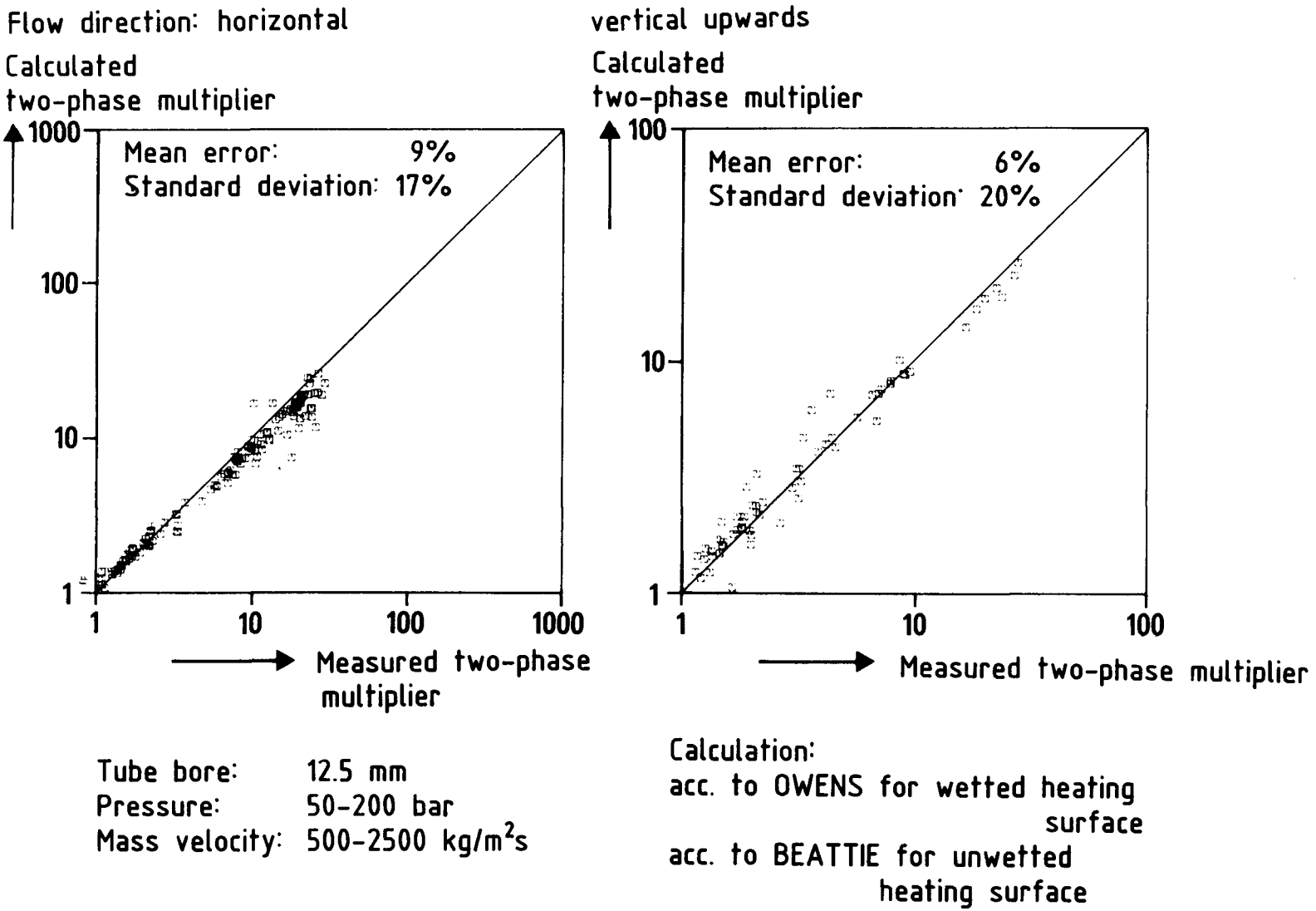


Figure 6-7 Comparison between measured and calculated two-phase multipliers

and those calculated with various correlations were compared to each other. Figure 6-8 shows this comparison for the suggested process and calculation according to LOMBARDI /60/ and FRIEDEL /61/. Plotted was the number of the measuring points which lies within a defined error range. The error was defined therein as follows:

$$Y = \frac{R_R - R_M}{R_M} \qquad (6\text{-}13)$$

With the suggested process with, e.g., an admissible error of ± 20% for horizontal and vertical flows, it is possible to verify approximately 80% of all measuring points. The other equations used for the comparison lead to considerably higher errors in the calculation since they do not consider the wetting state of the heating surface.

In addition to the experiments with heated tube flow there were analyzed pressure loss measurements on unheated tubes. Figure 6-9 shows a comparison of several correlations with measured values which were taken from a data bank /62/. The data bank contains essentially the values for the medium water of the data collection compiled by FRIEDEL /52/. The corresponding parameter regions are enumerated in Table 6-1. In this comparison were also included the newly developed STOREK /63/ model and the homogeneous model in the OWENS formulation /58/. It is of interest to observe that with horizontal flow the homogeneous model reproduces the test values better than the three relations used for the comparison.

The FRIEDEL equation furnishes the best agreement in the case of vertical tube flow. Also herein the homogeneous model presents advantages over the other two methods, since it covers all measuring values already with an error range of ±70% and does thus not produce any large "spreads." However, the OWENS homogeneous model has lead to errors during the transition to the steam flow, since herein the viscosity of the liquid phase is used for the determination of the friction coefficient.

### 6.2.3 Influence of the Heating and Entrance Effects

The influence of the heating on the friction pressure loss in the two-phase region was investigated on a horizontal tube. Figures 6-10 and 6-11 show the measured two-phase multiplier as a function of the steam quality. For the case of the heated flow, the friction pressure loss was obtained from the difference between the measured total pressure drop and the acceleration pressure drop (equation 6-6). The acceleration pressure drop, which due to the slight heating is only of secondary importance, was determined according to the homogeneous model. It can be seen that in the wetted region the pressure loss of the heated flow is practically identical with the pressure loss of the unwetted flow of the same steam quality. In the unwetted region the pressure loss of the heated flow lies below that of the unheated one.

From Figures 6-10 and 6-11 it can also be gathered that the pressure loss with partially wetted heating surface, in which in the horizontal tube the critical heat flux on the upper side of the tube was exceeded, lies between the values

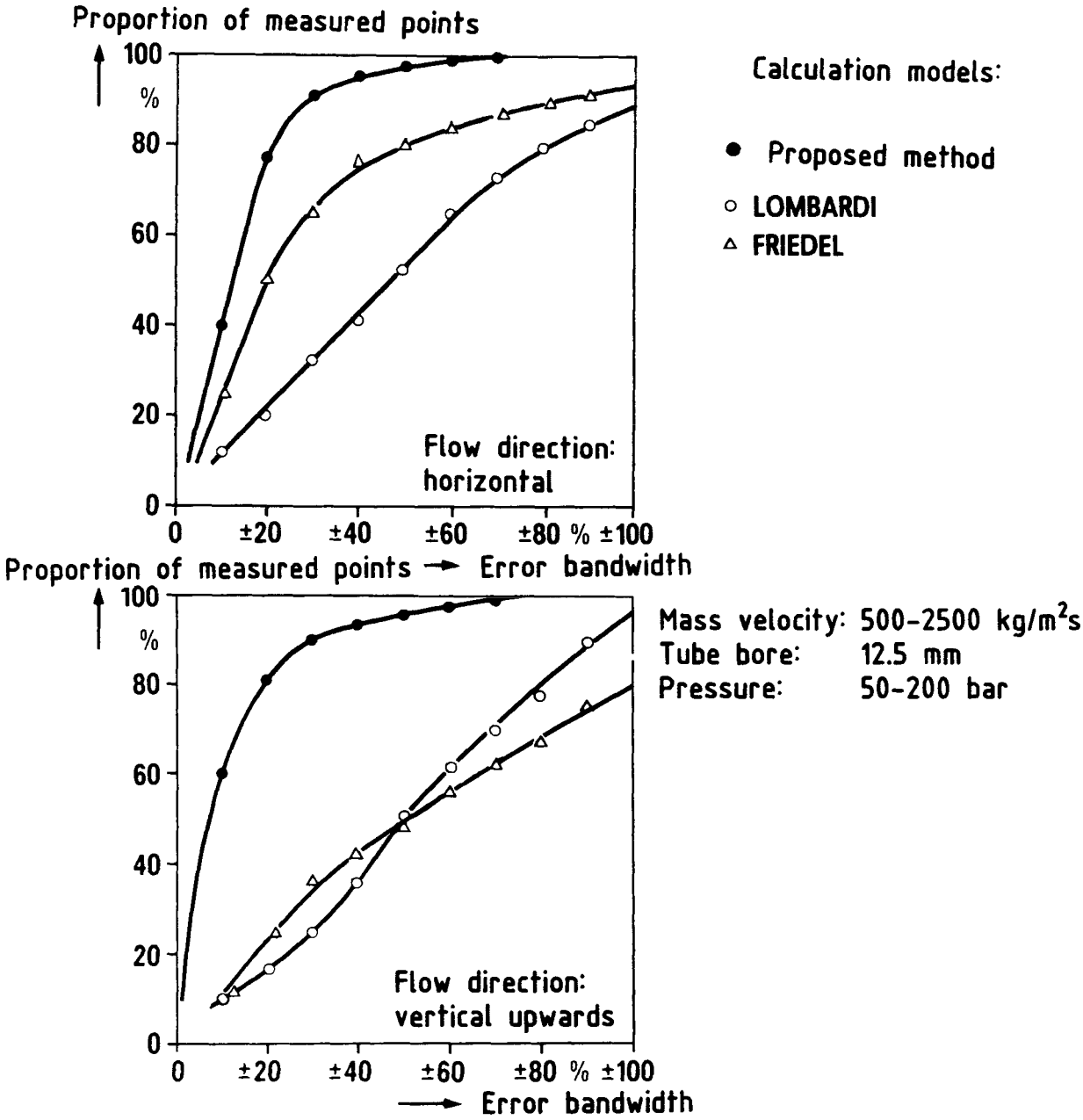


Figure 6-8 Number of measuring points within a defined error range (heated tube flow)

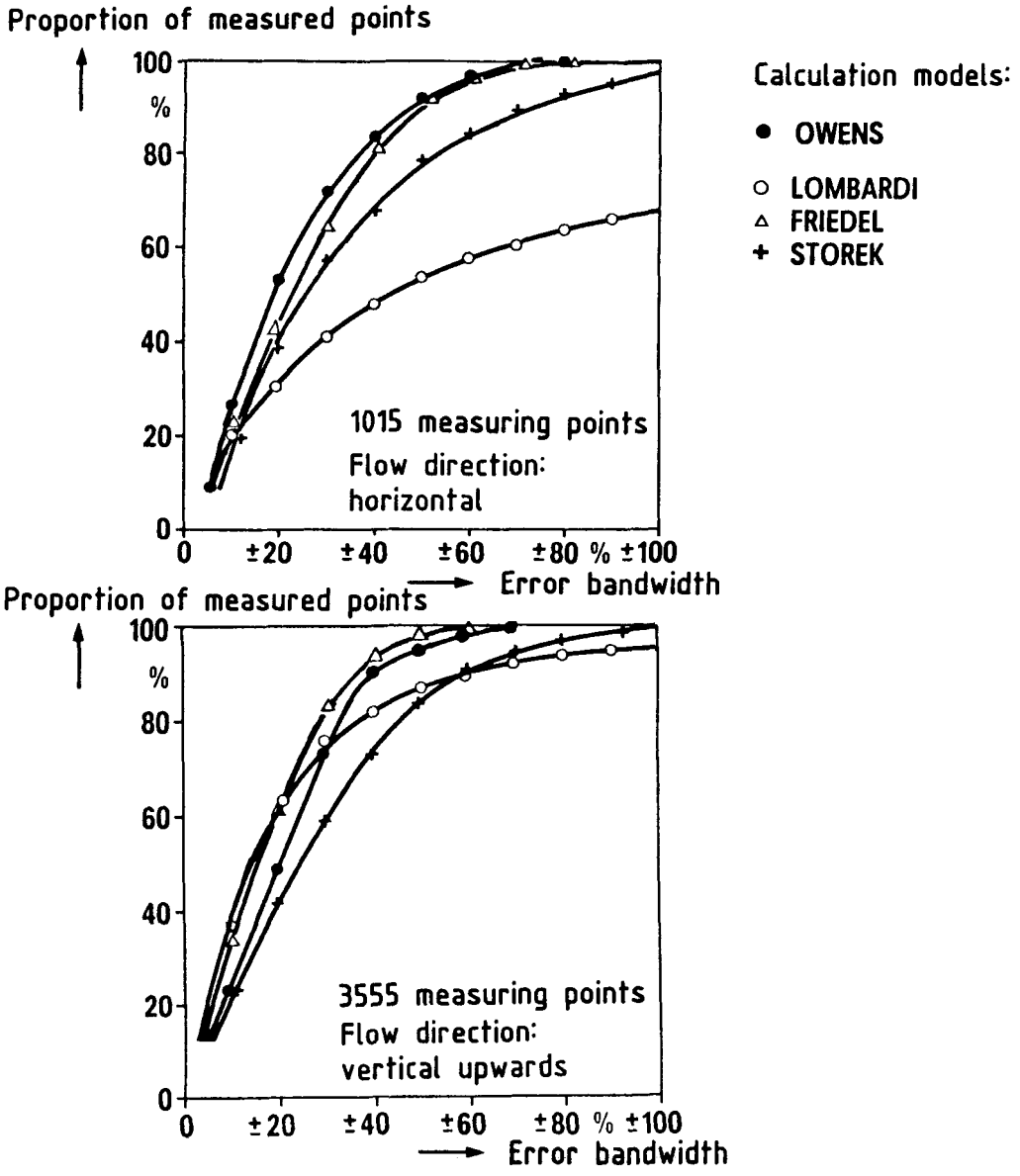


Figure 6-9 Number of the measuring points within a defined error range (unheated tube flow)

for the wetted and the unwetted heating surface. This can be seen especially in Figure 6-11 with a pressure of 100 bars. Herein the limiting curve for the unwetted wall (BEATTIE model) is obtained when the heating surface is unwetted around the entire circumference.

From Figure 6-10 it can be gathered that in the wetted region the pressure loss can lie still considerably above the values calculated according to the

Table 6-1 Parameter range of the experiments on unheated tubes

| Flow direction | Number (-) | Mass velocity ($kg/m^2s$) | Steam quality (-) | Pressure (bar) |
|---|---|---|---|---|
| Horizontal | 95 | 334 - 2739 | 0,05 - 0,98 | 41 - 97 |
| | 374 | 201 - 4458 | 0,01 - 0,99 | 1,7 - 97 |
| | 377 | 17 - 1615 | 0,07 - 0,99 | 1,4 - 19 |
| | 35 | 1004 - 4013 | 0,04 - 0,58 | 10 - 37 |
| | 134 | 112 - 1232 | 0,0 - 0,33 | 11 - 177 |
| Vertical upwards | 86 | 331 - 2751 | 0,04 - 0,98 | 41 - 97 |
| | 252 | 398 - 1835 | 0,0 - 0.04 | 1,0 - 1,7 |
| | 314 | 99 - 1532 | 0,01 - 0,36 | 11 - 197 |
| | 323 | 392 - 3995 | 0,02 - 0,87 | 17 - 100 |
| | 1877 | 497 - 4658 | 0,01 - 1,0 | 20 - 89 |
| | 347 | 961 - 4577 | 0,02 - 0,84 | 49 - 70 |
| | 101 | 500 - 3000 | 0,08 - 0,70 | 30 - 90 |
| | 40 | 500 - 1000 | 0,10 - 0,92 | 69 |
| | 156 | 397 - 1579 | 0,03 - 0,51 | 2,1 - 19 |
| | 17 | 990 - 4036 | 0,05 - 0,56 | 19 - 30 |
| | 42 | 481 - 2120 | 0,01 - 0,38 | 20 - 31 |

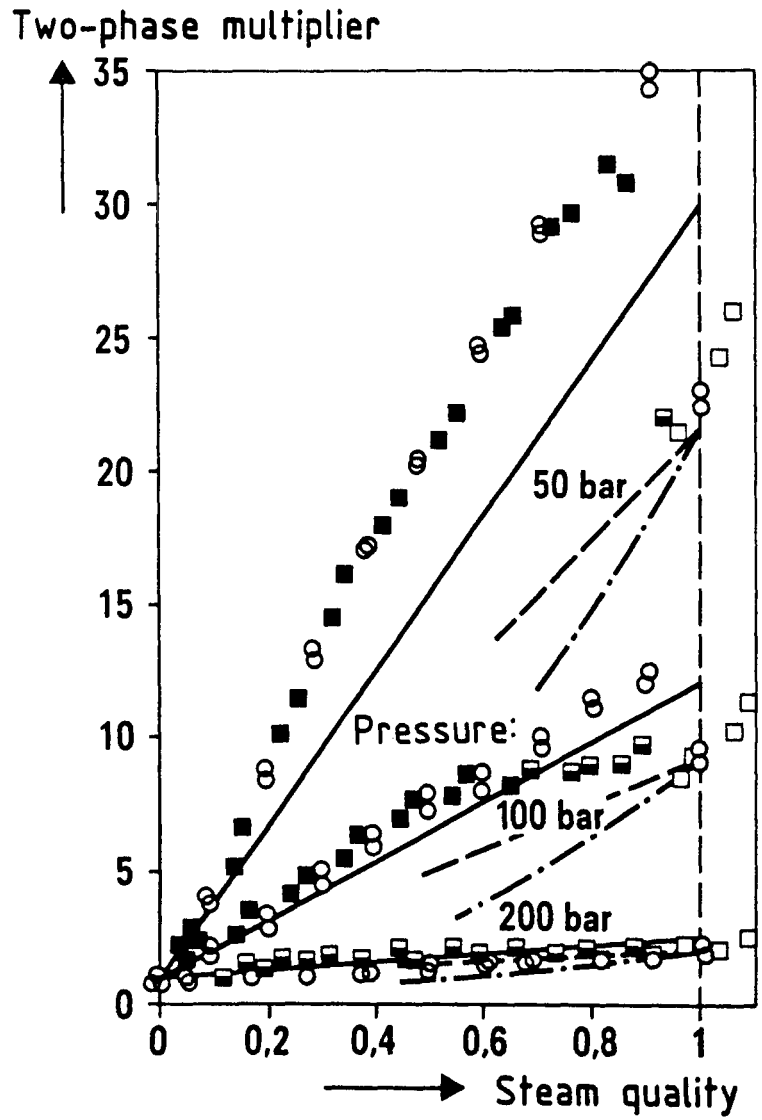


Measured values:

| Heating surface | Wetted | Partially wetted | Unwetted |
|---|---|---|---|
| Heated(100 kW/m$^2$) | ■ | ◪ | □ |
| Unheated | | ○ | |

Calculated values:

——— Homogeneous model acc. to OWENS

– – – – Homogeneous model with steam viscosity

—·—·— BEATTIE Model

Mass velocity: 750 kg/m$^2$s
Tube bore: 24.3 mm
Flow direction: horizontal

Figure 6-10 Influence of the heating on the two-phase multiplier

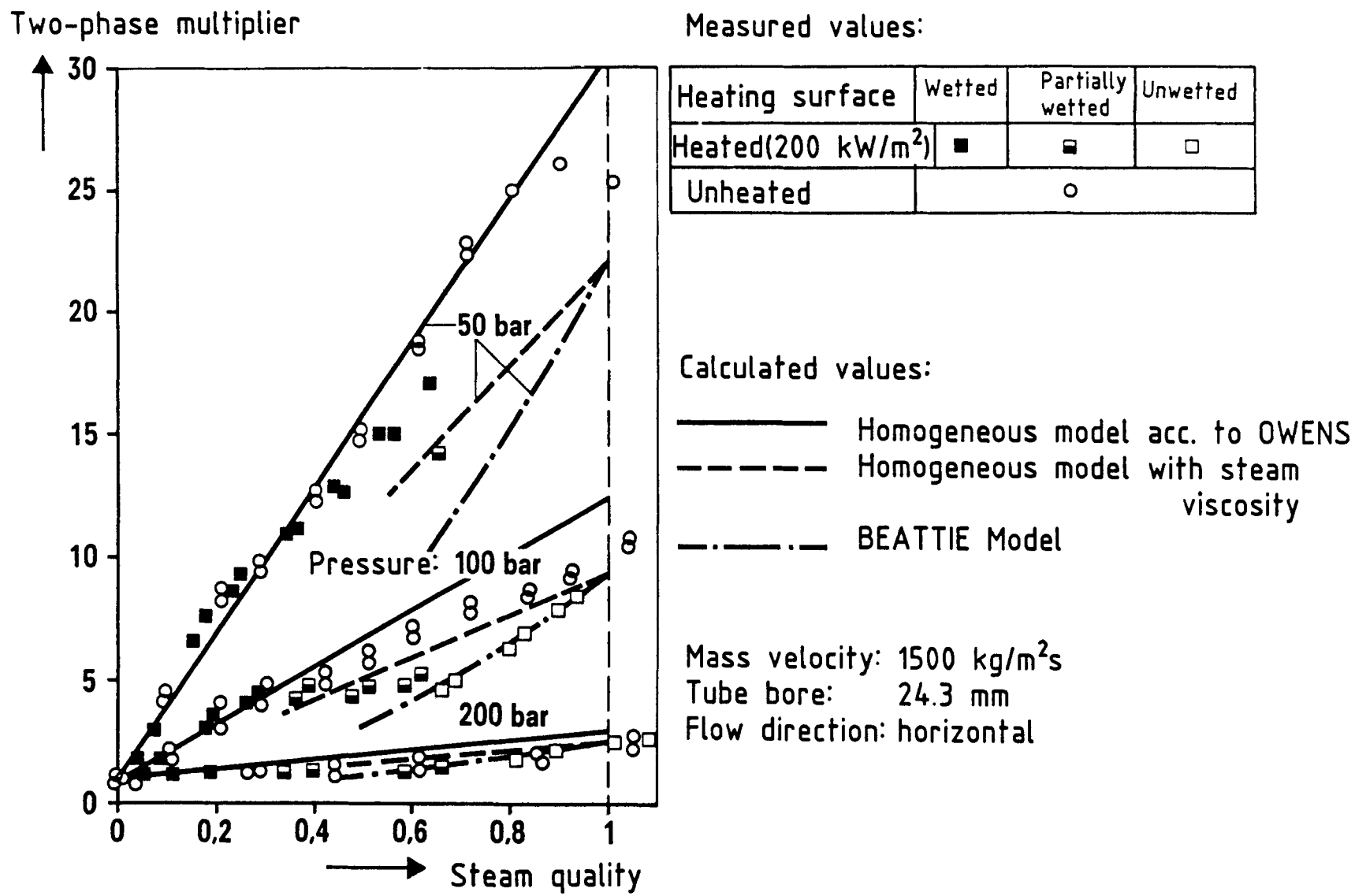


Figure 6-11 Influence of the heating on the two-phase multiplier

homogeneous model by OWENS. This has to be attributed to the influence of the deformation turbulence (cf. /63/) which, with low mass velocity and - as in this case - with large tube diameter cannot be neglected in respect to the influence of the Reynolds turbulence.

In the case of the heated tube, the transfer from the course of the pressure loss with wetted heating surface to that with unwetted heating surface is determined by the location of the boiling crisis which can be determined, e.g., according to Chapter 3.2 for conditions occurring in steam generator tubes. In the case of the unheated tube, when approaching the single-phase steam flow there can be sometimes observed a considerable drop of the friction pressure loss (Figure 6-10 at 50 and 100 bars) and with other parameters an increase of the friction pressure loss (Figure 6-11 at 100 bars). This has to be attributed to the different entrainment behavior of the two-phase flow. While in the first case, even with very high steam qualities, there is a water film on the wall which thus increases considerably the pressure loss, the wall in the second case would be essentially blown dry, whereby the considerably lower viscosity of the steam is decisive for the pressure loss.

The influence of the entrainment on the pressure loss was investigated on measurements by GASPARI /64/ on a vertical upflow adiabatic tube flow. Figure 6-12 shows the fraction of the liquid carried in the steam in the form of water drop lets for the transfer to the single-phase steam flow $\dot{x}$ 1) according to a method by HUHN /65/. In the case of high mass velocities, the entire liquid fraction is in the steam flow; thus, there is no longer a film on the wall and the pressure loss increases when approaching the single-phase flow as a result of the increasing flow velocity. On the other hand, with lower mass flow decreases the entrainment and there continues a water film which disappears only when approaching the single-phase steam flow. When the water film is removed with increasing steam quality, more steam comes comes into direct contact with the wall whereby the pressure loss decreases again. While with a heated flow this transition occurs in a very limited steam quality range, the change during the course of the pressure loss with an unheated flow occurs over a wider region.

In Figure 6-13, for GASPARI /64/ measurements, the two-phase multiplier is entered as function of the steam quality. It can be seen that with high mass velocities, also with an unheated flow, the pressure loss can drop again already at medium steam contents with increasing steam quality. In the Figure was also plotted the fraction of the water mass flow, calculated according to HUHN, which flows as film on the wall.

The steam quality range, in which can be observed a drop of the pressure loss with high mass flow, can therefore be assigned to the disappearance of the water film on the wall. From the comparison between the measured values and the calculation of the pressure loss according to the homogeneous model it can be gathered that, in the region with the low entrainment, the use of the fluid viscosity furnishes more accurate values for the determination of the tube friction coefficient while with high entrainment it is the steam viscosity.

The influence of entrance effects can be gathered from Figures 6-14 and 6-15. For a two-phase flow the literature /66/ mentions entrance effects up to a length to diameter ratio of 50. From the figures, it can be seen that in the investigated parameter range with a length to diameter ratio of 90, there is no longer present a noticeable influence of entrance effects in the two-phase region while

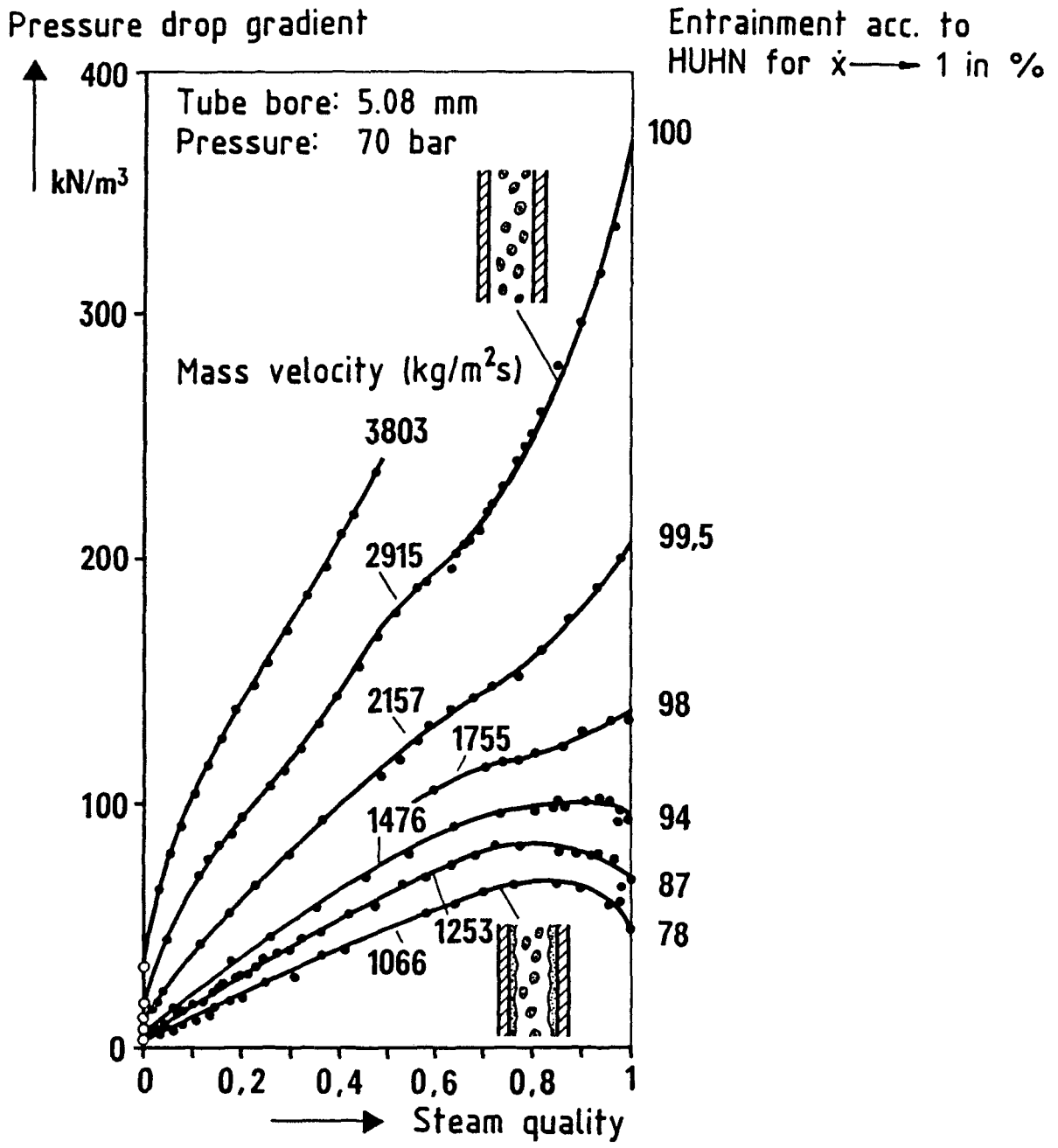


Figure 6-12 Connection between entrainment and pressure loss in an unheated flow

in the single-phase region they have disappeared almost completely with a relative length of 14. From the figures, it can also be gathered that the entrance effects are strongest in the medium steam quality region.

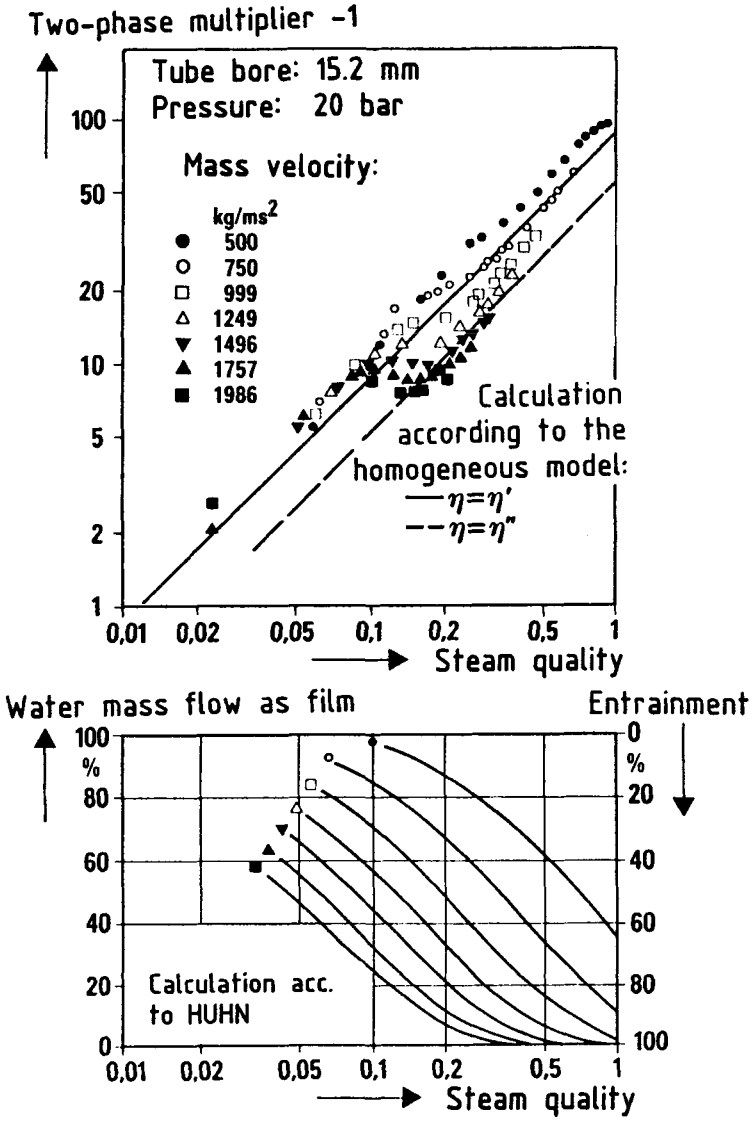


Figure 6-13 Connection between entrainment and pressure loss in an unheated flow

## 6.3 Recommendations for the Determination of the Friction Pressure Loss of a Two Phase-Flow

From the investigations described in the foregoing chapters it can be gathered that the wetting state of the wall has a decisive influence on the pressure loss. This applies both to heated as well as unheated-tube flows, wherein the transition from the wetted to the unwetted wall state takes place in the first case through the evaporation of the liquid film in connection with a droplets entrainment into the core flow and in the second case only by entrainment. However, during the transition to the single-phase flow even with a flow without entrainment there has to disappear the water film on the wall.

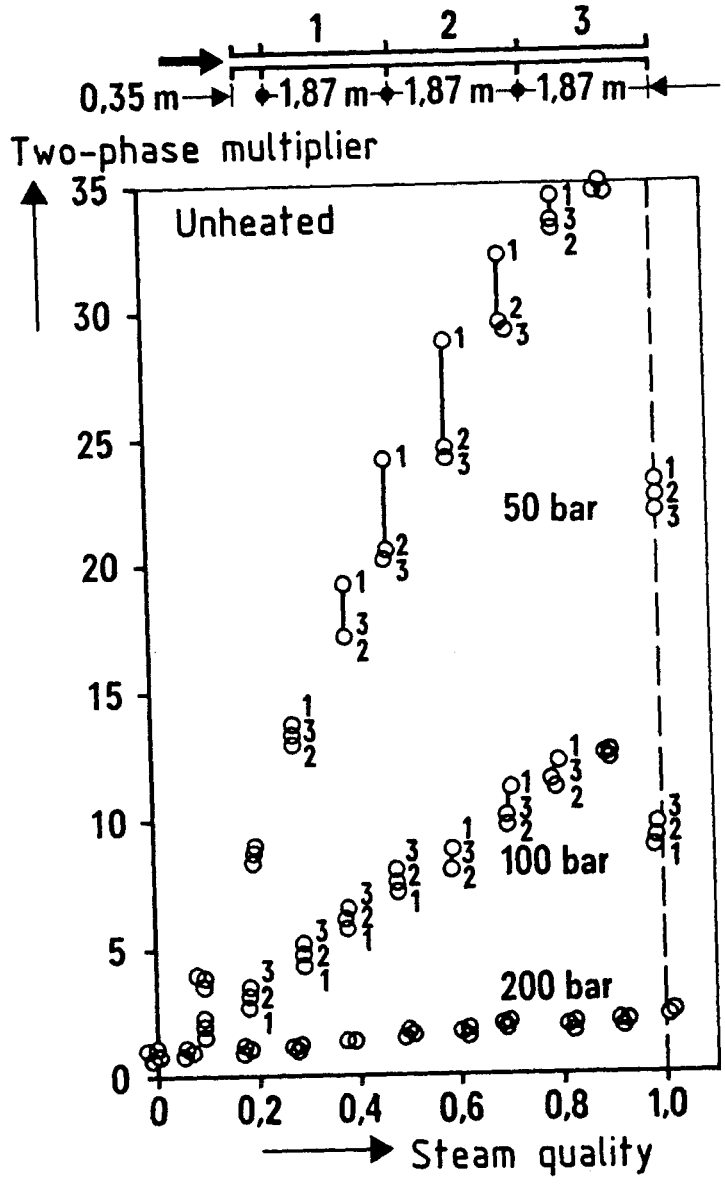


Mass velocity: 750 kg/m$^2$s
Tube bore: 24.3 mm
Tube orientation: horizontal
1, 2, 3 Number of section

Figure 6-14 Influence of entrance effects on the pressure loss

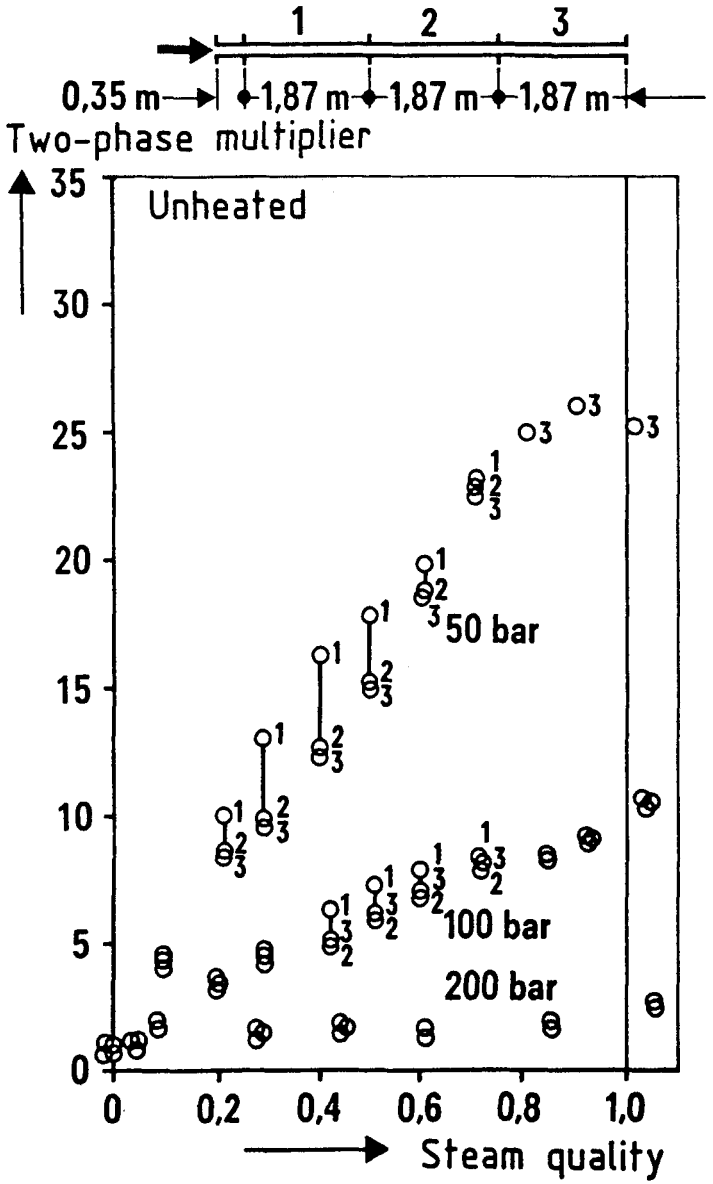


Mass velocity: 1500 kg/m$^2$s
Tube bore: 24.3 mm
Tube orientation: horizontal
1, 2, 3 Number of tube section

Figure 6-15 Influence of entrance effects on the pressure loss

The influence of the wetting state of the wall on the pressure loss can be easily represented according to formulae if one starts from a flow in which the deformation turbulence can be neglected in respect to the effect of the viscosity and the Reynolds turbulence. The process can be then described with the homogeneous, respectively with a quasi-homogeneous, model.

For the determination of the tube friction coefficient in the wetted region it is suggested to use the viscosity of the liquid phase, which leads to the two-phase multiplier used by OWENS /58/ (equation 6-11). The Reynolds number necessary for the determination of the tube friction coefficient is as follows:

$$Re = \frac{\dot{m} \cdot d}{\eta'} \tag{6-14}$$

For the determination of the tube friction coefficient in the case of an unheated flow with high entrainment it is suggested to use the steam viscosity. Thus the Reynolds number becomes:

$$Re = \frac{\dot{m} \cdot d}{\eta''} \tag{6-15}$$

and the two-phase multiplier becomes:

$$R = \frac{\eta''}{\eta'}^{n} \cdot 1 + \dot{x} \frac{\rho'}{\rho''} - 1 \tag{6-16}$$

The exponent n depends on the course of the tube friction coefficient $\xi$ as function of the Reynolds number in accordance with equation (6-17):

$$\xi \sim Re^{-n} \tag{6-17}$$

n decreases with increasing Reynolds number. For the investigated parameter range, according to COLBURN /67/, n can be fixed at 0.2. The decision if the two-phase multiplier shall be calculated according to equation (6-11) or (6-16) can be taken after a determination of the entrainment (e.g., according to HUHN /65/).

In the unwetted region of a heated tube flow the water component does not reach the wall. Therein, due to the higher wall temperature, the Leidenfrost temperature is exceeded most of the times. Between the water droplets and the tube wall, when the droplets approach the wall, steam is formed mainly on the side of the droplets facing the wall, preventing thus a contact between the droplets and the wall.

GARNIC and ROHSENOW /68/ investigated in an analytical manner the influence of the wall temperature on the droplet trajectories of evaporating nitrogen. As shown in Figure 6-16, the droplets cannot advance to the wall if a certain wall temperature is exceeded. This temperature depends on the deposition velocity of the droplets, on the droplets diameter, the mean flow velocity, the thickness of the laminar sub layer as well as on the properties of the liquid and gaseous phase. From the considerable drop of the friction pressure loss in the post-

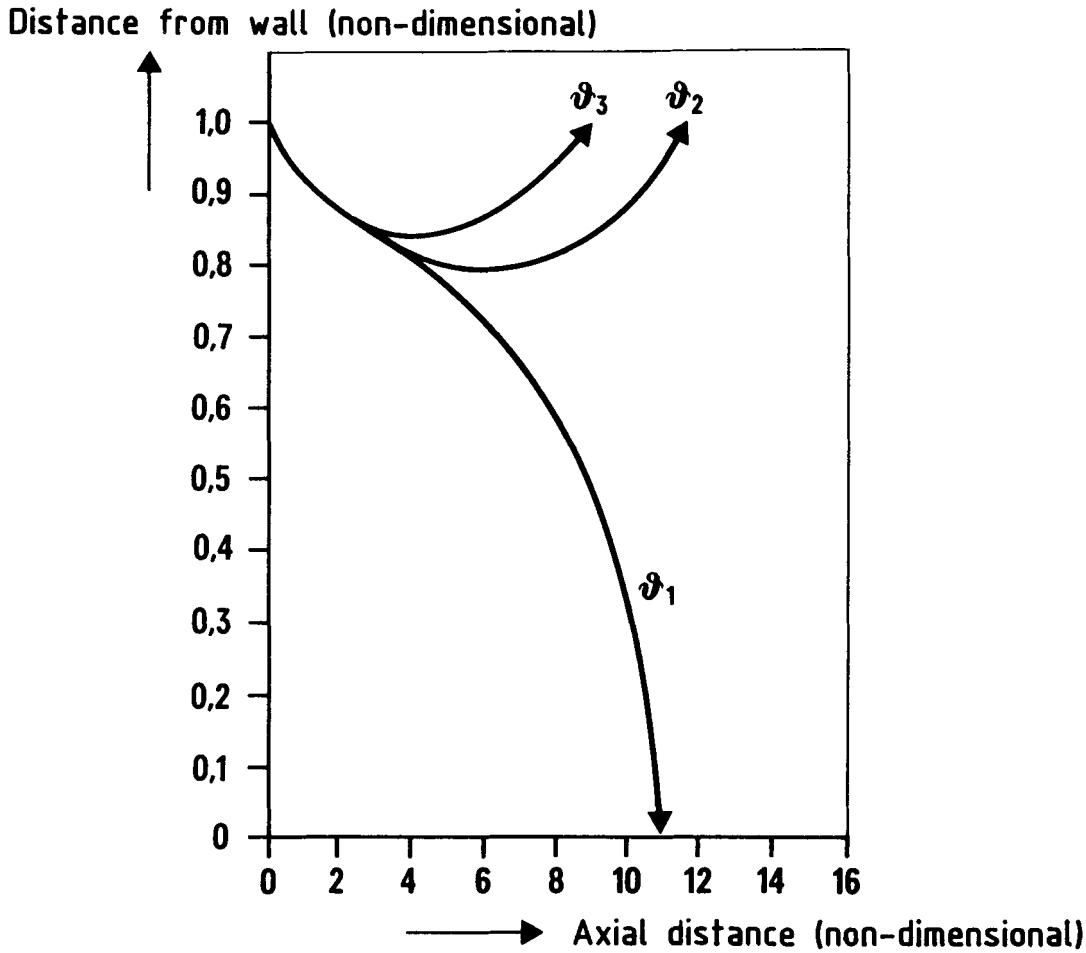


Figure 6-16 Influence of the wall temperature on the trajectories of evaporating nitrogen droplets (according to GARNIC and ROHSENOW)

dryout region, which can also be observed with lower heat fluxes and thus lower wall temperatures, it can be deduced that the wall temperature in the post-dryout region is most of the times so high, that droplets cannot reach the wall. Apparently, regardless if the wall temperature lies above or below the experimentally determined Leidenfrost temperature with forced convection (cf. Figure 4-13), the pressure loss is not influenced.

If one starts from the premise that in the unwetted region there a direct momentum transfer between water droplets and heating surface is not possible, the water droplets behave passively in respect to the pressure loss and increase by their presence merely the mean flow velocity. The pressure loss is then solely determined by the properties of the steam.

Thus, the Reynolds number necessary for the determination of the tube friction coefficient becomes

$$Re = \frac{w \cdot d}{\eta'' / \rho''} = \frac{\rho''}{\rho h} \cdot \frac{\dot{m} \cdot d}{\eta''} \tag{6-18}$$

and the pressure loss can be calculated as follows:

$$\Delta P_R = \xi \cdot \frac{L}{d} \cdot \frac{\rho''}{d} \cdot \left( \frac{m}{\rho_h} \right)^2 \tag{6-19}$$

With equations (6-2), (6-3), (6-9), (6-17), (6-18), and (6-19) the two-phase multiplier becomes

$$R = \left( \frac{\eta''}{\eta^T} \right)^n \cdot \left( \frac{\rho''}{\rho^T} \right)^{1-n} \cdot \left[ 1 + \dot{x} \left( \frac{\rho'}{\rho''} - 1 \right) \right]^{2-n} \tag{6-20}$$

For n = 0.2, the equation (6-20) is converted into the equation given by BEATTIE for the two-phase multiplier in the post-dryout region.

Figure 6-17 shows the transition from the wetted to the unwetted wall state for an unheated and a heated tube flow. In the case of unheated tubes, the two-phase multiplier can present in the transition region an increasing or decreasing tendency. The course depends on the length of the transition region and on the occurring changes of the pressure loss. In the case of horizontal tubes, the transition region is frequently longer than in vertical tubes due to separation phenomena. A transition region region occurs also in heated tubes if they are horizontal. The boiling crisis occurs therein on the upper side of the tube while the bottom side is still wetted. The length of the transition region in a heated tube flow can be determined according to Chapter 5.

In Figure 6-18 are summarized the calculation possibilities for the two-phase pressure loss with distinct Reynolds turbulence.

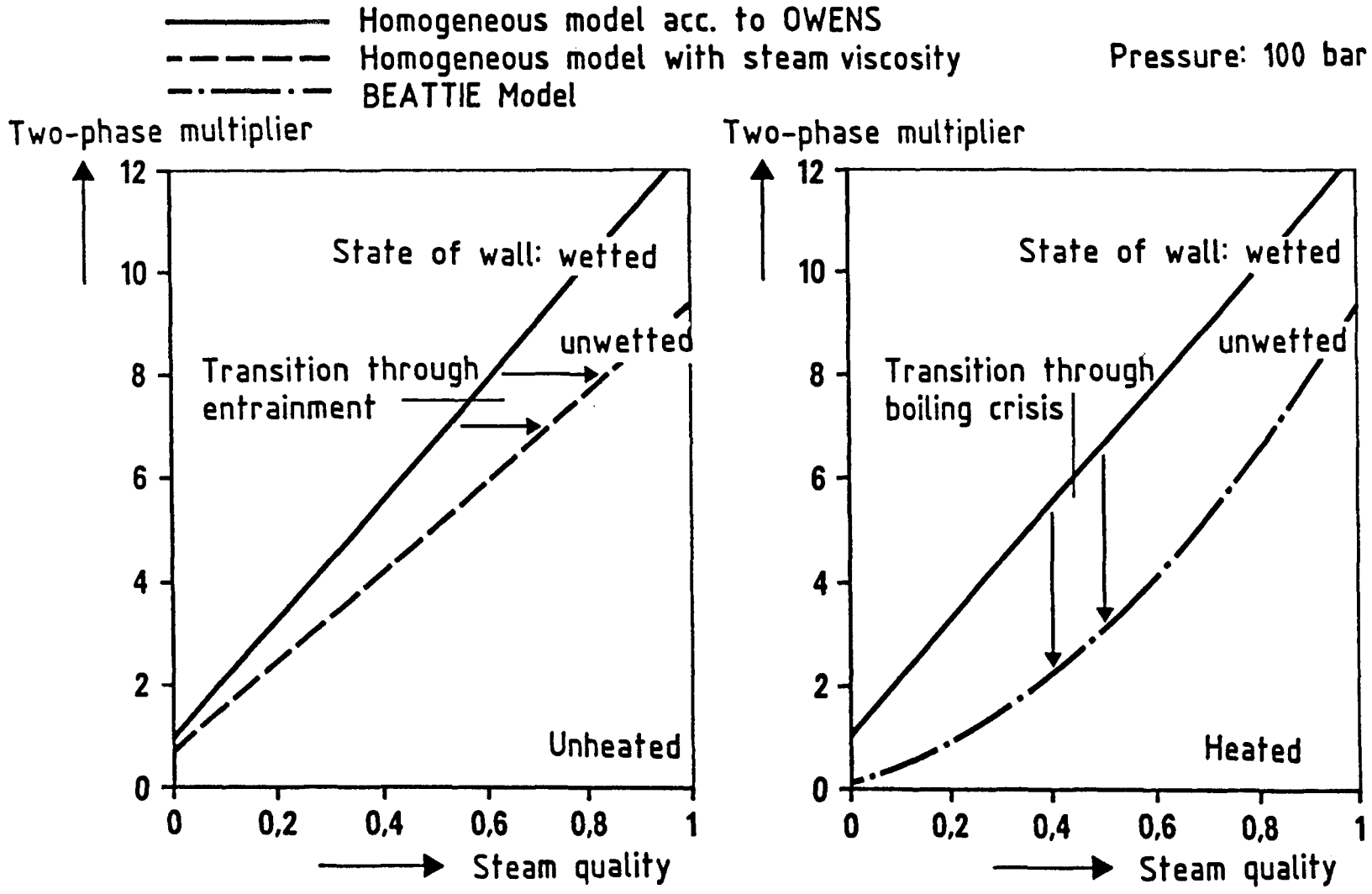


Figure 6-17 Recommended calculation possibilities for the two-phase pressure loss with distinct Reynolds turbulence

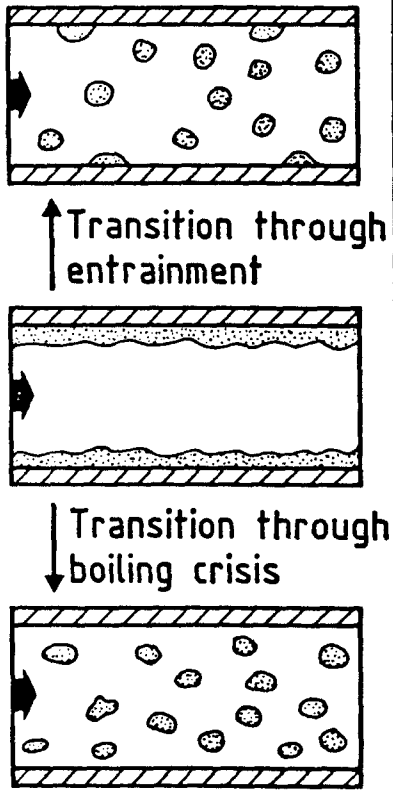


| State of wall | | Parameters determining pressure drop | | |
|---|---|---|---|---|
| | | Viscosity | Density | Two-phase multiplier |
| (almost) Unwetted | Unheated | $\eta''$ | $\varrho_h$ | $(\frac{\eta''}{\eta'})^n [1+x(\frac{\varrho'}{\varrho''}-1)]$ |
| Wetted | Heated or unheated | $\eta'$ | $\varrho_h$ | $1+x(\frac{\varrho'}{\varrho''}-1)$ |
| Unwetted | Heated | $\eta''$ | $\varrho''$ | $(\frac{\eta''}{\eta'})^n \cdot (\frac{\varrho''}{\varrho'})^{1-n} [1+x(\frac{\varrho'}{\varrho''}-1)]^{2-n}$ |

$n = 0{,}2$ for $10^4 < Re < 5 \cdot 10^6$

Figure 6-18 Recommended calculation possibilities for the two-phase pressure loss with distinct Reynolds turbulence

# 7 SUMMARY

The influence of the wetting state of the heating surface on the heat transfer and pressure loss was investigated for the parameter range of fossil-fired steam generators.

For the determination of the fundamental mechanisms one started at first from a steady state vertical upward tube flow. For this case a method was developed for the determination of critical boiling states in the entire steam quality region, which was compared to test results with the help of comparative calculations. The heat transfer after the exceeding of the boiling crisis was experimentally investigated. Based on these investigations there was developed a model for the heat transfer in the unwetted region, taking into consideration the thermal non-equilibrium between the water and the steam phase. This model is based on the simplified premise, that for each parameter combination there exists a value for the thermal non-equilibrium, through which the course of the heating surface temperature is determined. Thus, the heat transfer from the location of the minimum heat transfer until the transition to the single-phase steam flow can be described with sufficient accuracy.

The influence of pressure and enthalpy transients on the heat transfer in the unwetted region was experimentally investigated. Therein was observed a considerable ride of the wall temperature for transients, which occurred in the proximity of the critical pressure, which has to be attributed to a temporary non-wetting of a wetted heating surface in steady state. A semi-empirical model was developed for the advancing of the wetting front under pressure and enthalpy transients, which was verified with the obtained test results.

The influence of the tube orientation on the heat transfer was investigated in horizontal and vertical tubes. The tests showed that already in the region of the single-phase heat transfer with turbulent fluid flow there can occur considerable temperature differences between the upper and the bottom sides of the tube in the case of horizontal flow. The boiling crisis in the horizontal tube occurs in most cases much earlier on the upper side than on the bottom one. Due to the heat conduction in the wall material from the unwetted upper side to the wetted bottom side it is possible that the wall temperatures, after exceeding the boiling crisis, are distinctly lower in the horizontal tube than in the vertical one. Based on a force balance there was developed a method with which it can be determined at which parameter combination there can be expected an influence of the tube orientation on the location of the boiling crisis and on the heat transfer in the unwetted region.

Concomitantly with the heat transfer there was measured the pressure loss of the flow at horizontal and vertical tube orientation. Therein was observed a considerable influence of the wetting state of the heating surface on the pressure loss of a two-phase flow. The pressure loss is considerably lower in the unwetted region than in the wetted one. A method was developed with which it is possible to determine accurately the friction pressure loss with wetted and unwetted heating surfaces for the parameter range of fossil-fired steam generators. As shown by the analysis of measured friction pressure losses, the wall state has influence on the two-phase pressure loss also with an unheated tube flow. The transition from wetted to the unwetted state is herein effected by droplet entrainment into the core flow.

From the investigations on the pressure loss and heat transfer it can be gathered that in the considered parameter range with unwetted heating surface, the influence of the liquid droplets on the heat and momentum transfer with the heating surface can be disregarded.

## NOMENCLATURE

| | | |
|---|---|---|
| A | m | Laplace Constant |
| c | kJ/kgK | Specific thermal capacity |
| d | m | Tube bore |
| F | - | Surface of the water droplets per unit area of heated tube wall |
| Fr | - | Froude number |
| g | $m/s^2$ | Acceleration due to gravity |
| GR | | Grashof number |
| h | kJ/kg | Enthalpy |
| $\Delta h_v$ | kJ/kg | Specific evaporation enthalpy |
| $\Delta H$ | m | Height difference |
| L | m | Length |
| $\dot{m}$ | $kg/m^2s$ | Mass velocity |
| M | - | Mean value |
| n | - | Number of measurements; exponent |
| Nu | - | Nusselt number |
| $\overline{Nu}$ | - | Mean Nusselt number |
| p | bar | Pressure |
| $p_c$ | bar | Critical pressure |
| $\Delta p$ | $N/m^2$ | Pressure loss, pressure drop |
| Pr | _ | Prandtl number |
| $\dot{q}$ | $kW/m^2$ | Heat flux |
| $\dot{Q}$ | kW | Heat flux rate |
| R | - | Two-phase multiplier |
| $R_R$ | - | Calculated two-phase multiplier |
| $R_M$ | - | Measured two-phase multiplier |

| | | |
|---|---|---|
| Re | - | Reynolds number |
| u | m/s | Wetting front velocity |
| w | m/s | Flow velocity |
| $\dot{x}$ | - | Steam quality |
| $\dot{x}_{Lim}$ | - | Boundary steam quality |
| $\overline{\Delta\dot{x}}$ | - | Mean deviation of the steam quality |
| Y | - | Error magnitude |
| $\alpha$ | $kW/m^2K$ | Heat transfer coefficient |
| $\beta$ | 1/K | Coefficient of expansion |
| $\sigma$ | m | Tube wall thickness |
| $\varepsilon$ | - | Void fraction |
| $\dot{\omega}$ | - | Thermal non-equilibrium factor |
| $\eta$ | kg/ms | Dynamic viscosity |
| $\vartheta$ | °C | Temperature |
| $\Delta\vartheta_E$ | K | Inlet subcooling |
| $\Delta\vartheta_u$ | K | Superheating of the steam in the two-phase region |
| $\vartheta'_o$ | °C | Fictitious wall temperature on the upper side of the horizontal tube |
| $\Theta$ | rad | Angle of inclination |
| $\lambda$ | kW/mK | Heat conductivity |
| $\nu$ | $m^2/s$ | Kinematic viscosity |
| $\xi$ | - | Tube friction coefficient |
| $\rho$ | $kg/m^3$ | Density |
| $\bar{\rho}$ | $kg/m^3$ | Mean density |
| $\sigma$ | N/m | Surface stress |
| $\psi$ | rad | Peripheral angle |

Subscripts (or superscripts)

| | |
|---|---|
| B | Acceleration |
| Bil | According to balance |
| D | Steam |
| G | Hydrostatic |
| Ges | Total |
| h | Homogeneous |
| Kr | Critical boiling state |
| $Kr_R$ | Calculated critical boiling state |
| $Kr_M$ | Measured critical boiling state |
| L | Leidenfrost |
| o | Upper side of the horizontal tube |
| R | Friction |
| Real | Real (actual) |
| S | Saturation |
| Tr | Droplets |
| u | Bottom side of the horizontal tube |
| v | Vertical tube |
| W | Water, wall |
| $\alpha_{min}$ | Minimum heat transfer coefficient |
| ' | Saturation state of water |
| " | Saturation state of steam |
| 1ph, w | Single-phase, water |
| 2ph | Two-phase |

## BIBLIOGRAPHY


1. Hein, D., Keil, H. and Koehler, W. The BENSON Test Rig, VGB-Kraftwerkstechnik, 57th Annual Series, No. 6, June 1977.

2. Govier, G. W., Radford, B. A. and Dunn, J. S. C. The Upward Vertical Flow of Air-Water Mixtures, Canad, J. Chem. Eng. Bd. 35, No. 2, pp. 58-70 (1975).

3. Bennet, A. W. et al. Flow Visualization Studies of Boiling at High Pressure, Inst. Mech. Eng., Proc. 1965 - 1966, 180, Part 3C, 260 - 270, 1965.

4. Taitel, Y., Dukler, A. E. Flow Regime Transitions for Vertical Upward Gas-Liquid Flow, A Preliminary Approach through Physical Modelling, IACheE, 10 Annual meeting, New York, Session on Fundamental Research in Fluid Mechanics (1977).

5. Cumo, M., Palazzi, G., Urbani, G. C. On the Limiting Critical Quality and the "Deposition Controlled Burnout," CNEN-RT/ING (79)4-(1979).

6. Doroshchuk, V. E., Levitan, L. L., Lantsmann, F. P. Recommendations for Calculating Burnout in a Round Tube with Uniform Heat Release, Teploenergetika 22 (1975) No. 12, pp. 60-70.

7. Academy of Sciences, USSR: Tabular Data for Calculating Burnout when Boiling Water in Uniformly Heated Round Tubes, Thermal Eng. Vol. 23 (1977) No. 9, pp. 77-79.

8. Kemner, H. CHF Table for KWU Fuel Assemblies with Spacers without Vanes and their Application, Working Report KWU-R 123-171/80 (1980).

9. Fechner, B. The Heat Transfer after the Exceeding of the Critical Heat Flux Density, Diploma Thesis at the Institute A for Thermodynamics at the TU Munich (1976).

10. Kon'Kov, A. S. Experimental Study of the Conditions under which Heat Exchange Deteriorates when a Steam-Water Mixture Flows in Heated Tubes, Teploenergetika, Vol. 13 (1965) No. 12, p. 77.

11. Tong, I. S., Currin, H. B., Engle, F. C. DNB Studies in an open Lattice Core, WCAP-3736, Vol. I and II (1964).

12. Becker, K. M. An Analytical and Experimental Study of Burnout Conditions in Vertical Round Ducts, Aktiebolaget Atomenergie AE-178 (1965).

13. Becker, K. M. Burnout Studies in Round Tubes at 140 Bars, AE-RTL-974 (1968).

14. Thompson, B., Macbeth, R. C. Boiling Water Heat Transfer Burnout in Uniformly Heated Round Tubes, A Compilation of World Date with Accurate Correlations, AEEW-R356 (1964).

15. Exercise on Reproducibility of Critical Heat Flux Data Meeting of the European Two Phase Flow Group, Milano 1970.

16. Bailey, N. A. Dryout and Post Dryout Heat Transfer at Low Flow in a Single Tube Test Section, AEEW-R-1068, Jan. 1977.

17. Bailey, N. A. The Interaction of Droplet Deposition and Forced Convection in Post-Dryout Heat Transfer at High Subcritical Pressures, European Two-Phase Flow Group Meeting, Rome 1972.

18. Smolin, V. N. et al. Experimental Study of a Heat Transfer Crisis, Soviet Atomic Energy, Vol. 16 (1964) No. 5, pp. 515-521.

19. Becker, M., Ling, C.-H. Burnout Measurements in a Round Tube of 7100 mm Heated Length, European Two-Phase Flow Group Meeting, Milano 1970.

20. Hein, D., Köhler W., Krätzer, W. Experimental and Analytical Studies on the Heat Transfer in Steam Generator Tubes, KWU-R 513, January 1979.

21. Cumo, M., Urbani, G. Post Burnout Exercise: Comparison of the Experimental Data, European Two-Phase Flow Group Meeting, Harwell 1974.

22. Hein, D., et al. Compilation of Working Papers for the Determination of the Critical Heat Flux and the Minimum Heat Transfer Coefficients with Film Boiling, MAN-Report No. 282.03.01, July 1971.

23. Iloeje, O. C. Three Step Model of Dispersed Flow Heat Transfer, Third Water Reactor Safety Research Information Meeting, Washington (1975).

24. Mayinger, F. Flow and Heat Transfer in Gas-Fluid Mixtures, Vienna (1982).

25. Bennett, A. W., Hewitt, G. F., et al. Heat Transfer to Steam Water Mixtures Flowing in Uniformly Heated Tubes in which the Critical Heat Flux Has Been Exceeded, AERE-R 5373 (1967).

26. Dougall, R. D., Rohsenow, W. M. Filmboiling on the Inside of Vertical Tubes with Upward Flow of the Fluid at Low Qualities, MIT 9079-26 (1963).

27. Bishop, A. A., Sandberg, R. O., Tong, L. S. High Temperature Supercritical Pressure Water Loop, Part V: Forced Convection Heat Transfer to Water after the Critical Heat Flux at High Subcritical Pressures, WCAP-2056 (Part 5) (1964).

28. Heinemann, J. B. An Experimental Investigation of Heat Transfer to Superheated Steam in Round and Rectangular Channels, ANL-6213 (1960).

29. Miropol'skiy, Z. L. Heat Transfer in Film Boiling of Steam-Water Mixture in Steam Generating Tubes, Teploenergetika Vol. 10, No. 5, pp. 49-53 (1963).

30. Groeneveld, D. C. Post-Dryout Heat Transfer at Reactor Operating Conditions, ANS Conf. 730304 (1973), pp. 321-350.

31. Plummer, D. N. Post Critical Heat Transfer to Flowing Liquid in a Vertical Tube, Ph.D. Thesis, MIT (1974).

32. Groeneveld, D. C., Delorme, G. G. J. Prediction of Thermal Non-Equilibrium in the Post-Dryout Regime, Nuclear Engineering and Design 36, pp. 17-26 (1976).

33. Saha, P., Shiralkar, B. S. and Dix, G. E. A Post-Dryout Heat Transfer Model Based on Actual Vapor Generation Rate in Dispersed Droplet Regime, ASME Publication at AICHE-ASME Heat Transfer Conf., Salt Lake City, Utah, August 1977.

34. Koizumi, Y., Ueda, T., Tanaka, H. Post-Dryout Heat Transfer to R 113 Upward Flow in a Vertical Tube, Int. J. Heat Mass Transfer, Vol. 22, pp. 669-678 (1979).

35. Schnittger, R. B. Investigations on the Heat Transfer with Vertical and Horizontal Tube Flows in the Post-Dryout Region, Dissertation, University of Hannover (1982).

36. Gnielinski, V. New Equations for the Heat and Mass Transfer in Tube and Channels with Turbulent Flows, Forsch. Ing.-Wes. 41, No. 1 (1975).

37. Herkenrath, H., Mörk-Mörkenstein, P. et al. Heat Transfer to Water with Forced Flow in the Pressure Range of 140 to 250 bars, EUR 3658 d - EURATOM Ispra (1967).

38. Jens, W. H. and Lottes, P. A. Analysis of Heat Transfer, Burnout, Pressure Drop, and Density Data for High Pressure Water, USAEC Report ANL-4627 (1951).

39. Lausterer, G. K., Franke, J. and Eitelberg, E. Mathematical Modelling of a Steam Generator, Dig. Comp. Appli. to Process Control, Proceeding of VI IFAC/IFIP - Int. Conf., Dusseldorf Oct. (1980).

40. Nukijama, S. Maximum and Minimum Values of Heat Transmitted from Metal to Boiling Water under Atmospheric Presure J. Soc. Mech. Eng. Jap. 37 (1934) 367/74 and 53/54.

41. Bergles, A. E., Collier, J. G., Delhaye, J., Hewitt, G. F., Mayinger, F. Two-Phase Flow and Heat Transfer in the Power and Process Industries, Washington, Hemisphere Publishing (1981).

42. Yamanouchi, A. Effect of Core Spray Cooling in Transient State after Loss of Coolant Accident, J. Nucl. Sci. Technol. 5 (1968) 547-558.

43. Hein, D. Models for the Rewetting by Flooding, Dissertation, University of Hannover (1980).

44. Kefer, V. The Influence of Pressure on the Wetting Behavior, Diploma Thesis at the Institute A for Thermodynamics at the TU Munich (1982).

45. Baker, O. Simultaneous Flow of Oil and Gas, Oil and Gas Journal 53, No. 12 (1954), pp. 185-195.

46. Mandhane, J. M., Gregory, G. A., Aziz, K. A Flow Pattern Map for Gas - Liquid Flow in Horizontal Pipes, Int. Multiphase Flow, Vol. 1, pp. 537-553 (1974).

47. Taitel, Y., Dukler, A. E. A Model for Predicting Flow Regime Transitions in Horizontal and Near Horizontal Gas-Liquid Flow, AICHE Journal Vol. 22, No. 1, Jan. 1976, pp. 47-54.

48. Petukhov, B. S., Polyakov, A. F., Kuleshow, V. A., Shekhter, Yu.L. Turbulent Flow and Heat Transfer in Horizontal Tubes with Substantial Influence of Thermogravitational Forces, 5th Int. Heat Transfer Conf. Tokyo (1974), Vol. 3, pp. 164-168.

49. Cumo, M., Fabrizi, F., Palazzi, G. The Influence of Inclination of CHF in Steam Generator Channels, CNEN RT/ING (78) 11 (1978).

50. Wallis, G. B. One-dimensional Two-Phase Flow, New York, McGraw-Hill (1969).

51. Schnittger, R. B. and Mayinger, F. Post-Dryout Heat Transfer in Horizontal Tubes European Two-Phase Flow Group Meeting, Paris (1982).

52. Friedel, L. Pressure Drop with the Flow of Gas/Steam-Liquid-Mixtures in Tubes, Chem.-Ing.-Techn. 50, No. 3 (1978).

53. Tarasova, N. V. and Leontiev, A. I. Hydraulic Resistance with a Steam-Water Mixture Flowing in a Vertical Heated Tube, High Temp, Vol. 3, No. 1, pp. 102-108 (1965).

54. Tarasova, N. V., Leontiev, A. I., Hlopushin, V. I. and Orolov, V. M. Pressure Drop of Boiling Subcooled Water and Steam-Water Mixture Boiling, Proc. 3rd Int. Heat Transfer Conf. (1966).

55. Beattie, D. R. H. A Note on the Calculation of Two-Phase Pressure Losses Nucl. Engng. and Design 25, pp. 395-402 (1973).

56. Beattie, D. R. H. Friction Factors and Regime Transitions in High Pressure Steam-Water Flows, ASME 75-WA/HT-4 (1975).

57. Whitcutt, R. D. B. and Chojnowski, B. Two-Phase Pressure Drop in High Pressure Steam Generating Tubes, European Two-Phase Flow Group Meeting, Brussels (1973).

58. Owens, W. L. Two-Phase Pressure Gradient, Int. Developm. in Heat Transfer, ASME pp. 363-368 (1963).

59. Delhaye, J. M., Giot, M. and Riethmüller, M. L. Thermohydraulics of Two-Phase Systems for Industrial Design and Nuclear Engineering, Washington (1981).

60. Lombardi, C., Pedrocchi, E. A Pressure Drop Correlation in Two-Phase Flow, Energia Nucleare, Vol. 19, No. 2 (1972).

61. Friedel, L. A Dimensionless Relation for the Friction Pressure Drop with Two-Phase Flow of Water and R 12, Verfahrenstechnik 13, No. 4 (1979).

62. Köhler, W. Data Compilation on Measurements of the Two-Phase Pressure Loss and on the Volumetric Steam Quality of Flowing Water/Water-Steam Mixtures, Working Report KWU-R 513/33/79 (1979).

63. Storek, H. and Brauer H. Pressure Loss of Adiabatic Gas-Liquid Flows in Horizontal and Vertical Tubes, VDI-Forsch.-Heft 599 (1980).

64. Gaspari, G. P., Lombardi, C., Peterlongo, G. Pressure Drops in Steam-Water Mixtures, Report R-83 CISE, Milano (1964).

65. Huhn J. and Wolf, J. Two-Phase Flow, VEB Fachbuchverlag Leipzig (1975).

66. Collier, J. G. Two-Phase Gas-Liquid Pressure Drop and Void Fraction - A Review of the Current Position, European Two-Phase Flow Group Meeting, Paper B1, Harwell (June 1974).

67. Colburn, A. P. Trans, A.I. Ch.E., Vol. 29, 174 (1933).

68. Ganić, E. N. and Rohsenow, W. M. On the Mechanism of Liquid Drop Deposition in Two-Phase Dispersed Flow, Trans. ASME, Vol. 101, May (1979).